

The Dissertation Committee for Sarp Akcay  
certifies that this is the approved version of the following dissertation:

## **Boosted Apparent Horizons**

Committee:

---

Richard Matzner, Supervisor

---

Richard Hazeltine

---

Larry Shepley

---

Pawan Kumar

---

Duane Dicus

# **Boosted Apparent Horizons**

by

**Sarp Akcay, B.S.**

## **Dissertation**

Presented to the Faculty of the Graduate School of

The University of Texas at Austin

in Partial Fulfillment

of the Requirements

for the Degree of

**Doctor of Philosophy**

**The University of Texas at Austin**

August 2009

## Acknowledgments

I would like to extend my gratitude toward my adviser Richard Matzner whose door was always open for countless sessions of answering dumb graduate student questions. His guidance and physical intuition have been of invaluable help in creating this work as well as assisting me find my way in other projects. His rigor and tireless editing have made all my written work much more concise than I could have ever singlehandedly accomplished. It is my hope that I was not a complete disappointment. I look forward to our future collaborations.

To my friends, I can not thank enough for being there through the good and the bad, the ups and the downs, for putting up with my endless antics and coming to my aid in my darkest hours. You will not be forgotten.

And finally, my parents and family who have given up so much and left their home country in order for me to pursue a career in physics. Words would not do justice to how indebted I am to all of you. Never once was I told to give up physics and opt for a more lucrative career, never once was I discouraged from studying science and perhaps even more importantly, my mind was always kept free from the oppression of superstition and religious beliefs. I must indeed be one of the few privileged individuals in the world for having been brought up by such progressive parents. You have made the ultimate sacrifice and I hope that this doctorate will at least partly count toward making up for what you gave up. I hope that I have succeeded in

making you proud to some degree. *Bu tezi size hediye ediyorum. Yaptığınız fedakarlıkların bir simgesi olarak kabul edin.*

SARP AKÇAY

*The University of Texas at Austin  
August 2009*

# Boosted Apparent Horizons

Publication No. \_\_\_\_\_

Sarp Akcay, Ph.D.

The University of Texas at Austin, 2009

Supervisor: Richard Matzner

Boosted black holes play an important role in General Relativity (GR), especially in relation to the binary black hole problem. Solving Einstein vacuum equations in the strong field regime had long been the holy grail of numerical relativity until the significant breakthroughs made in 2005 and 2006. Numerical relativity plays a crucial role in gravitational wave detection by providing numerically generated gravitational waveforms that help search for actual signatures of gravitational radiation exciting laser interferometric detectors such as LIGO, VIRGO and GEO600 here on Earth. Binary black holes orbit each other in an ever tightening adiabatic inspiral caused by energy loss due to gravitational radiation emission. As the orbits shrinks, the

holes speed up and eventually move at relativistic speeds in the vicinity of each other (separated by  $\sim 10M$  or so where  $2M$  is the Schwarzschild radius). As such, one must abandon the Newtonian notion of a point mass on a circular orbit with tangential velocity and replace it with the concept of black holes, cloaked behind spheroidal event horizons that become distorted due to strong gravity, and further appear distorted because of Lorentz effects from the high orbital velocity. *Apparent horizons* (AHs) are 2-dimensional boundaries that are trapped surfaces. Conceptually, one can think of them as ‘quasi-local’ definitions for a black hole horizon. This will be explained in more detail in chapter 2. Apparent horizons are especially important in numerical relativity as they provide a computationally efficient way of describing and locating a black hole horizon. For a stationary spacetime, apparent horizons are 2-dimensional cross-sections of the event horizon, which is itself a 3-dimensional null surface in spacetime. Because an AH is a 2-dimensional cross-section of an event horizon, its area remains invariant under distortions due to Lorentz boosts although its shape changes. This fascinating property of the AH can be attributed to the fact that it is a cross-section of a *null* surface, which, under the boost, still remains null and the total area does not change. Although this invariance of the area is conceptually easy to see it is less straightforward to derive this result. We present two different ways to show the area invariance. One is based on the spin-boost transformation of the null tetrad and the other a direct coordinate transformation of the boosted metric under the Lorentz boost. Despite yielding identical results the two methods differ significantly and we elaborate on this in much more detail. We furthermore show that the use of the spin-boost transformation is not well-suited for binary

black hole spacetime and that the spin-boost is fundamentally different from a Lorentz boost although the transformation equations look very similar. We also provide a way to visualize the distorted horizons and look at the multipole moments of these surfaces under small boosts. We finish by summarizing our main results at the end and by commenting on the binding energy of the binary and how the apparent horizon is distorted due to presence of another black hole.

# Table of Contents

<b>Acknowledgments</b>	<b>iii</b>
<b>Abstract</b>	<b>v</b>
<b>List of Tables</b>	<b>x</b>
<b>List of Figures</b>	<b>xi</b>
<b>Chapter 1. Introduction</b>	<b>1</b>
<b>Chapter 2. Apparent Horizons</b>	<b>14</b>
2.1 Apparent Horizon in Schwarzschild Spacetime . . . . .	14
2.2 Apparent Horizons in Kerr Spacetime . . . . .	21
<b>Chapter 3. Boosted Apparent Horizons</b>	<b>28</b>
3.1 Boosted Schwarzschild Black Holes . . . . .	29
3.2 Numerical Results . . . . .	34
3.3 Boosted Kerr Black Holes . . . . .	42
<b>Chapter 4. Visualization</b>	<b>53</b>
4.1 Discrete Tracer Line Method . . . . .	55
4.2 Distorted Polar Coordinate Method . . . . .	61
4.2.1 Overlap Between The Two Methods . . . . .	68
4.3 Adding The Third Dimension . . . . .	68
4.4 Elliptical Coordinates . . . . .	71
4.4.1 Elliptical Coordinates for Boosted Horizons . . . . .	74



<b>Chapter 5. Area Invariance under Spin-Boost Transformations</b>	<b>77</b>
5.1 Poisson's Derivation . . . . .	78
5.2 Null Tetrad Formalism . . . . .	81
5.3 Spin-Boost Transformation for the Schwarzschild Spacetime .	87
<b>Chapter 6. Perturbations of a Boosted Black Hole</b>	<b>104</b>
6.1 Boosted Schwarzschild Black Hole . . . . .	110
6.2 Slow Spin Kerr as a Perturbation of Schwarzschild . . . . .	121
6.2.1 Slow Spin Kerr Boosted . . . . .	122
6.3 Boosted Schwarzschild to Second Order . . . . .	125
<b>Chapter 7. Conclusions</b>	<b>131</b>
<b>Appendix</b>	<b>135</b>
<b>Appendix 1. Maple Code for The Tracer Line Method</b>	<b>136</b>
<b>Appendix 2. Maple Code for the Polar Plot Method</b>	<b>143</b>
<b>Appendix 3. Maple Code for Plotting using Ellipsoidal Coordinates</b>	<b>149</b>
<b>Appendix 4. Maple Code for using Tilted Ellipsoidal Coordinates</b>	<b>153</b>
<b>Bibliography</b>	<b>157</b>
<b>Vita</b>	<b>164</b>

## List of Tables

- 4.1 Numerically determined values yielding the length of the distorted ellipse's long and short axes  $a'_1, a'_2$  as well as the angular locations  $\theta'_{max}$  of those axes. In each column, the top two rows correspond to  $a'_1$  and bottom two to  $a'_2$ . . . . . 65
- 6.1 Summary of all perturbations that contribute to the background Schwarzschild metric. Here, we have included the Kerr metric in the slow spin ( $a \ll 1$ ) limit as a perturbation to the Schwarzschild background. Quadratic terms give modes up to  $\ell = 2$ . However, as expected, there is no radiation coming from these modes. . . . . 130

## List of Figures

1.1	The spacelike Cauchy hypersurface $\Sigma$ with a 2-dimensional trapped surface $S$ in it. $t^\mu$ is timelike and normal to $\Sigma$ whereas $r^\mu$ is spacelike and lies in $\Sigma$ but is normal to $S$ . $\ell^\mu$ and $n^\mu$ are null linear combinations of $t^\mu$ and $r^\mu$ and are orthogonal to $S$ . . . .	6
1.2	Finkelstein and Penrose diagrams for a spacetime containing a star collapsing to form a black hole and a shell of dust collapsing onto that black hole later. The green and black curves on the left represent outgoing light rays that become trapped inside the event horizon. The 2-dimensional apparent horizons are zero-expansion surfaces that intersect $t = \text{constant}$ spacelike slices. Note that a surface that is marginally trapped at $t = t_1, t_2$ becomes fully trapped later on. The green curve in the right diagram is the 3-dimensional world tube of 2-dimensional apparent horizons. Note that it starts from inside the event horizon at first and later becomes a spacelike surface during the infall of dust to finally coincide with the event horizon after all dynamical processes have settled down. Finally, the event horizon in the left diagram only becomes a zero-expansion surface as $t \rightarrow \infty$ , which is consistent with its technical definition. Its expansion asymptotically goes to zero as $t \rightarrow \infty$ . . . . .	11
3.1	The cylinders represent the 3-dimensional event horizons whose 2-dimensional $t = \text{constant}$ cross-sections are the apparent horizons (AHs). The AH on the left is unboosted and the one on the right is boosted. As can be seen from the figure, the boost simply tilts the $t = \text{constant}$ cuts of the cylinder. One dimension has been suppressed for convenience. Each circle is topologically equivalent to a 2-sphere . . . . .	30

3.2	<p>Negative of the binding Energy <math>-E_b</math> versus the inverse coordinate separation <math>1/r</math> for the cases with boosts speed <math>\beta = 0, 0.1, 0.5</math> represented by the green, black and blue curves, respectively. The red line is the Newtonian binding energy which scales as <math>1/r</math>. Ideally, it should be tangent to the <math>\beta = 0</math> curve (green) at large <math>r</math> (<math>1/r \rightarrow 0</math>) but here it is slightly shifted due to numerical errors. As can be seen in the figure, the binding energy matches the Newtonian limit very well for large separations (<math>1/r \rightarrow 0</math>), it grows faster than <math>1/r</math> as the black holes are closer (<math>1/r \rightarrow \infty</math>). This is due to changes in horizon masses because of the distortions induced by the black holes on each other. It (<math>-E_b</math>) also becomes more negative for large boosts reflecting the unbound nature of distant rapidly moving black holes where the kinetic energy of the black holes overwhelms the negative potential energy. . . . .</p>	40
3.3	<p>Horizon mass <math>M_H</math> and ADM mass <math>M_{ADM}</math> versus inverse distance <math>1/r</math> for boost speeds of <math>\beta = 0, 0.1, 0.5</math>. <math>M_{ADM}</math> (the upper, approximately parallel curves) is given by the the pink dashed line (<math>v=0.5</math>) and by the closely overlapping blue line (<math>v=0</math>) and the red X marks (“×”). As expected, the ADM mass remains constant regardless of the separation <math>r</math> but varies as <math>\gamma M_{ADM 0}</math> for varying boost speeds <math>\beta</math>. <math>M_H</math> (the lower curves) is represented by closely overlapping red and green curves for the <math>v=0</math> and <math>v=0.1</math> cases, and by the higher black curve for <math>v=0.5</math>. Note that the horizon mass grows larger as the black holes are nearer i.e. as <math>1/r \rightarrow \infty</math>. The horizon mass is invariant under boosts. For <math>r \geq 10</math> (i.e. <math>1/r \leq 0.1</math>) the horizon mass curves for different boosts overlap perfectly. Apparently because of the nonlinear interaction of the black hole geometries in the full solution, for larger boosts and for small separations the horizon mass does increase slightly. . . . .</p>	41
3.4	<p>The tilted cylindrical coordinates <math>(\bar{r}_{  }, \bar{r}_{\perp}, \bar{\phi}_{cyl})</math> along with the radial coordinate <math>r</math> and Kerr-Schild Cartesian coordinates <math>(\bar{x}, \bar{y}, \bar{z})</math>. The vector <math>\beta</math> points along the boost direction, which is parallel to the symmetry axis of the cylinder. . . . .</p>	45
4.1	<p>x-z cross sections of an unboosted (solid) and a z-direction boosted (dotted) Kerr black hole with <math>a = M/2</math>, which gives <math>r_+ = 1 + \sqrt{3}/2 = 1.866M</math>. This gives <math>a_1 = 1.932M</math>, <math>a_2 = 1.866M</math> for the x-,z-axes, respectively. The Lorentz boost factor is <math>\gamma = 2</math>. In the figure and henceforth, we will set <math>M = 1</math>. . . . .</p>	55

4.2	A schematic representation of the general lay-out for the tracer-line method. The red line is the tracer-line, which is parallel to the boost direction and sweeps the undistorted ellipse from left to right. The dashed line is perpendicular to the solid lines. $\theta_\beta$ is the boost direction given by the polar angle $\theta$ lying in the x-z plane. The x-direction here does not necessarily coincide with the overall x-direction of the grid. We always rotate the coordinate grid so that the azimuthal boost direction $\phi_\beta$ is reset to zero. . . . .	58
4.3	A $\beta = \sqrt{3}/2$ ( $\gamma = 2$ ) boost of an extremal ( $a = 1$ ) Kerr black hole in the direction $\theta_\beta = 30^\circ$ . The solid curve (the ellipse) is the undistorted horizon with semi-major axis $a_1 = \sqrt{2}$ and semi-minor axis $a_2 = 1$ . The distance units are normalized in terms of black hole mass $M$ . The dotted warped/tilted ellipse is the new black hole horizon distorted under the Lorentz boost. . . . .	60
4.4	A $\beta = \sqrt{2}/2$ ( $\gamma = \sqrt{2}$ ) boost of a Kerr black hole with spin $a = 0.75$ in the direction $\theta_\beta = 45^\circ$ . The solid curve (the ellipse) is the undistorted horizon with semi-major axis $a_1 = 1.822875656$ and semi-minor axis $a_2 = 1.661437828$ . As before, the dotted tilted ellipse is the Lorentz contracted black hole horizon. . . . .	62
4.5	Schematic diagram showing the various angles and vectors used in determining the location of the distorted ellipse. The ellipses drawn here do not represent the actual distorted shapes. . . . .	63
4.6	Horizon of a Kerr black hole with $a = 1$ distorted by a Lorentz boost with $\gamma = 2$ in the direction $\theta_\beta = 30^\circ$ . This was plotted using the <i>polar plot</i> method. . . . .	67
4.7	The overlap of the methods showing a perfect match. This figure shows an undistorted Kerr black hole with $a = 1$ and the same black hole distorted by a $\gamma = 2$ Lorentz boost with angle $\theta_\beta = 30^\circ$ with respect to the z-axis. . . . .	69
4.8	Different cross-sections of the triaxial ellipsoid which is an extremal Kerr black hole of spin $a = 1$ distorted from its original shape by a $\gamma = 2$ Lorentz boost toward $\theta_\beta = 30^\circ$ direction which lies on the x-z plane. Starting from the upper left and going clockwise, the x-y, x-z, y-z cuts and the view from a random angle are displayed. The “jaws of doom” effect is an artifact of insufficient resolution, or rather, number of points used in generating the plots. Here, each plot contains 10,000 points. One can ‘close’ the jaws by increasing the number of particles at the expense of computing time. . . . .	70
4.9	Ellipsoidal coordinates for two Kerr black holes with spins $a = 1, 0.5$ respectively. The innermost ellipses are the horizons. The hyperbolae are curves of $\theta = 60^\circ, 45^\circ, 30^\circ$ , respectively. . . . .	74

4.10	Tilted ellipsoidal coordinates for two Kerr black holes with spins $a = 1, 0.5$ respectively. The innermost ellipses are the horizons. The boost is in the x-z plane given by polar angle $\theta_\beta = 30^\circ$ with $\gamma = 2$ as before. The untilted ellipses represent the unboosted horizons. One can visually compare these figures with the figures obtained in sections 4.1, 4.2. . . . .	75
5.1	3+1 ADM foliation of a spacetime into 3-dimensional spacelike hypersurfaces $\Sigma$ . $T^\mu$ is normal to each hypersurface and $\Phi^\mu$ provides a direction of time flow. $\beta^i$ accounts for the shift of each point on a given hypersurface. Two spatial dimensions have been suppressed. . . . .	91

# Chapter 1

## Introduction

Although one usually refers to the event horizon of a black hole when one speaks of ‘the horizon’, because of its unusual features, a black hole event horizon does not always make for a practical physical boundary. This stems from the fact that it is difficult to properly define a ‘region of no escape’ in the strict mathematical sense. This notion of no escape was mathematically formulated by introducing the concept of a black hole event horizon (EH), which is defined as a three-dimensional null surface in a spacetime that is the “future boundary of the causal past of future asymptotic null infinity  $\mathcal{I}^+$ ” [2]. Also in [2], Hawking and Ellis provide a more technical version of the above quoted definition with the following statement: “The event horizon is an achronal boundary which is generated by null geodesic segments which may have past endpoints but which can have no future endpoints.” An achronal set is one that contains no two points in it that are timelike separated. So, achronal sets are made up of spacelike and null segments. In more physical terms, the definition given in [2] means that an event horizon is described as the boundary in spacetime between null geodesics that escape to infinity, and those that fall into the singularity. Because it takes an infinite amount of

time to reach infinity, one must wait till ‘the end of time’ (end of spacetime actually) to locate the event horizon of a given spacetime. One determines the position of the event horizon by finding that one null ray at that neither falls into the black hole, nor escapes to null infinity  $\mathcal{I}^+$ . Then, one simply traces that special ray backward in time to locate the event horizon at each instant of time. Because of this requirement to know the entire future of the spacetime, event horizons are said to be *teleological* and non-local.

Furthermore, the non-local nature of the event horizon causes it to evolve in non-intuitive ways. This can be seen by looking at how the rate of change of horizon area evolves (2nd time derivative of the area). Using the Raychaudhuri equation ([3]) one obtains

$$\frac{d^2\tilde{\epsilon}}{d\lambda^2} = \left( \frac{1}{2}\Theta_{(\ell)}^2 - \sigma_{(\ell)\mu\nu}\sigma_{(\ell)}^{\mu\nu} - 8\pi T_{\mu\nu}\ell^\mu\ell^\nu \right) \tilde{\epsilon}. \quad (1.1)$$

Above  $\tilde{\epsilon}$  is the area 2-form of a 2-dimensional spacelike cross-section of the EH,  $\Theta_{(\ell)}$  is the expansion of the null geodesics  $\ell^\mu$  tangent to the event horizon (the growth rate of area along  $\ell^\mu$ ) and  $\sigma_{(\ell)}^{\mu\nu}$  is the tidal shearing (simply called “shear”) of that vector field.  $\lambda$  is the affine parameter to the geodesics  $\ell^\mu$ . All these terms will be explained in more detail later on. For now, it suffices to note that Eq.(1.1) tells one about the behavior of the rate of change of the growth rate of the horizon area. When there is no matter falling in (vacuum) both  $\sigma_{(\ell)}^{\mu\nu}$  and  $T_{\mu\nu}$  equal zero, which means that in the case of  $\Theta_{(\ell)} \neq 0$  (expanding horizon), the horizon expansion has maximum acceleration when no matter is falling. In other words, the infall of matter slows the expansion rate down,



which is very counterintuitive to say the least. Obviously, this picture severely contrasts with what one might expect in dynamical processes such as matter accretion by a black hole. This behavior of the growth not being related to the rate of infalling matter is another strange feature of event horizons along with their teleological nature. Another unusual property is the fact that event horizons are only defined for spacetimes containing a future null infinity  $\mathcal{I}^+$  (cf. [2]).

It is precisely these properties that make event horizons impractical for use in ‘local’ (in space and time) physics. This is because in order for one to locate the horizon, one would have to know the entire future of the spacetime. Once that is known, one can then trace the appropriate null rays backward in time and draw this boundary that one calls the event horizon. In more technical terms, one would have to solve the Cauchy problem for the whole future development of a given partial Cauchy surface [2]. A partial Cauchy surface is a spacelike hypersurface which no non-spacelike curve intersects more than once. “Whole future development” is presently unattainable in computational practice. Current numerical simulations have total run times of fractions of a second in real time. A typical simulation time might at best last for  $10^4 M = 5\mu s \times 10^4 (M/M_\odot) = 0.05s (M/M_\odot)$  where  $M$  is the mass of the black hole of interest and  $M_\odot = 1.99 \times 10^{30}\text{kg}$  is a solar mass. It is easy to see that this is far from being the null infinity one must reach in order to track the event horizon. In short, the non-local nature of an event horizon can be even more troubling in numerical relativity.

Apparent horizons (AH), on the other hand, are not plagued by such prescient definitions. They are *quasilocal* in nature and are more straightforward to locate in a given spacetime. Apparent horizons were first introduced by Penrose and Hawking in [1]&[2]. An apparent horizon is defined as the outermost marginally trapped surface on a given (partial) Cauchy slice  $\Sigma$ . A trapped surface is a smooth, closed 2-surface which has both of its forward-in-time, normal-to-the-surface null directions  $\ell^\mu$  and  $n^\mu$  have negative expansions  $\Theta_{(\ell)}$  and  $\Theta_{(n)}$  everywhere. That is, a 2-surface  $S$  is trapped if

$$\Theta_{(\ell)} \equiv q^{\mu\nu} \nabla_\mu \ell_\nu < 0 \quad \text{and} \quad \Theta_{(n)} \equiv q^{\mu\nu} \nabla_\mu n_\nu < 0 \quad (1.2)$$

where

$$q_{\mu\nu} \equiv g_{\mu\nu} + (\ell_\mu n_\nu + n_\mu \ell_\nu) / (-\ell \cdot n) \quad (1.3)$$

is the 2-metric induced on  $S$  and  $g_{\mu\nu}$  is the spacetime 4-metric. Here and henceforth,  $\ell^\mu$  denotes the outgoing null normal and  $n^\mu$  the ingoing one unless specified otherwise (see Fig. 1.1). One can apply this definition of a trapped surface to Minkowski spacetime. There, the outgoing normals have positive expansion everywhere, thus telling us that there are no trapped surfaces in Minkowski spacetime whatsoever as one should expect. Physically, the expansion of a vector field  $\Theta$  corresponds to the projection of the divergence of that vector field onto the 2-surface  $S$ . One can show that this expansion corresponds to the rate of change of the area of the 2-surface  $S$  (see [38] for a nice derivation of this).

A Marginally Trapped Surface (MTS) is one that has  $\Theta_{(\ell)} = 0$  and  $\Theta_{(n)} < 0$ . It is possible to have more than one MTS in a given region of spacetime. For example, during merger simulations of binary black holes in numerical relativity, one often finds an MTS around each black hole and a larger MTS enveloping the entire binary. Of these MTSs, one picks the outermost surface and calls that one the *apparent horizon*. The existence of an apparent horizon implies the existence of an event horizon outside it or coinciding with it. However, the converse is not true: It is possible to have no apparent horizons whatsoever inside an event horizon [2], [4]. Hawking imposed additional global assumptions for the existence of an apparent horizon, namely that the spacetime is “regular predictable”. This basically forbids the existence of any *naked* singularities to the future of the Cauchy slice. Such a spacetime is called *future asymptotically predictable*. Several additional conditions are needed to make this regular predictable (see [2], section 9.3). These are much more severe restrictions than one encounters in contemporary definitions of apparent horizons. One being, in particular, that the apparent horizon, much like the event horizon, is only defined for asymptotically flat spacetimes. There are less restricted, more conventional ways of defining an apparent horizon. For example, one can define an apparent horizon as a topologically spherical 2-dimensional surface on which the expansion of the outgoing null rays orthogonal to that surface is zero [5]. Thus, it is a surface where gravity is so strong that putative outgoing null rays can only “hover” against the gravitational force. The presence of such a trapped surface in a

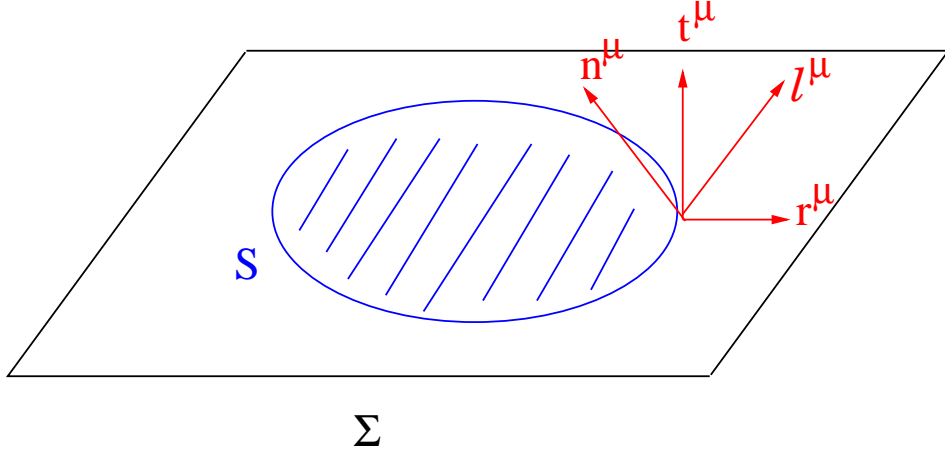


Figure 1.1: The spacelike Cauchy hypersurface  $\Sigma$  with a 2-dimensional trapped surface  $S$  in it.  $t^\mu$  is timelike and normal to  $\Sigma$  whereas  $r^\mu$  is spacelike and lies in  $\Sigma$  but is normal to  $S$ .  $\ell^\mu$  and  $n^\mu$  are null linear combinations of  $t^\mu$  and  $r^\mu$  and are orthogonal to  $S$ .

spacetime implies the existence of a singularity at least in the sense of a caustic (inextendible geodesic) [2],[6],[7]. Additionally, unlike event horizons, which are globally defined as the boundary in spacetime between null geodesics that escape to infinity, and those that fall into the singularity, apparent horizons are local objects, computable at one instant of time, hence much more accessible in numerical simulations and in computations that deal with non-isolated black holes. Examples of non-isolated black holes can be binary black holes, accreting black holes or a black hole merging with a neutron star. Moreover, apparent horizons can be extended into 3-dimensional world tubes, where every 2-dimensional cross-section of the world tube is an apparent horizon. Furthermore, these 3-dimensional hypersurfaces - the tubes - need not be only null, they can be spacelike and still have *time = constant cuts* that are apparent

horizons.

In stationary spacetimes, apparent horizons and event horizons coincide. For example, in the stationary Kerr spacetime in Boyer-Lindquist coordinates, the apparent and the event horizons are located at radial coordinate  $r = r_+ \equiv M + \sqrt{M^2 - a^2}$ , where  $M$  is the mass of the black hole and  $a$  is the spin parameter for the Kerr black hole given by  $a \equiv J/M$ , with  $J$  being the angular momentum of the black hole. Clearly, the two horizons also coincide in Schwarzschild spacetime at  $r = 2M$  (Here,  $r$  is the Schwarzschild radial coordinate.) as this spacetime is the  $a = 0$  limit of the more general Kerr solution to Einstein vacuum equations. [Technically speaking Schwarzschild spacetimes are not subsets of the more general Kerr spacetimes because static spacetimes (such as Schwarzschild) are invariant under time reversal whereas stationary spacetimes (such as the rotating Kerr black hole solution) are not.]

It should be added that Ashtekar has extended the apparent horizon concept to his Isolated/ Dynamical Horizon formalism [8], [9], [10]. Isolated horizons (IHs) mostly found their use in black hole entropy calculations in Loop Quantum Gravity ([11], [12]). They are null 3-dimensional surfaces that are defined as the boundary of black holes in complete isolation at a given time in a spacetime manifold  $\mathcal{M}$  with metric  $g_{\mu\nu}$ . More specifically, a given 3-surface  $H$  is an isolated horizon if: (1) It is null and topologically  $S^2 \times \mathbb{R}$ , (2) Any null vector field  $\ell^\mu$  normal to  $H$  will have a vanishing expansion on  $H$  i.e.

$$\Theta_{(\ell)} \equiv h^{\mu\nu} \nabla_\mu \ell_\nu = 0 \tag{1.4}$$

where  $h_{\mu\nu}$  is a degenerate 3-dimensional metric of signature  $(0,+,+)$  on  $H$  (degenerate because  $H$  is null) and  $\nabla_\mu$  is the covariant derivative compatible with spacetime metric  $g_{\mu\nu}$ . Technically, there are a few more requirements in order for  $H$  to be an isolated horizon, however, they are not relevant here. The reader is encouraged to read more about this subject in [9] or [10]. Although the locations of the IHs and EHs coincide in stationary and static spacetimes, one should keep in mind that an IH is defined locally and will usually be a subset of the EH of a given spacetime. To see this, consider, for example, the case of dust falling onto a black hole for some time interval  $t_1 < t < t_2$ . In this case, the black hole will have 2 separate isolated horizons of differing sizes (one before  $t_1$  and another after  $t_2$ ). However, only the second IH will coincide with the event horizon.

A Dynamical Horizon (DH), on the other hand, is a spacelike black hole boundary whose structure accommodates dynamical processes such as gas accretion or merger events involving a black hole. A nice feature of the use of DHs as black hole boundaries is the recent success of Ashtekar and collaborators in deriving the laws of black hole mechanics for Dynamical horizons [9]. A dynamical horizon is defined as follows: First, one takes a 3-dimensional spacelike, smooth surface  $H$  foliated by 2-surfaces  $S_i$  such that on each leaf  $S_i$  one has a transverse congruence of null outgoing geodesics  $\ell^\mu$  and null ingoing geodesics  $n^\mu$  (labeled as before). Then, one looks at the expansion of those geodesics on the leaf  $S_i$ ; a dynamical horizon exists if  $\Theta_{(\ell)} = 0$  and  $\Theta_{(n)} < 0$  on  $S_i$ . These 2-dimensional cross-sections,  $S_i$ , are topologically equivalent to

2-spheres ( $S^2$ ) but technically are not apparent horizons despite the fact that DHs are, by definition, the outermost marginally trapped surfaces. This is because the strict definition of an apparent horizon requires a Cauchy slicing of spacetime meaning that it is tied too rigidly to the choice of spacelike 3-surfaces. Despite this restriction, we feel compelled to state that such caveats are more relevant to mathematicians and less important for numerical simulations.

Although the conditions imposed on the ingoing and outgoing expansions seem sufficient to identify a surface as the right black hole boundary, in [13], it is shown that certain vanishing scalar invariant spacetimes contain marginally trapped tubes (e.g. a dynamical horizon) but not any trapped surfaces or other signatures of black holes. Furthermore, Carter has found black hole solutions with a cosmological constant [14] where there is a second cosmological ‘apparent horizon’ satisfying the expansion conditions of Eqs.(1.2) that does not cloak a spacetime singularity beyond it. To rectify this, Hayward (in [15]) introduced a third condition for an MTS to be considered a black hole boundary. By looking at the Lie derivative of the outgoing expansion, Hayward classified a given surface as a *trapping horizon* if  $\mathcal{L}_n\Theta_{(\ell)} \neq 0$  (along with the  $\Theta_{(\ell)} = 0$  and  $\Theta_{(n)} \neq 0$  conditions from before). For  $\Theta_{(n)} < 0$ , the trapped surface is called *future*. Furthermore, if  $\mathcal{L}_n\Theta_{(\ell)} < 0$  the trapped surface is called *outer* while if  $\mathcal{L}_n\Theta_{(\ell)} > 0$  it is called *inner*. In stationary spacetimes, a black hole event horizon would be an example for a *future outer trapping horizon* (FOTH) whereas a black hole Cauchy horizon (as in the inner hori-

zon  $r_-$  of Reissner-Nordström and Kerr spacetimes) is a *future inner trapping horizon*.

Even with all the above descriptions for possible candidates for a black hole boundary, it is generally agreed in the relativity community that the outermost  $\Theta_{(\ell)} = 0$  cross-section of a 3-dimensional hypersurface is much more convenient to work with than either an event horizon or an apparent horizon as strictly defined in [2]. In fact, the classical definition of an apparent horizon is widely ignored in numerical relativity and other practical applications and instead one uses the term *apparent horizon* for the outermost  $\Theta_{(\ell)} = 0$  surface ([16]). This is the definition that we will adopt in this thesis along with the condition that  $\Theta_{(n)} < 0$ . Since we deal with stationary and static spacetimes such as Kerr and Schwarzschild here, the apparent and the event horizons will coincide. We therefore need not worry about all the intricacies mentioned above.

A final word of caution should be added here about one's preference to use apparent horizons instead of event horizons. There are several issues that crop up when one looks at apparent horizons in dynamical spacetimes. One such situation arises in binary black hole mergers where there could be up to three apparent horizons inside an event horizon at a given time [17], [18]. In a near merger situation, each black hole has its own AH with a third AH enveloping the entire binary system. And as this spacetime is far from settling down to a stationary state the third AH is inside the clairvoyant event horizon. Another common problem is the so-called 'horizon jumps' that can



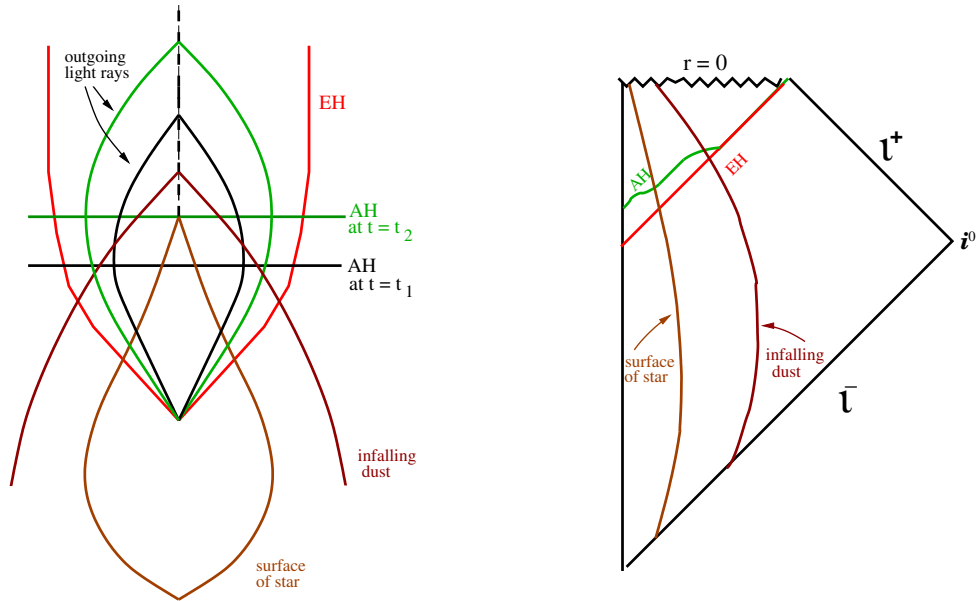


Figure 1.2: Finkelstein and Penrose diagrams for a spacetime containing a star collapsing to form a black hole and a shell of dust collapsing onto that black hole later. The green and black curves on the left represent outgoing light rays that become trapped inside the event horizon. The 2-dimensional apparent horizons are zero-expansion surfaces that intersect  $t = \text{constant}$  spacelike slices. Note that a surface that is marginally trapped at  $t = t_1, t_2$  becomes fully trapped later on. The green curve in the right diagram is the 3-dimensional world tube of 2-dimensional apparent horizons. Note that it starts from inside the event horizon at first and later becomes a spacelike surface during the infall of dust to finally coincide with the event horizon after all dynamical processes have settled down. Finally, the event horizon in the left diagram only becomes a zero-expansion surface as  $t \rightarrow \infty$ , which is consistent with its technical definition. Its expansion asymptotically goes to zero as  $t \rightarrow \infty$ .

occur in situations such as when a timelike dust shell falls onto a spherically symmetric black hole [16], [19], [20], [21], [17]. Once again the AH is inside the event horizon but instead of smoothly growing, the AH can suddenly jump to its final location. Or it can move outward at a rate faster than the speed of light. In this case, the three dimensional world tube of successive apparent horizons would make up a dynamical horizon (see Fig.1.2). Despite all these shortcomings, the ubiquitously accepted definition of apparent horizons will be used as the black hole boundary of choice for this thesis. And as mentioned before, since we will only be dealing with stationary spacetimes, we will not have to worry about the aforementioned complications.

We will proceed as follows: In Chapter 2 we will look at apparent horizons in Schwarzschild and Kerr spacetimes. This will be followed by the boosted black holes in Chapter 3 where we will also show the area invariance under boosts and accompany this with some numerical results. In Chapter 4, we will introduce several methods to visualize the distorted horizons in two or three spatial dimensions. Chapter 5 will deal with area invariance under spin-boost transformations and its implications. In Chapter 6, we will use black hole perturbation theory to investigate the multipole moments of a black hole distorted by a Lorentz boost. Finally, we will close with a summary of the work and an outlook on potential follow-ups. Throughout this thesis, we will use the natural or ‘God given units’ which set  $G = c = 1$ . As always,  $G = 6.67 \times 10^{-11} \text{ Nm}^2/\text{kg}^2$  is Newton’s gravitational constant and  $c = 3 \times 10^8 \text{ m/s}$  is the speed of light. We will normalize all dimensions in terms of the black hole

mass  $M$ . This will inevitably cause some confusion with units. Some useful conversion factors are

- Length:  $M \rightarrow GM/c^2$  e.g.  $1M = 1.5(M/M_\odot)$  km.
- Time:  $M \rightarrow GM/c^3$  e.g.  $1M = 5 \times 10^{-6}(M/M_\odot)$  sec.
- Angular Momentum:  $M^2 \rightarrow GM^2/c$  e.g.  $M^2 = 3 \times 10^{41}(M/M_\odot)^2 \text{kg m}^2/\text{sec}$ .

Our conventions for the index notation will be the usual choices. The Greek letters  $\alpha, \beta, \dots, \mu, \nu$  will denote the spacetime indices, e.g.  $\mu = 0, 1, 2$  or  $3$ . The Roman letters  $i, j$  etc. will denote the spatial indices, e.g.  $i = 1, 2$  or  $3$ .

## Chapter 2

### Apparent Horizons

Although we have already stated that in stationary spacetimes the apparent horizon coincides with the event horizon, it is nevertheless instructive to make use of the definition of the apparent horizon provided above to determine its location. Here, we do this for both Schwarzschild and Kerr spacetimes.

#### 2.1 Apparent Horizon in Schwarzschild Spacetime

First discovered by Karl Schwarzschild while in the trenches of the Russian front in 1915, the Schwarzschild metric describes the unique (by Birkhoff's theorem [29]) spherically symmetric solution to Einstein's equations in vacuum. In spherical coordinates  $(r, \theta, \phi)$  the metric is

$$\begin{aligned} ds^2 &\equiv g_{\mu\nu} dx^\mu dx^\nu \\ &= -\left(1 - \frac{2M}{r}\right) dt^2 + \left(1 - \frac{2M}{r}\right)^{-1} dr^2 + r^2(d\theta^2 + \sin^2\theta d\phi^2). \end{aligned} \tag{2.1}$$

Here,  $M$  is the mass of the black hole and the event horizon is located at  $r = 2M$ . It is a 3-dimensional null surface in the static Schwarzschild spacetime

and its 2-dimensional cross-sections in time are spheres of radius  $2M$ . These spheres are the apparent horizons, which here correspond to the  $t = \text{constant}$  cuts of the event horizon. Let us see if we can apply the formalism of outgoing and ingoing expansions of chapter 1 to obtain the same location for the apparent horizons.

Since the spacetime is spherically symmetric, the apparent horizon should be a surface of  $t = \text{constant}$ ,  $r = \text{constant}$ . Therefore, we need to determine the radially ingoing and outgoing null geodesics of the Schwarzschild spacetime. We denote these geodesics by  $n^\mu$  and  $\ell^\mu$  as before. In the coordinate basis, they are given to be

$$\ell^\mu = \left( \left(1 - \frac{2M}{r}\right)^{-1}, 1, 0, 0 \right), \quad (2.2)$$

$$n^\mu = \frac{1}{2} \left( 1, - \left(1 - \frac{2M}{r}\right), 0, 0 \right). \quad (2.3)$$

Using the metric of Eq.(2.1) one can easily verify that  $\ell^\mu$  and  $n^\mu$  are null, that is  $\ell^2 = n^2 = 0$ . The normalization factor in front of the vectors is chosen such that  $\ell \cdot n \equiv g_{\mu\nu} \ell^\mu n^\nu = -1$ . This is not a necessary condition and is a choice made by convention because it gives a simpler form for the 2-metric  $q_{\mu\nu}$  (c.f Eq.(1.3)) of the  $t = \text{constant}$ ,  $r = \text{constant}$  2-surfaces. The 2-metric is the pullback of the spacetime metric  $g_{\mu\nu}$  onto spheres of constant radius at a given instant of time. More specifically, the 2-metric equals

$$q_{\mu\nu} = g_{\mu\nu} + \ell_\mu n_\nu + n_\mu \ell_\nu. \quad (2.4)$$

Comparing this with Eq.(1.3), we immediately see the convenience of the choice for the normalization of  $\ell^\mu$  with respect to  $n^\mu$ .

Recall that the expansion of any vector field (or flow in spacetime) is the projection of the divergence of that field onto the 2-surface to which it is orthogonal. This gives

$$\begin{aligned}\Theta_{(\ell)} &= q^\mu_\nu \nabla_\mu \ell^\nu \\ &= (g^\mu_\nu + \ell^\mu n_\nu + n^\mu \ell_\nu) \nabla_\mu \ell^\nu \\ &= \nabla_\mu \ell^\mu + n_\nu \ell^\mu \nabla_\mu \ell^\nu + n^\mu \ell_\nu \nabla_\mu \ell^\nu\end{aligned}\tag{2.5}$$

$$= \frac{1}{\sqrt{-g}} \partial_\mu (\sqrt{-g} \ell^\mu) - \kappa.\tag{2.6}$$

In the last line above, we made use of several well known identities in General Relativity (GR). The first term in Eq.(2.6) is the standard identity for the 4-divergence of any vector field (cf. [30], [6] or any other standard GR text), the second term was obtained using the geodesic equation

$$\ell^\nu \nabla_\nu \ell^\mu = \kappa \ell^\mu\tag{2.7}$$

in its more general non-affinely parametrized form.  $\kappa = 0$  only for an affinely parametrized geodesic. We also used  $n_\mu \ell^\mu = -1$  in the second term. Finally, the third term in Eq.(2.5) disappears because it equals  $1/2 n^\mu \nabla_\mu (\ell^2)$  which, by definition, is zero because  $\ell^2 = 0$ . A quick computation yields  $\kappa = 0$  for

the null geodesic given in Eq.(2.2). Thus, for the expansion we are left with

$$\Theta_{(\ell)} = \frac{1}{\sqrt{-g}} \partial_{\mu} (\sqrt{-g} \ell^{\mu}) = \frac{2}{r}. \quad (2.8)$$

If we are to follow our prescription for locating the apparent horizon, we must solve  $\Theta_{(\ell)} = 0$  for  $r$  next. Solving Eq.(2.8) yields  $r = \infty$  for the location of the apparent horizon! With such a meaningless result, one is compelled to ask what went wrong here. The problem is with the form of  $\ell^{\mu}$  in Eq.(2.2). As it is written in that equation,  $\ell^{\mu}$  has a component that blows up at  $r = 2M$ . What we need to do is rewrite  $\ell^{\mu}$  in a non-singular form by rescaling it

$$\ell^{\mu} = \left( 1, \left( 1 - \frac{2M}{r} \right), 0, 0 \right). \quad (2.9)$$

$n^{\mu}$  would also be rescaled accordingly. Once again, it is easily verified that this is a null vector and a geodesic of the spacetime. However, this new version of  $\ell^{\mu}$  is no longer an affine geodesic; as such it will give  $\kappa \neq 0$  in the geodesic equation. We explicitly mention these caveats and display the details of the algebra as this problem will crop up again when we look at spinning black holes. Computing the expansion once again, we get

$$\begin{aligned} \Theta_{(\ell)} &= \frac{1}{\sqrt{-g}} \partial_{\mu} (\sqrt{-g} \ell^{\mu}) - \kappa \\ &= \frac{2}{r} - \frac{2M}{r^2} - \frac{2M}{r^2} \\ &= \frac{2}{r} \left( 1 - \frac{2M}{r} \right). \end{aligned} \quad (2.10)$$

This expression for the expansion of  $\ell^{\mu}$  gives us the desired result, namely

$\Theta_{(\ell)} = 0$  at  $r = 2M$ , that is, the apparent horizon is located at  $r = 2M$ . To make sure that this is a trapped surface, we also compute  $\Theta_{(n)}$ . Using the rescaled version of  $n^\mu$  given by

$$n^\mu = \frac{1}{2} \left( \left( 1 - \frac{2M}{r} \right)^{-1}, -1, 0, 0 \right), \quad (2.11)$$

we get

$$\Theta_{(n)} = -\frac{1}{r} < 0. \quad (2.12)$$

This is negative for all values of  $r$ . With the conditions  $\Theta_{(\ell)} = 0$  and  $\Theta_{(n)} < 0$  satisfied, we have that the 2-surfaces  $r = 2M$  of the Schwarzschild spacetime are apparent horizons. Of course, one could have drawn this conclusion a priori since one knows that in Schwarzschild spacetime, the event horizon is located at  $r = 2M$  and since the spacetime is static, the apparent horizons simply are  $t = \text{constant}$  cuts of the event horizon.

Let us digress here for a little and present a case where apparent horizon can actually be a spacelike surface located inside the event horizon of a black hole. In order for this to happen, the spacetime must be dynamical. The example of null dust collapsing onto a black hole will suffice as a nice illustration. This collapse problem was first investigated by Vaidya in [22]. Let us begin with the Schwarzschild metric written in outgoing Eddington-Finkelstein coordinates (First devised by Eddington in [23] then rediscovered by Finkelstein in [24])

$$ds^2 = - \left( 1 - \frac{2M(v)}{r} \right) dv^2 + 2 dvdr + r^2 (d\theta^2 + \sin^2 \theta d\phi^2). \quad (2.13)$$



Here,  $v$  is the null outgoing ‘time’ coordinate defined as follows

$$v \equiv t + \int \left(1 - \frac{2M(v)}{r}\right)^{-1} dr. \quad (2.14)$$

The black hole mass increases due to the infalling null dust, thus the black hole mass is now a function of  $v$  i.e.  $M \rightarrow M(v)$  with  $dM/dv > 0$ . Let the dust fall in during a null time interval  $v_1 < v < v_2$ . So, for the mass of the black hole we can write

$$M(v) = \begin{cases} M_1 & \text{for } v < v_1 \\ M_{12}(v) = M_1 + \delta m(v) & \text{for } v_1 < v < v_2 \\ M_2 = M_1 + \delta M & \text{for } v > v_2 \end{cases}$$

Above  $\delta m(v)$  is an arbitrary function that represents the mass of the infalling dust, which starts from zero mass at  $v = v_1$  and reaches  $\delta M$  at  $v = v_2$ . Before  $v_1$  and after  $v_2$  the spacetime is static, therefore the apparent horizon is null and located at  $r = 2M_1$  and  $r = 2(M_1 + \delta M) = 2M_2$ , respectively. However, for  $v_1 < v < v_2$ , the apparent horizon is a spacelike surface. One sees this by determining the norm of the vector field tangent to the apparent horizon’s 3-dimensional world tube. Looking at the expansion of the null outgoing geodesics, one has

$$\Theta_{(\ell)} \propto r - 2M(v). \quad (2.15)$$

Then, the location of the apparent horizon can be written as a constraint

$$\Phi = r - 2M(v) = 0. \quad (2.16)$$

Thinking of  $\Phi$  as a potential, we look at its gradient

$$\Phi_{,\mu} = \left( -\frac{dM}{dv}, 1, 0, 0 \right). \quad (2.17)$$

$\Phi_{,\mu}$  is a one-form dual to the vector  $V^\mu \equiv g^{\mu\nu}\Phi_{,\nu}$ . The vector field  $V^\mu$  is orthogonal to the apparent horizon. This is analogous to what happens in electrostatics with electric potentials that can be thought of as level surfaces and electric fields which are the gradients of those potentials and orthogonal to the level surfaces. However, in keeping with this analogy, one must keep in mind that in 3-dimensional Euclidean space, there is no distinction between vectors and one-forms. This exceptional property of vectors and one-forms only holds in 3-dimensions. Coming back to General Relativity in 4-dimensional spacetime, we see that at  $r = 2M(v)$ , the norm-squared of this one-form is

$$\begin{aligned} g^{\mu\nu}\Phi_{,\mu}\Phi_{,\nu} &= 2\Phi_{,v}\Phi_{,r} + \Phi_{,r}^2 \left( 1 - \frac{2M}{r} \right)_{r=2M(v)} \\ &= -4\frac{dM}{dv}. \end{aligned} \quad (2.18)$$

Since  $dM/dv > 0$ ,  $\Phi_{,\mu}$  has a negative norm i.e. it is timelike and since  $\Phi_{,\mu}$  is normal to the horizon, the horizon itself must be spacelike. So, we see that during  $v_1 < v < v_2$ , the apparent horizon becomes spacelike and outside that time interval it is null. On the other hand, being *teleological* in nature, the event horizon is located at  $r = 2M(v_2) = 2(M + \delta M) = 2M_2$  for the entire history of the spacetime. The apparent horizon coincides with the event horizon only for  $v \geq v_2$ . This situation is illustrated in figure 1.2.

In this section, we saw that in Schwarzschild spacetime (spherically symmetric and static), the apparent horizon is located at  $r = 2M$ . Even in the dynamical yet spherically symmetric case of the Vaidya spacetime (null dust collapsing onto a preexisting Schwarzschild black hole), the apparent horizon is still at  $r = 2M(v)$ . In that example, the mass of the black hole is a function of the null time coordinate  $v$ , hence the use of  $M(v)$ . In both cases, the apparent horizon is the outermost marginally trapped surface satisfying the conditions  $\Theta_{(\ell)} = 0$  and  $\Theta_{(n)} < 0$ .

## 2.2 Apparent Horizons in Kerr Spacetime

Although the spherically symmetric black hole solutions (Schwarzschild, Reissner-Nordström [25], [26]) were quickly discovered soon after Einstein revealed his theory in 1915; the axially symmetric, spinning black hole solution remained elusive for almost a half century. Finally in 1963, Roy Kerr presented the correct description of a rotating black hole in [27]. This was a very crucial discovery as it is generally believed that the end-product of the collapse of a rotating star is a rotating black hole which carries angular momentum because of conservation of angular momentum. This means that all *astrophysical* black holes are Kerr black holes with the exception of a few that might form in a binary where exact angular momentum cancellation occurs (a very improbable but not impossible situation, see [28]). We have now reached a point where strong astrophysical evidence supports the existence of these spinning black holes ([31], [32],[33]) and manipulating this spacetime has become a frequent

task in computational astrophysics. The angular momentum of the spinning black hole automatically selects a preferred direction, the spin axis, and the Kerr hole is axially symmetric around this direction.

We begin with the Kerr metric in the standard Boyer-Lindquist (BL) coordinates. The metric components are

$$g_{tt} = -\left(1 - \frac{2Mr}{\rho^2}\right), \quad (2.19)$$

$$g_{t\phi} = g_{\phi t} = -\frac{2Mar \sin^2 \theta}{\rho^2}, \quad (2.20)$$

$$g_{rr} = \frac{\rho^2}{\Delta}, \quad g_{\theta\theta} = \rho^2, \quad (2.21)$$

$$g_{\phi\phi} = \frac{\Sigma}{\rho^2} \sin^2 \theta \quad (2.22)$$

$$(2.23)$$

where  $\rho^2 = r^2 + a^2 \cos^2 \theta$ ,  $\Delta = r^2 - 2Mr + a^2$  and  $\Sigma = (r^2 + a^2)^2 - a^2 \Delta \sin^2 \theta$ . Here,  $M$  is once again the mass of the black hole,  $a$  is called the spin parameter and is defined as  $a \equiv J/M$  where  $J$  is the angular momentum of the rotating black hole in units of mass<sup>2</sup>. The event horizon is located at  $r_{EH} \equiv r_+ = M + \sqrt{M^2 - a^2}$ , which satisfies  $\Delta(r = r_+) = 0$ . The Kerr metric is an example of a stationary spacetime in which a time reversal transformation ( $t \rightarrow -t$ ) changes the rotation direction of the black hole and the sign of  $g_{t\phi} dt d\phi$  term in the metric. This is what separates stationary spacetimes from static ones despite the fact that both spacetimes are time independent.

As with the Schwarzschild spacetime, we are once again interested in

locating the apparent horizon. Therefore, we must look at the expansion of the outgoing and ingoing null geodesics of the Kerr spacetime. Using the same notation as in section 2.1, we have the following null, radially outgoing geodesic:

$$\ell^\mu = \left( \frac{r^2 + a^2}{\Delta}, 1, 0, \frac{a}{\Delta} \right) \quad (2.24)$$

Assuming we have a good choice for  $\ell^\mu$ , we can compute its expansion  $\Theta_{(\ell)}$  to determine where it equals zero. That value marks the location of the outermost trapped surface, namely, the apparent horizon. One can straightforwardly confirm that this is an affinely parametrized geodesic, which gives  $\kappa = 0$  in the geodesic equation. This leaves  $\Theta_{(\ell)} = \frac{1}{\sqrt{-g}}(\sqrt{-g} \ell^r)_{,r}$  in Eq.(2.6), which in the case of the  $\ell^\mu$  of Eq.(2.24) gives

$$\begin{aligned} \Theta_{(\ell)} &= \partial_r (\ln \sqrt{-g}) = \frac{2r}{r^2 + a^2 \cos^2 \theta} \\ &= \frac{2r}{\rho^2}. \end{aligned} \quad (2.25)$$

Just like in section 2.1, we ended up with an equation that gives  $r = \infty$  for the location of AH. As before, this incorrect solution to  $\Theta_{(\ell)} = 0$  is the result of a poor choice of components for the null outgoing normal  $\ell^\mu$ , some of which are singular at the horizon i.e.  $\ell^t$  and  $\ell^\phi$  blow up at  $r = r_+$  since by definition  $\Delta(r = r_+) = 0$ . So, although it is affinely parametrized, our initial choice for  $\ell^\mu$  is not well suited for calculating the expansion. We fix this problem by simply multiplying the vector field above by  $\Delta$  (rescaling) and using that for our null normal. Once again,  $n^\mu$  will be rescaled accordingly to keep  $\ell \cdot n = -1$ .

The new outgoing null normal is given by

$$\ell^\mu = ((r^2 + a^2), \Delta, 0, a). \quad (2.26)$$

Obviously, written in this form,  $\ell^\mu$  is no longer an affinely parametrized geodesic. Evaluating the expression in Eq.(2.6) with the new components for  $\ell^\mu$  results in

$$\begin{aligned} \Theta_{(\ell)} &= \frac{1}{\sqrt{-g}}(\sqrt{-g} \Delta)_{,r} - \kappa & (2.27) \\ &= 2 \frac{a^2 r \cos^2 \theta - a^2 M \cos^2 \theta + a^2 r + 2r^3 - 3Mr^2}{r^2 + a^2 \cos^2 \theta} - 2(r - M) \\ &= 2r \frac{r^2 - 2Mr + a^2}{r^2 + a^2 \cos^2 \theta} \\ &= 2r \frac{\Delta}{\rho^2} & (2.28) \end{aligned}$$

where  $\Delta$  and  $\rho$  are defined immediately below Eq.(2.23). As we can see from the equation above, the apparent horizon is located at  $\Delta = 0$ , which gives us the anticipated  $r_{AH} = r_+ = M + \sqrt{M^2 - a^2}$ .

We can also reach the very same result using a nonsingular coordinate system from the start. In an analogous way to Eddington-Finkelstein coordinates for the Schwarzschild metric, we transform from the Boyer-Lindquist basis  $(t, r, \theta, \phi)$  to ingoing Kerr coordinates  $(u, r, \theta, \chi)$  via

$$\begin{aligned} u &= t - \hat{r} \\ \chi &= \phi - \tilde{r} \end{aligned} \quad (2.29)$$

where

$$\frac{d\hat{r}}{dr} = \frac{r^2 + a^2}{\Delta} \quad \text{and} \quad \frac{d\tilde{r}}{dr} = \frac{a}{\Delta}. \quad (2.30)$$

In these ingoing coordinates the metric becomes

$$ds^2 = - \left(1 - \frac{2Mr}{\rho^2}\right) - 2du dr + 2a \sin^2 \theta dr d\chi \\ - \frac{4Mar \sin^2 \theta}{\rho^2} dud\chi + \rho^2 d\theta^2 + \frac{\Sigma}{\rho^2} \sin^2 \theta d\chi^2 \quad (2.31)$$

Next, we set out to calculate the expansion of  $\ell^\mu$  once again. Because Eq.(2.27) is a scalar equation, it is invariant under coordinate transformations and it still applies. Furthermore, it turns out that the  $r$ -component of  $\ell^\mu$  remains the same because the coordinate transformation only shifts the  $t$  and the  $\phi$  coordinates. Therefore, the divergence term in the expansion (Eq.(2.27)) yields exactly the same answer as before. The non-affinity parameter  $\kappa$  also is calculated to be identical to the above expression. So, we end up with  $r_{AH} = r_+$  once again. We have omitted the details of the algebra here as it is hardly any more enlightening. The more rigorous reader can convince him/herself of this result. It is useful to keep in mind that the second coordinate system (ingoing Kerr) we use here actually is a spheroidal version of the Kerr-Schild coordinates, which we introduce in chapter 3. As a last note, we should add that using outgoing Eddington-Finkelstein coordinates still results in the same expression for the expansion as one should expect.

We must also compute  $\Theta_{(n)}$  to make sure that it is negative on and

inside the horizon. The ingoing null normal is given by

$$n^\mu = \left( \frac{r^2 + a^2}{2\rho^2}, -\frac{\Delta}{2\rho^2}, 0, \frac{a}{2\rho^2} \right). \quad (2.32)$$

Next, we calculate the expansion of the rescaled version of Eq.(2.32).  $n^\mu$  must be rescaled by a factor of  $\Delta^{-1}$  so as to still yield  $\ell \cdot n = -1$ . For the expansion, we are left with

$$\Theta_{(n)} = -\frac{r}{\rho^2(r^2 + a^2)}. \quad (2.33)$$

This result for the ingoing expansion is negative everywhere as it was in the Schwarzschild case. Note that the outgoing expansion  $\Theta_{(\ell)}$  is proportional to  $\Delta$  as can be seen from Eq.(2.28).  $\Delta$  is a quadratic function in  $r$  which can be written as  $\Delta = (r - r_+)(r - r_-)$  where  $r_\pm = M \pm \sqrt{M^2 - a^2}$  are the roots of  $\Delta = 0$ . These roots physically correspond to the inner ( $r_-$ ) and outer ( $r_+$ ) Kerr horizons. Clearly,  $\Delta < 0$  only for  $r_- < r < r_+$ , which tells us that the spheroidal 2-surfaces to which  $\ell^\mu$  and  $n^\mu$  are normal are only trapped for  $r_- < r < r_+$ .  $\Theta_{(\ell)} > 0$  outside the interval  $r \in [r_-, r_+]$  so there are no trapped surfaces inside  $r_-$  and outside  $r_+$ . The fact that there are no trapped surfaces inside  $r_-$  is a somewhat surprising but well known result in General Relativity and it explained in detail in the standard textbooks of Wald [6]; Misner, Thorne and Wheeler (MTW) [30]; and Hawking & Ellis [2].

The results obtained from Eqs.(2.28), (2.33) indicate that the surface  $r = r_+$  in Kerr spacetime has zero outgoing expansion ( $\Theta_{(\ell)} = 0$ ) and negative ingoing expansion ( $\Theta_{(n)} < 0$ ). It is therefore the outermost trapped surface



and thus the apparent horizon in the Kerr spacetime. This was the expected result since the Kerr solution is a stationary spacetime and therefore has the event and the apparent horizons coinciding at  $r = r_+$ . Now that we have explicitly located the apparent horizon in Schwarzschild and Kerr spacetimes, let us move on to the case of boosted black holes.

## Chapter 3

### Boosted Apparent Horizons

In this chapter we consider only Schwarzschild and Kerr spacetimes in Kerr-Schild (KS) coordinates as given in Eq.(3.1) below. This form of the metric contains a “natural” Minkowski background, and hence a natural definition of a Lorentz boost [34]. It is found (cf. [35], [36], [37]) that the apparent horizon of a black hole will appear distorted in these coordinates when boosted; the longitudinal coordinate direction undergoes a Lorentz contraction. However, this is an effect only in coordinates; the point of this chapter is an explicit calculation to show that the area of the apparent horizon 2-surface, recomputed in the spatial frame of the boosted observer, remains unchanged, that is:  $Area = 4\pi (r_+^2 + a^2)$  for the Kerr case and  $Area = 16\pi M^2$  for the Schwarzschild black hole. This result is of course necessary on general principles.

The invariance of the area depends on the observation that the event horizon of a stationary black hole is a null 3-dimensional submanifold of the spacetime with vanishing expansion. And null surfaces naturally remain null under Lorentz transformations. In fact, the area of any 2-dimensional cross section of the horizon remains invariant under any redefinition of the 3-space

$t = \text{constant}$  (that is legitimately spacelike). Two cross-sections of the event horizon that differ by a redefinition of  $t = \text{constant}$  slice can be put in a point-wise 1-to-1 correspondence along the null generators of the horizon. These null offsets do not contribute to the area which is transverse to the null generators. This situation is schematically illustrated in Fig.3.1. The ‘unboosted’ horizon is on the left and is depicted as two parallel vertical lines in the figure. One computes the 2-dimensional area of the apparent horizon by taking a  $t = \text{constant}$  *cut* of the 3-dimensional event horizon (one angular dimension is suppressed in the figure). When the black hole is boosted, the event horizon still remains null, thus it is still represented by vertical lines in the figure. However, in the boosted frame,  $t = \text{constant}$  slices become tilted so they now give distorted cross-sections for the boosted apparent horizon. But as we will see below, these null contributions do not change the area of the apparent horizon.

We give a quick derivation of the Schwarzschild case then present the most general calculation for the astrophysically realistic spacetimes, namely, the Kerr black hole boosted along an arbitrary direction.

### 3.1 Boosted Schwarzschild Black Holes

The special case of the nonspinning Schwarzschild (i.e. spherical) black hole provides an illuminating guide to the features of the full Kerr case. Because the spacetime is spherically symmetric, a boost of the Schwarzschild metric in an arbitrary direction can always be rotated so that it points along

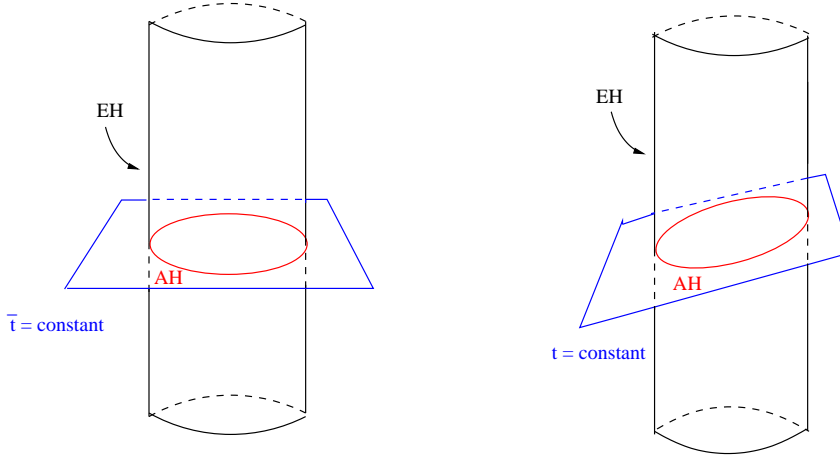


Figure 3.1: The cylinders represent the 3-dimensional event horizons whose 2-dimensional  $t = \text{constant}$  cross-sections are the apparent horizons (AHs). The AH on the left is unboosted and the one on the right is boosted. As can be seen from the figure, the boost simply tilts the  $t = \text{constant}$  cuts of the cylinder. One dimension has been suppressed for convenience. Each circle is topologically equivalent to a 2-sphere

the  $z$ -direction. Although this does not make a difference for the Schwarzschild case, when we deal with the boost of the Kerr black hole, working out the case with the  $z$ -boost first is helpful because it retains the axisymmetry of the Kerr metric and thus is simpler.

The Kerr-Newman vacuum solution to Einstein's equation can be written in a special form called the Kerr-Schild form of the metric. This form is, in general ([30], [38], [39], [40]),

$$g_{\mu\nu} = \eta_{\mu\nu} + 2Hl_{\mu}l_{\nu} \quad (3.1)$$

where  $H$  is a function of spacetime coordinates,  $\eta_{\mu\nu}$  is the Minkowski metric of

flat spacetime and  $l^\mu$  is a null vector with respect to both  $g_{\mu\nu}$  and  $\eta_{\mu\nu}$ . Clearly, this is a special form, and the metric of a general spacetime cannot be put in this form. But the Kerr vacuum black hole can be so written. Under a Lorentz boost (a coordinate transformation with the form of a Lorentz transformation on the  $t, x, y, z$  coordinates describing the flat space with metric  $\eta_{\mu\nu}dx^\mu dx^\nu$ ), the Kerr-Schild metric will preserve the general form that it has in Eq.(3.1). We will denote the coordinates in the unboosted frame by placing bars over them. Unbarred coordinates refer to those in the boosted frame.

Let us now turn to the business of actually boosting the Schwarzschild metric. Eq.(3.1) for this case is

$$g_{\mu\nu}d\bar{x}^\mu d\bar{x}^\nu = -d\bar{t}^2 + d\bar{x}^2 + d\bar{y}^2 + d\bar{z}^2 + \frac{2M}{\bar{r}} (d\bar{t} + d\bar{x} + d\bar{y} + d\bar{z})^2 \quad (3.2)$$

which, in cylindrical coordinates  $(\bar{r}_\parallel, \bar{r}_\perp, \bar{\phi}_{cyl})$  can be written as

$$g_{\mu\nu}d\bar{x}^\mu d\bar{x}^\nu = -d\bar{t}^2 + d\bar{r}_\parallel^2 + d\bar{x}_\perp^2 + d\bar{y}_\perp^2 + \frac{2M}{\bar{r}} \left( d\bar{t} + \frac{\bar{r}_\parallel}{\bar{r}} d\bar{r}_\parallel + \frac{\bar{x}_\perp}{\bar{r}} d\bar{x}_\perp + \frac{\bar{y}_\perp}{\bar{r}} d\bar{y}_\perp \right)^2 \quad (3.3)$$

where  $\bar{x}_\perp = \bar{r}_\perp \cos \bar{\phi}_{cyl}$  and  $\bar{y}_\perp = \bar{r}_\perp \sin \bar{\phi}_{cyl}$ . The coordinate system  $(\bar{r}_\parallel, \bar{r}_\perp, \bar{\phi}_{cyl})$  aligns  $\bar{r}_\parallel$  with the axis of the cylinder parallel to the boost direction  $\vec{\beta}$ ;  $\bar{r}_\perp, \bar{\phi}_{cyl}$  are the polar coordinates of the circular plane orthogonal to the axis of the cylinder (see Fig.(3.4)). Note that  $\bar{x}^2 + \bar{y}^2 + \bar{z}^2 = \bar{r}_\parallel^2 + \bar{r}_\perp^2$ .

The boosted (unbarred) coordinates are related to the unboosted frame

by

$$\begin{aligned}
\bar{t} &= \gamma(t - \beta r_{\parallel}) \\
\bar{r}_{\parallel} &= \gamma(r_{\parallel} - \beta t) \\
\bar{r}_{\perp} &= r_{\perp}, \quad \bar{\phi}_{cyl} = \phi_{cyl}.
\end{aligned} \tag{3.4}$$

The boost parameters are the usual dimensionless speed  $\beta \equiv v/c$ , and the ‘gamma factor’  $\gamma = (1 - \beta^2)^{-1/2}$ ; both are defined as usual in the background Minkowski spacetime. The apparent horizon is defined in a given 3-space ( $t = \text{constant}$ ) and the horizon area will be independent of  $t$ , so without loss of generality we take  $t = 0$ . The  $t = 0$  (boosted) 3-metric is

$$ds^2|_{t=0} = dr_{\parallel}^2 + d\bar{x}_{\perp}^2 + d\bar{y}_{\perp}^2 + \frac{2M}{\bar{r}^3} (-\bar{r}\gamma\beta dr_{\parallel} + \bar{r}_{\parallel}d\bar{r}_{\parallel} + \bar{x}_{\perp}d\bar{x}_{\perp} + \bar{y}_{\perp}d\bar{y}_{\perp})^2. \tag{3.5}$$

We have strategically kept some terms expressed using unboosted (barred) forms. They can be straightforwardly substituted using Eq.(3.4). In this form, however, we can easily restrict the metric to the horizon surface, since

$$\bar{r}d\bar{r} = \bar{r}_{\parallel}d\bar{r}_{\parallel} + \bar{x}_{\perp}d\bar{x}_{\perp} + \bar{y}_{\perp}d\bar{y}_{\perp} = 0 \tag{3.6}$$

on the horizon where  $\bar{r}$  is a constant ( $= 2M$ ). Thus on the horizon:

$$\begin{aligned}
ds^2|_{t=0, \bar{r}=2M} &= \left[ \gamma^{-2}d\bar{r}_{\parallel}^2 + d\bar{x}_{\perp}^2 + d\bar{y}_{\perp}^2 + \frac{2M}{\bar{r}}(\beta^2 d\bar{r}_{\parallel}^2) \right]_{\bar{r}=2M} \\
&= (d\bar{r}_{\parallel}^2 + d\bar{x}_{\perp}^2 + d\bar{y}_{\perp}^2)|_{\bar{r}=2M}.
\end{aligned} \tag{3.7}$$

Above, we made use of  $d\bar{t} = -\gamma\beta dr_{\parallel}$  and  $d\bar{r}_{\parallel} = \gamma dr_{\parallel}$ . In Cartesian  $(\bar{x}, \bar{y}, \bar{z})$

coordinates this is

$$ds^2|_{t=0, \bar{r}=2M} = (d\bar{x}^2 + d\bar{y}^2 + d\bar{z}^2)|_{\bar{r}=2M} . \quad (3.8)$$

This can be put in a more familiar form using spherical coordinates  $(\bar{r}, \bar{\theta}, \bar{\phi})$  which now gives

$$ds^2|_{t=0, \bar{r}=2M} = (2M)^2 (d\bar{\theta}^2 + \sin^2 \bar{\theta} d\bar{\phi}^2) . \quad (3.9)$$

Thus the area of the horizon is  $4\pi(2M)^2$  as expected. Importantly, note that Eq.(3.7) describes the boosted apparent horizon; the simple form (Eq.(3.8)) that allows immediate evaluation of the surface area is the expression of this area in terms of coordinates appropriate first of all to the unboosted frame. On the horizon the contribution from the time transformation exactly cancels the Lorentz contraction of  $\bar{r}_\parallel$ .

In section 3.3, we will show the area invariance for a boosted Kerr black hole by performing a coordinate transformation to facilitate boosting the spacetime, followed by another coordinate transformation that simplifies the extraction of the 2-dimensional metric by restricting to the horizon. With the 2-dimensional metric we will straightforwardly compute the horizon area. But before we move on the Kerr case, we take a numerical digression and present results from computer simulations boosting Schwarzschild black holes toward (or away from) each other.

## 3.2 Numerical Results

Before looking at the horizon of a boosted spinning black hole, we demonstrate some numerical applications of these concepts, concentrating in this section on only nonspinning black holes. Recent breakthroughs in numerical relativity ([41], [42], [43], [44], [45], [46]) have enabled the community to investigate various physical scenarios involving interacting black holes. There are many different approaches to numerically evolving the physical system. The use of a particular structure, *puncture initial data* ([47]) has become ubiquitous for numerical codes. Puncture initial data are conformally flat. Solution of the constraint equations (elliptic equations describing a nonlinear generalization of Newtonian gravity) produces a mathematically correct configuration. But if boosted, the puncture is not physically relaxed, so when the solved (mathematically correct) data are evolved, the black hole emits short wavelength gravitational radiation. Some of this spurious radiation propagates out to infinity and some falls onto the black hole, increasing the horizon mass.

One can instead use *superposed Kerr-Schild* ([48]) initial data. This takes the Kerr-Schild metric for a single black hole and creates a background metric for two black holes by adding a second ‘mass term’ to the flat background:

$$g_{\mu\nu} = \eta_{\mu\nu} + H_1 l_{\mu}^{(1)} l_{\nu}^{(1)} + H_2 l_{\mu}^{(2)} l_{\nu}^{(2)}. \quad (3.10)$$

Here  $H_1, H_2$  are scalar functions that depend on coordinates from the centers of each black hole as well as the black holes’ masses and spins. They are identical



in form to single black hole terms centered at the locations of the two holes (cf. Eq. (3.11) below; there is also a prescription for superposing the momentum associated with this combination, in the initial data). Although Kerr-Schild initial data exactly solve Einstein's equation for a single boosted black hole and thus satisfy the constraint equations, this is not the case for superposed Kerr-Schild, which is only an educated guess. However, by starting out with this initial guess as a conformal background metric (in the same sense that puncture data has a flat conformal background), one can solve the constraint equations, so Kerr-Schild data can be adjusted to become proper initial data. The solution of the elliptic initial data equations modifies the configuration to be an exact (modulo numerical error) description of a gravitational configuration. In practice, unless the black holes are very close together, the correction for superposed Kerr-Schild data is small; less than one percent.

The code being developed at University of Texas Austin is called *openGR* [49]. Among the suite of programs comprising *openGR*, there is a finite element initial data code, which can produce either puncture or superposed Kerr-Schild initial data. The evolution code treats the dynamics of binary black hole systems and the extraction of gravitational waves from the merger of the black holes. The code is a fourth order accurate adaptive mesh refinement code with sixth order interpolation between coordinate patches. Our initial physical setup is very similar to those of [50] and [51], which also evolve the data. [50] solves conformally flat puncture data instead of our superposed Kerr-Schild data, and treats higher boosts than we consider. [51] describes the nonax-

isymmetric almost-head-on collision of two Schwarzschild black holes. Their initial data is an unsolved superposed version of Schwarzschild initial data in isotropic coordinates.

The total mass/energy of the spacetime is given by the ADM mass  $M_{ADM}$  ([60]) computed at spatial infinity (numerically, “near” the outer grid boundary). The ADM mass corresponds to the apparent Newtonian mass measured at large distances from the sources, measured for instance by observing the period of distant satellites around the central mass. Suppose the individual black hole masses are given by Kerr-Schild mass parameters  $m_1$  and  $m_2$ . Then the *background* gives an ADM mass  $M_{ADM\ bkgd} = m_1 + m_2$ . As noted, solving the constraint equation changes the superposed Kerr-Schild data slightly, so the solved ADM mass closely approximates  $M_{ADM} \approx m_1 + m_2$ , though it does have some dependence on the parameters of the data, particularly on the separation of the black holes.

Of interest in the design of data is the binding energy  $E_b$  of the configuration. We can compute this as the measured ADM mass minus the intrinsic mass of the constituent black holes. The difficulty lies in defining an *intrinsic* black hole mass. We choose the horizon mass. (For nonspinning black holes, we have  $M_H = (A_H/16\pi)^{1/2}$ , where  $A_H$  is the area of the apparent horizon; *openGR* includes an apparent horizon finder.) Classically the area of the horizon can increase, but we also know that the horizon area is an adiabatic invariant; it is only slightly affected by slow motions. “Slow” means slow compared to the normal frequencies of oscillation of the hole, which are

high frequency; the lowest frequency is on the order  $f \sim (20M_H)^{-1}$ , and most frequencies in binary evolution are lower than this frequency. Hence we are confident that the apparent horizon mass provides an (almost) constant intrinsic mass. Binding is indicated by  $E_b \equiv M_{ADM} - (M_{H1} + M_{H2}) < 0$ . If the data describe black holes in motion, then the kinetic energy also contributes (positively) to the total energy. For a boosted black hole the ADM mass acquires a factor  $\gamma$ :  $M_{ADM\ 0} \rightarrow \gamma M_{ADM\ 0}$  where  $M_{ADM\ 0}$  is  $m$ , the metric mass parameter in the single hole case. Thus we expect that for a given boost parameter  $\gamma$ , the binding energy may be negative (i.e. bound) if the holes are close together, but positive (unbound) if the data are set with the black holes far apart. Furthermore, for the nonlinear small separation limit (and/or for significant  $\gamma$ ) cases, Newtonian arguments become obscure because of the change in metric due to the presence of the second hole, and due to coordinate ambiguities.

We construct an equal mass binary black hole system (nonspinning Schwarzschild black holes) with initial coordinate separation  $r$ . The configuration is axisymmetric; the black holes are boosted toward or away from each other with Lorentz boost velocity  $\beta \equiv v/c$  (or instantaneously at rest with  $\beta = 0$ ); the boosts are equal but opposite in the computational frame. The axisymmetry allows extremely high resolution computational simulation. The code is a finite element code, with an adaptive resolution of  $1/100 M_{ADM}$  near the holes and  $1 M_{ADM}$  at the outer boundary. The computational domain is a sphere of radius  $256 M_{ADM}$ .

We plot the the negative of binding energy  $-E_b$  of the binary in figure 3.2. Here, we define the binding energy to be  $E_b \equiv M_{ADM} - 2M_H$ . Since the configuration is axisymmetric, the black holes have the same horizon mass  $M_H$ , hence the factor of 2. We display our results in units of the total parameter ADM mass which is normalized to equal 1 ( $M_{ADM}^{bgd} = m_1 + m_2 = 0.5 + 0.5 = 1$ ). In Fig. 3.2,  $r$  is the coordinate separation between the two black holes also given in units of  $M_{ADM}$  (e.g.  $r = 10$  translates to  $r = 10 GM_{ADM}/c^2$ ). The binding energy scales as  $1/r$  at the Newtonian limit; this Newtonian limit is plotted as a red straight line in Fig. 3.2. Bonning et al. [52] had analytically predicted this Newtonian limit (see that paper for details). Previous computational work by Hawley et al. [53] failed to show the Newtonian limit, because of insufficient domain size to eliminate outer boundary effects. We clearly see that for every rest configuration the binding energy for large separations agrees with the Newtonian prediction ([52]), but there is a deviation to stronger binding for closer coordinate separation. The cause for this will be discussed below as it related to the distortion of black holes' horizons near each other. One can in principle use expressions from post-Newtonian theory to give the next order correction to  $E_b$ . These terms scale as  $((\text{Mass})/r)^2$ .

It is of interest to understand *how* the binding energy is achieved in the initial data. Fig. 3.3 is a plot of  $M_{ADM}$  and horizon mass  $M_H$  versus  $1/r$  for boosts of  $\beta = 0, 0.1, 0.5$  represented by the red, green and black curves for  $M_H$ , respectively. For the  $M_{ADM}$  versus  $1/r$  plot, we use a blue solid line, red “ $\times$ ” marks and pink dashed line for  $\beta = 0, 0.1, 0.5$ , respectively. Note

the confirmation of the analytical expectation above that the ADM mass is essentially constant for the binary pair regardless of the coordinate distance between them. However, although we construct all data with the same parameter values  $m$ , we see different constant ADM masses for different  $|\beta|$  (motion with the same  $|\beta|$  together or apart yields the same ADM mass, constant across the possible separations). This is because the ADM mass scales as  $\gamma M_{ADM0}$  for a boosted black hole. Thus, for example, the ratio of ADM masses between the pink dashed line ( $\beta = 0.5$ ) and the blue line ( $\beta = 0$ ) in Fig. 3.3 should be  $(1 - 0.5^2)^{-1/2} = 1.154$ . This is easily seen in Fig. 3.3. We estimate the numerical error of about one percent in this quantity by looking at the ADM mass for the  $\beta = 0$  case (blue line) which, in principle, should give  $M_{ADM} = 1$  but actually is located slightly higher at  $M_{ADM} = 1.01$ . The most significant cause of this 1% discrepancy is the fact that we numerically computed the ADM mass right at the computational boundary as opposed to slightly inside it.

Though  $M_{ADM}$  stays almost constant for differing separation, the binding becomes stronger for smaller separation, even in the Newtonian limit, of course. As described in [52], when the parameter  $m$  is held constant for each hole, the *horizon* area of the constituent black holes increases with decreasing separation. The modification of the geometry by the *other* black hole modifies the horizon area so that it is no longer the  $16\pi m^2$  which would be computed for an isolated hole, but  $16\pi M_H^2$  with  $M_H > m$ . If we imagine the initial data constructed by adiabatically moving the holes from infinite separation, it

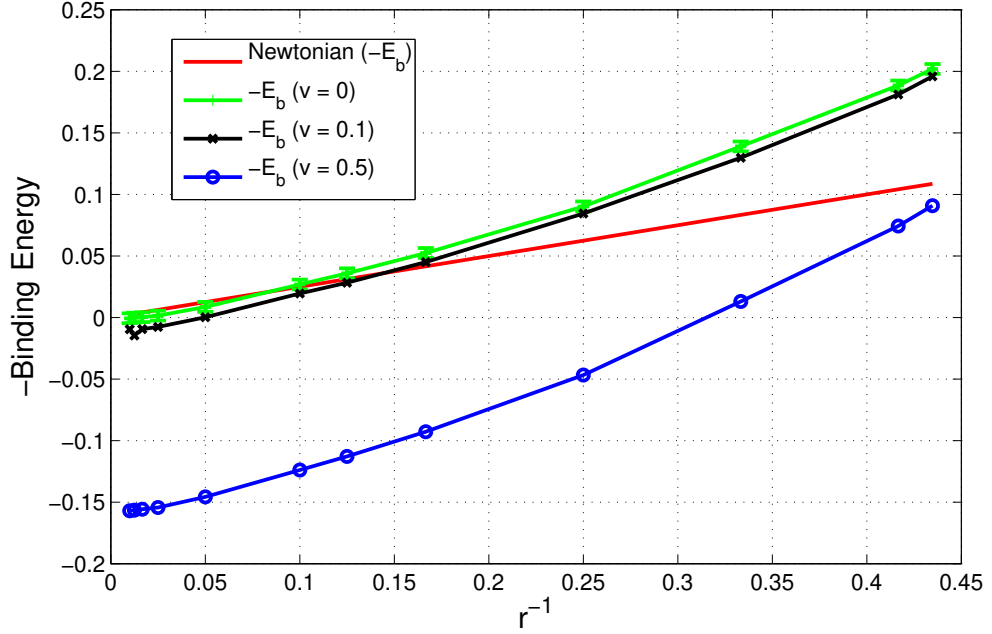


Figure 3.2: Negative of the binding Energy  $-E_b$  versus the inverse coordinate separation  $1/r$  for the cases with boosts speed  $\beta = 0, 0.1, 0.5$  represented by the green, black and blue curves, respectively. The red line is the Newtonian binding energy which scales as  $1/r$ . Ideally, it should be tangent to the  $\beta = 0$  curve (green) at large  $r$  ( $1/r \rightarrow 0$ ) but here it is slightly shifted due to numerical errors. As can be seen in the figure, the binding energy matches the Newtonian limit very well for large separations ( $1/r \rightarrow 0$ ), it grows faster than  $1/r$  as the black holes are closer ( $1/r \rightarrow \infty$ ). This is due to changes in horizon masses because of the distortions induced by the black holes on each other. It ( $-E_b$ ) also becomes more negative for large boosts reflecting the unbound nature of distant rapidly moving black holes where the kinetic energy of the black holes overwhelms the negative potential energy.

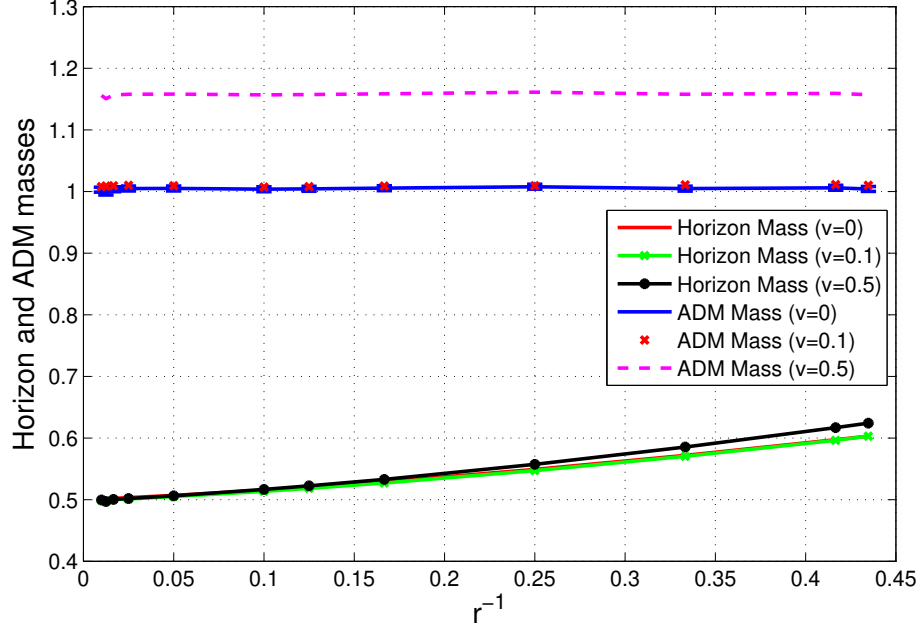


Figure 3.3: Horizon mass  $M_H$  and ADM mass  $M_{ADM}$  versus inverse distance  $1/r$  for boost speeds of  $\beta = 0, 0.1, 0.5$ .  $M_{ADM}$  (the upper, approximately parallel curves) is given by the pink dashed line ( $v=0.5$ ) and by the closely overlapping blue line ( $v=0$ ) and the red X marks (“ $\times$ ”). As expected, the ADM mass remains constant regardless of the separation  $r$  but varies as  $\gamma M_{ADM 0}$  for varying boost speeds  $\beta$ .  $M_H$  (the lower curves) is represented by closely overlapping red and green curves for the  $v=0$  and  $v=0.1$  cases, and by the higher black curve for  $v=0.5$ . Note that the horizon mass grows larger as the black holes are nearer i.e. as  $1/r \rightarrow \infty$ . The horizon mass is invariant under boosts. For  $r \geq 10$  (i.e.  $1/r \leq 0.1$ ) the horizon mass curves for different boosts overlap perfectly. Apparently because of the nonlinear interaction of the black hole geometries in the full solution, for larger boosts and for small separations the horizon mass does increase slightly.

would be this mass  $M_H$  which is adiabatically invariant. This was predicted analytically by [52] for nonspinning, instantaneously nonmoving black holes; it was predicted qualitatively for moving black holes.

The horizon mass is expected to remain invariant under boosts, and in single boosted black holes this is what we observe. But for fully solved data – the result of solving a nonlinear elliptic system, Fig. 3.3 shows that the horizon mass in the  $\beta = 0.5$  case is somewhat above that of the  $\beta = 0$  one for close separations (‘close’ meaning black hole separations less than  $r = 10$ ). Indeed, for  $r > 10$  (i.e.  $1/r < 0.1$ ), the overlap of the red, green and black curves is perfect to within less than one percent error. This is an interesting result depending on both the boost and the separation. The *growth* of the horizon area for large boosts is an effect due to the proximity of the two black holes. For sufficiently large separations, the boost does not change the horizon mass, hence does not change the horizon area.

### 3.3 Boosted Kerr Black Holes

We return to the analytic study of black hole horizons, now including spin. Strong astrophysical evidence supports the existence of spinning (Kerr) black holes ([31], [32],[33]); manipulating description of this spacetime is a frequent task in computational astrophysics. The angular momentum of the spinning black hole automatically selects a preferred direction and the Kerr hole is axially symmetric around the spin axis. Written in Kerr-Schild coordinates the Kerr spacetime formally admits a boost.



We will begin with the unboosted Kerr metric written in standard Kerr-Schild coordinates. We will then rewrite the metric in cylindrical coordinates where the symmetry axis of the cylinder points toward the boost direction. (We transform to cylindrical coordinates only to facilitate the boosting of the spacetime.) Once the spacetime is boosted, we will look at the spatial 3-metric on a (boosted)  $t = \text{constant}$  hypersurface. Since we are ultimately interested in the 2-metric we will perform one final coordinate transformation from cylindrical to spheroidal coordinates and consider  $\bar{r} = r_+$  (the expected horizon location). Once we have our 2-metric, we will compute the area of the apparent horizon and show that it indeed equals the unboosted, stationary value, which is  $Area = 4\pi (r_+^2 + a^2)$ .

The Kerr spacetime in Kerr-Schild coordinates is ([38], [30], [39],[40]):

$$\begin{aligned}
ds^2 &= -d\bar{t}^2 + d\bar{x}^2 + d\bar{y}^2 + d\bar{z}^2 \\
&\quad + \frac{2M\bar{r}^3}{\bar{r}^4 + a^2\bar{z}^2} \left[ d\bar{t} + \frac{\bar{r}\bar{x} + a\bar{y}}{\bar{r}^2 + a^2} d\bar{x} + \frac{\bar{r}\bar{y} - a\bar{x}}{\bar{r}^2 + a^2} d\bar{y} + \frac{\bar{z}}{\bar{r}} d\bar{z} \right]^2 \\
&= -d\bar{t}^2 + d\bar{x}^2 + d\bar{y}^2 + d\bar{z}^2 \\
&\quad + \frac{2M\bar{r}^3}{\bar{r}^4 + a^2\bar{z}^2} \left[ d\bar{t} + \frac{\bar{r}}{\bar{r}^2 + a^2} (\bar{x}d\bar{x} + \bar{y}d\bar{y}) + \frac{a(\bar{y}d\bar{x} - \bar{x}d\bar{y})}{\bar{r}^2 + a^2} + \frac{\bar{z}d\bar{z}}{\bar{r}} \right]^2
\end{aligned} \tag{3.11}$$

where we rewrote the Kerr metric in the second line in a form that will be useful in the following. In the  $a \rightarrow 0$  limit, we recover the Schwarzschild metric in Kerr-Schild coordinates. The radial coordinate  $\bar{r}$  is related to the fundamental coordinates  $\bar{x}, \bar{y}, \bar{z}$  by the equation of an oblate ellipsoid

$$\frac{\bar{x}^2 + \bar{y}^2}{\bar{r}^2 + a^2} + \frac{\bar{z}^2}{\bar{r}^2} = 1 \tag{3.12}$$

which is equivalent to a quadratic equation in  $\bar{r}^2$

$$\bar{r}^4 - \bar{r}^2(\bar{x}^2 + \bar{y}^2 + \bar{z}^2 - a^2) - a^2\bar{z}^2 = 0, \quad (3.13)$$

and the horizon is located at  $\bar{r} = r_+ = M + \sqrt{M^2 - a^2}$ . Eq. (3.12) motivates spheroidal coordinates:

$$\begin{aligned} \bar{x} &= \sqrt{\bar{r}^2 + a^2} \sin \bar{\theta} \cos \bar{\phi}, \\ \bar{y} &= \sqrt{\bar{r}^2 + a^2} \sin \bar{\theta} \sin \bar{\phi}, \\ \bar{z} &= \bar{r} \cos \bar{\theta}. \end{aligned} \quad (3.14)$$

We now explicitly reintroduce the cylindrical coordinates  $(\bar{r}_\parallel, \bar{r}_\perp, \bar{\phi}_{cyl})$  of the previous section :

$$\begin{aligned} \bar{x} &= \bar{r}_\parallel \sin \theta_\beta \cos \phi_\beta + \bar{r}_\perp (\cos \theta_\beta \cos \phi_\beta \cos \bar{\phi}_{cyl} - \sin \phi_\beta \sin \bar{\phi}_{cyl}) \\ \bar{y} &= \bar{r}_\parallel \sin \theta_\beta \sin \phi_\beta + \bar{r}_\perp (\cos \theta_\beta \sin \phi_\beta \cos \bar{\phi}_{cyl} + \cos \phi_\beta \sin \bar{\phi}_{cyl}) \\ \bar{z} &= \bar{r}_\parallel \cos \theta_\beta - \bar{r}_\perp \sin \theta_\beta \cos \bar{\phi}_{cyl} \end{aligned} \quad (3.15)$$

The angles  $\theta_\beta, \phi_\beta$  specify the direction of the Lorentz boost  $\beta$  in spherical coordinates based on  $\bar{x}, \bar{y}, \bar{z}$ :  $\beta = (\beta \sin \theta_\beta \cos \phi_\beta, \beta \sin \theta_\beta \sin \phi_\beta, \beta \cos \theta_\beta)$ . With

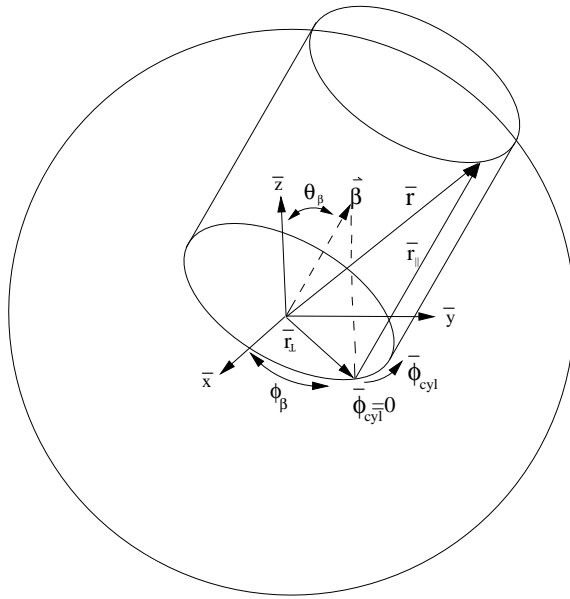


Figure 3.4: The tilted cylindrical coordinates  $(\bar{r}_\parallel, \bar{r}_\perp, \bar{\phi}_{cyl})$  along with the radial coordinate  $r$  and Kerr-Schild Cartesian coordinates  $(\bar{x}, \bar{y}, \bar{z})$ . The vector  $\beta$  points along the boost direction, which is parallel to the symmetry axis of the cylinder.

the coordinate transformation in Eq. (3.15) the Kerr metric becomes

$$\begin{aligned}
ds^2 &= -d\bar{t}^2 + d\bar{r}_{\parallel}^2 + d\bar{r}_{\perp}^2 + \bar{r}_{\perp}^2 d\bar{\phi}_{cyl}^2 \\
&+ \frac{2M\bar{r}}{\bar{r}^4 + a^2 (\bar{r}_{\parallel} \cos \theta_{\beta} - \bar{r}_{\perp} \sin \theta_{\beta} \cos \bar{\phi}_{cyl})^2} \\
&\times \left[ \frac{d\bar{t} + \frac{\bar{r}}{\bar{r}^2 + a^2} (\bar{x}d\bar{x} + \bar{y}d\bar{y}) + \frac{\bar{z}d\bar{z}}{\bar{r}}}{+ \frac{a(\sin \theta_{\beta} [\bar{r}_{\perp} d\bar{r}_{\parallel} - \bar{r}_{\parallel} d(\bar{r}_{\perp} \sin \bar{\phi}_{cyl})] - \cos \theta_{\beta} \bar{r}_{\perp}^2 d\bar{\phi}_{cyl})}{\bar{r}^2 + a^2}} \right]^2. \quad (3.16)
\end{aligned}$$

We now carry out a boost along the selected cylindrical axis. Unbarred coordinates will denote the boosted observer frame. They are related to the barred rest-frame coordinates via Eq. (3.4). After boosting this metric, we will look at it on an arbitrary  $t = \text{constant}$  hypersurface, which we take as  $t = 0$  since this choice simplifies the expressions, to project out the spatial geometry of the hypersurface in which the apparent horizon lies. This will leave us with  $d\bar{t} = -\gamma\beta dr_{\parallel}$  and  $\bar{r}_{\parallel} = \gamma r_{\parallel}$ . With these changes substituted into Eq. (3.16) we obtain the spatial part of the boosted Kerr metric on a  $t = 0$  hypersurface:

$$\begin{aligned}
ds^2|_{t=0} &= dr_{\parallel}^2 + dr_{\perp}^2 + r_{\perp}^2 d\phi_{cyl}^2 \\
&+ \frac{2M\bar{r}}{\bar{r}^4 + a^2 (\gamma r_{\parallel} \cos \theta_{\beta} - r_{\perp} \sin \theta_{\beta} \cos \phi_{cyl})^2} \\
&\times \left[ \frac{-\gamma\beta dr_{\parallel} + \frac{\bar{r}}{\bar{r}^2 + a^2} (\bar{x}d\bar{x} + \bar{y}d\bar{y}) + \frac{\bar{z}d\bar{z}}{\bar{r}}}{+ \frac{a(\sin \theta_{\beta} \gamma [r_{\perp} dr_{\parallel} - r_{\parallel} d(r_{\perp} \sin \phi_{cyl})] - \cos \theta_{\beta} r_{\perp}^2 d\phi_{cyl})}{\bar{r}^2 + a^2}} \right]^2 \quad (3.17)
\end{aligned}$$

where a few terms involving  $\bar{x}, \bar{y}, \bar{z}, \bar{r}$  in Eqs. (3.16), (3.17) were left untouched with the next step in mind. If one wishes, one could also write all of these terms as functions of  $r_{\parallel}, r_{\perp}$  and  $\phi_{cyl}$ . Let us remember what we are after; the

2-metric of the boosted geometry projected out by the condition  $\bar{r} = r_+$ . Eq. (3.12) implies

$$\frac{\bar{x}d\bar{x} + \bar{y}d\bar{y}}{\bar{r}^2 + a^2} + \frac{\bar{z}d\bar{z}}{\bar{r}^2} = \left( \frac{\bar{x}^2 + \bar{y}^2}{(\bar{r}^2 + a^2)^2} + \frac{\bar{z}^2}{\bar{r}^4} \right) \bar{r}d\bar{r} \longrightarrow 0 \quad \text{at} \quad \bar{r} = r_+. \quad (3.18)$$

Thus if  $d\bar{r} = 0$  (e.g. on the horizon,  $\bar{r} = r_+$ ), the left hand side of Eq. (3.18) vanishes. This is the analogue of Eq. (3.6) for the Schwarzschild case of Section ???. This simplification reduces the complexities of Eq. (3.17) substantially:

$$ds^2|_{t=0, \bar{r}=r_+} = \left[ \begin{array}{l} dr_{\parallel}^2 + dr_{\perp}^2 + r_{\perp}^2 d\phi_{cyl}^2 + \frac{2Mr_+}{r_+^4 + a^2 (\gamma r_{\parallel} \cos \theta_{\beta} - r_{\perp} \sin \theta_{\beta} \cos \phi_{cyl})^2} \\ \times \left[ -\gamma\beta dr_{\parallel} + \frac{a(\sin \theta_{\beta} \gamma [r_{\perp} dr_{\parallel} - r_{\parallel} d(r_{\perp} \sin \phi_{cyl})] - \cos \theta_{\beta} r_{\perp}^2 d\phi_{cyl})}{r_+^2 + a^2} \right]^2 \end{array} \right]_{\bar{r}=r_+}. \quad (3.19)$$

However, it is difficult to translate the horizon condition  $\bar{r} = r_+$  into something meaningful in cylindrical coordinates. Therefore, we must rewrite Eq. (3.19) in spheroidal coordinates to impose the condition  $\bar{r} = r_+$  to extract the 2-metric of the apparent horizon. We do this by going back to Eqs. (3.15) and rewriting them as a matrix equation for both boosted and unboosted coordinates

$$\begin{pmatrix} \bar{x} \\ \bar{y} \\ \bar{z} \end{pmatrix} = \hat{M} \begin{pmatrix} \bar{r}_{\perp} \cos \bar{\phi}_{cyl} \\ \bar{r}_{\perp} \sin \bar{\phi}_{cyl} \\ \bar{r}_{\parallel} \end{pmatrix} = \hat{M} \begin{pmatrix} r_{\perp} \cos \phi_{cyl} \\ r_{\perp} \sin \phi_{cyl} \\ \gamma r_{\parallel} \end{pmatrix} \quad (3.20)$$

where the components of the matrix  $\hat{M}$  can be determined from Eqs. (3.15). The radial coordinate  $\bar{r}$  in Eq. (3.14) is related to the Cartesian and cylindrical coordinates via  $\bar{x}^2 + \bar{y}^2 + \bar{z}^2 = \bar{r}_{\perp}^2 + \bar{r}_{\parallel}^2 = \bar{r}^2 + a^2 \sin^2 \bar{\theta}$ . Since  $\bar{r}_{\parallel} = \gamma r_{\parallel}$  on the  $t = 0$  hypersurface, we also have  $r_{\perp}^2 + \gamma^2 r_{\parallel}^2 = \bar{r}^2 + a^2 \sin^2 \bar{\theta}$  (cf. [38]). Setting

Eq. (3.20) equal to Eq. (3.14) and multiplying by  $\hat{M}^{-1}$ , we get

$$\begin{pmatrix} r_{\perp} \cos \phi_{cyl} \\ r_{\perp} \sin \phi_{cyl} \\ \gamma r_{\parallel} \end{pmatrix} = \hat{M}^{-1} \begin{pmatrix} \sqrt{\bar{r}^2 + a^2} \sin \bar{\theta} \cos \bar{\phi} \\ \sqrt{\bar{r}^2 + a^2} \sin \bar{\theta} \sin \bar{\phi} \\ \bar{r} \cos \bar{\theta} \end{pmatrix}.$$

Expanding this we obtain

$$\begin{aligned} r_{\perp} \cos \phi_{cyl} &= \cos \theta_{\beta} \cos \phi_{\beta} \sqrt{\bar{r}^2 + a^2} \sin \bar{\theta} \cos \bar{\phi} \\ &\quad + \cos \theta_{\beta} \sin \phi_{\beta} \sqrt{\bar{r}^2 + a^2} \sin \bar{\theta} \sin \bar{\phi} - \sin \theta_{\beta} \bar{r} \cos \bar{\theta} \\ r_{\perp} \sin \phi_{cyl} &= -\sin \phi_{\beta} \sqrt{\bar{r}^2 + a^2} \sin \bar{\theta} \cos \bar{\phi} + \cos \phi_{\beta} \sqrt{\bar{r}^2 + a^2} \sin \bar{\theta} \sin \bar{\phi} \\ \gamma r_{\parallel} &= \sin \theta_{\beta} \cos \phi_{\beta} \sqrt{\bar{r}^2 + a^2} \sin \bar{\theta} \cos \bar{\phi} \\ &\quad + \sin \theta_{\beta} \sin \phi_{\beta} \sqrt{\bar{r}^2 + a^2} \sin \bar{\theta} \sin \bar{\phi} + \cos \theta_{\beta} \bar{r} \cos \bar{\theta}. \end{aligned} \quad (3.21)$$

In the limit  $\theta_{\beta} = \phi_{\beta} = 0$ , the equations above reduce to Eq. (3.14) with the cylindrical coordinates replacing  $(\bar{x}, \bar{y}, \bar{z})$ . This is the case of boosting along the z-axis, and we briefly treat that here before proceeding. For boost along the z-axis, with  $\bar{r} = r_+$  (i.e. on the horizon) we have

$$ds^2|_{t=0, \bar{r}=r_+} = \left[ dx^2 + dy^2 + dz^2 + \frac{r_+^2 (r_+^2 + a^2)}{r_+^4 + \gamma^2 a^2 z^2} \left[ -\gamma \beta dz + \frac{a(ydx - xdy)}{r_+^2 + a^2} \right]^2 \right]_{\bar{r}=r_+}. \quad (3.22)$$

Because of the boost in the z-direction, only the terms involving z ( $-\gamma \beta dz$  in the numerator and  $\gamma^2 a^2 z^2$  in the denominator) differ from the unboosted case. In Eq. (3.22) we still have to evaluate some of the terms at  $\bar{r} = r_+$ . Using

spheroidal coordinates

$$\begin{aligned}
x &= \sqrt{r_+^2 + a^2} \sin \bar{\theta} \cos \bar{\phi} \\
y &= \sqrt{r_+^2 + a^2} \sin \bar{\theta} \sin \bar{\phi} \\
\gamma z &= r_+ \cos \bar{\theta}
\end{aligned} \tag{3.23}$$

we get

$$\begin{aligned}
ds^2|_{t=0, \bar{r}=r_+} &= (r_+^2 + a^2)(\cos^2 \bar{\theta} d\bar{\theta}^2 + \sin^2 \bar{\theta} d\bar{\phi}^2) + \frac{r_+^2}{\gamma^2} \sin^2 \bar{\theta} d\bar{\theta}^2 \\
&+ \frac{r_+^2 + a^2}{r_+^2 + a^2 \cos^2 \bar{\theta}} [\beta r_+ \sin \bar{\theta} d\bar{\theta} - a \sin^2 \bar{\theta} d\bar{\phi}]^2 .
\end{aligned} \tag{3.24}$$

With further simplifications, this becomes

$$ds^2|_{t=0, \bar{r}=r_+} = (r_+^2 + a^2 \cos^2 \bar{\theta}) d\bar{\theta}^2 + \frac{\sin^2 \bar{\theta}}{r_+^2 + a^2 \cos^2 \bar{\theta}} [-\beta a r_+ \sin \bar{\theta} d\bar{\theta} + (r_+^2 + a^2) d\bar{\phi}]^2 . \tag{3.25}$$

In the  $a \rightarrow 0$  limit, Eq. (3.25) gives precisely the expression we obtained for the boosted Schwarzschild metric. Let us now look at the 2-metric  $g_{AB}(A, B =$

$\theta, \phi$ ) for the apparent horizon component by component.

$$\begin{aligned}
g_{\bar{\theta}\bar{\theta}} &= (r_+^2 + a^2 \cos^2 \bar{\theta}) + \left( \frac{\gamma \beta a r_+ \sin^2 \bar{\theta}}{\sqrt{r_+^2 + a^2 \cos^2 \bar{\theta}}} \right)^2, \\
g_{\bar{\phi}\bar{\phi}} &= \left( \frac{(r_+^2 + a^2) \sin \bar{\theta}}{\sqrt{r_+^2 + a^2 \cos^2 \bar{\theta}}} \right)^2, \\
g_{\bar{\theta}\bar{\phi}} &= - \left( \frac{(r_+^2 + a^2) \sin \bar{\theta}}{\sqrt{r_+^2 + a^2 \cos^2 \bar{\theta}}} \right) \left( \frac{\gamma \beta a r_+ \sin^2 \bar{\theta}}{\sqrt{r_+^2 + a^2 \cos^2 \bar{\theta}}} \right). \tag{3.26}
\end{aligned}$$

For any  $2 \times 2$  matrix of the form

$$H_{AB} = \begin{pmatrix} A^2 + B^2 & BC \\ BC & C^2 \end{pmatrix} \tag{3.27}$$

the determinant is  $\det H_{AB} = A^2 C^2$ . The 2-dimensional metric is of this form, so

$$\sqrt{\det(g_{AB})} = (r_+^2 + a^2) \sin \bar{\theta} \tag{3.28}$$

Since

$$\text{Area} = \int \sqrt{\det(g_{AB})} d\bar{\theta} d\bar{\phi} \tag{3.29}$$

we obtain an area of  $4\pi (r_+^2 + a^2)$  as expected, identical to the unboosted horizon area.

Going back to our boost in an arbitrary direction, we rewrite the 3-metric in Eq. (3.19) using the spheroidal coordinates of Eq. (3.21). After some algebra using a well known algebraic relation for the Kerr spacetime ( $2Mr_+ = r_+^2 + a^2$ ) to simplify, and setting  $\bar{r} = r_+$  in most places, we end up



with a result surprisingly similar to Eq. (3.25)

$$ds^2|_{t=0, \bar{r}=r_+} = (r_+^2 + a^2 \cos^2 \bar{\theta}) d\bar{\theta}^2 + \frac{\sin^2 \bar{\theta}}{r_+^2 + a^2 \cos^2 \bar{\theta}} [a\gamma\beta dr_{||} + (r_+^2 + a^2) d\bar{\phi}]^2 \quad (3.30)$$

Using the last one of Eqs. (3.21), we now expand the terms containing  $dr_{||}$  and obtain the components of the 2-metric for the apparent horizon:

$$g_{\bar{\theta}\bar{\theta}} = (r_+^2 + a^2 \cos^2 \bar{\theta}) + \frac{\beta^2 a^2 \sin^2 \bar{\theta}}{r_+^2 + a^2 \cos^2 \bar{\theta}} \left( \sqrt{r_+^2 + a^2} \sin \theta_\beta \cos \bar{\theta} \cos(\bar{\phi} - \phi_\beta) - r_+ \cos \theta_\beta \sin \bar{\theta} \right)^2, \quad (3.31)$$

$$g_{\bar{\phi}\bar{\phi}} = \frac{(r_+^2 + a^2) \sin^2 \bar{\theta}}{r_+^2 + a^2 \cos^2 \bar{\theta}} \left( \sqrt{r_+^2 + a^2} - \beta a \sin \theta_\beta \sin \bar{\theta} \sin(\bar{\phi} - \phi_\beta) \right)^2, \quad (3.32)$$

$$g_{\bar{\theta}\bar{\phi}} = \frac{\beta a \sqrt{r_+^2 + a^2} \sin^2 \bar{\theta}}{r_+^2 + a^2 \cos^2 \bar{\theta}} \quad (3.33)$$

$$\times \left[ \begin{aligned} & \left( \sqrt{r_+^2 + a^2} \sin \theta_\beta \cos \bar{\theta} \cos(\bar{\phi} - \phi_\beta) - r_+ \cos \theta_\beta \sin \bar{\theta} \right) \\ & \times \left( \sqrt{r_+^2 + a^2} - \beta a \sin \theta_\beta \sin \bar{\theta} \sin(\bar{\phi} - \phi_\beta) \right) \end{aligned} \right] \quad (3.34)$$

$$(3.35)$$

The  $\beta \rightarrow 0$  limit of equations (3.31) through (3.32) yields the standard 2-metric of the Kerr spacetime given in Boyer-Lindquist coordinates. The  $a \rightarrow 0$  limit gives the standard Schwarzschild (spherical) 2-metric. The  $\theta_\beta = 0$  limit yields the metric of Eq. (3.26). Eqs. (3.31)-(3.33) show that  $g_{AB}$  is again of the form

of Eq. (3.27). Hence the square root of the determinant of the metric is

$$\sqrt{\det(g_{AB})} = (r_+^2 + a^2) \sin \bar{\theta} - \beta a \sqrt{r_+^2 + a^2} \sin \theta_\beta \sin^2 \bar{\theta} \sin(\bar{\phi} - \phi_\beta). \quad (3.36)$$

The first term above is the familiar contribution from the unboosted Kerr metric. To determine the area, we integrate the square root of the determinant of the 2-metric over the angular variables of the spheroidal coordinate system.

$$\begin{aligned} \text{Area} &= \int \sqrt{\det(g_{AB})} d\bar{\theta} d\bar{\phi} \\ &= \int_0^{2\pi} d\bar{\phi} \int_0^\pi d\bar{\theta} \left[ (r_+^2 + a^2) \sin \bar{\theta} - \beta a \sqrt{r_+^2 + a^2} \sin \theta_\beta \sin^2 \bar{\theta} \sin(\bar{\phi} - \phi_\beta) \right] \\ &= 4\pi (r_+^2 + a^2). \end{aligned} \quad (3.37)$$

Above, the second term disappears because of the  $\bar{\phi}$  integral. Our calculation shows that the area of the apparent horizon of a Kerr black hole remains invariant under arbitrary Lorentz boosts, as expected.

We have now shown that the area of the apparent horizon remains invariant under Lorentz boosts and yields the usual value  $\text{Area} = 4\pi r_{horizon}^2$  for a static or stationary black hole. This could be seen as an unexpected result as the horizon becomes distorted because of Lorentz contraction along the boost direction. Next, we will look at these distortions in detail and show how they change the shape of the 2-dimensional apparent horizon.

## Chapter 4

### Visualization

Schwarzschild spacetime is spherically symmetric. Therefore, the apparent horizons of an isolated (unperturbed), unboosted Schwarzschild black hole are 2-spheres. Under a Lorentz boost, the sections of these spheres that are parallel to the boost direction get Lorentz contracted. The resulting shape is always an oblate spheroid regardless of the boost direction. This will not be the case with the apparent horizon of a Kerr black hole because the horizon of an unboosted Kerr black hole is an oblate ellipsoid to begin with. This is clear from Eq.(3.12); the Boyer-Lindquist ‘radial’ coordinate  $r$  in Kerr spacetime is not spherically symmetric like the radial coordinate  $r$  of the Schwarzschild spacetime. Let us display Eq.(3.12) here once more

$$\frac{x^2 + y^2}{r^2 + a^2} + \frac{z^2}{r^2} = 1. \quad (4.1)$$

The horizon is located at  $r = r_+$  which, in these Kerr-Schild Cartesian coordinates, gives an oblate ellipsoid, which has a circular cross section of radius  $\sqrt{r_+^2 + a^2}$  at  $z = 0$  and an elliptical cross section in the  $x, y = \text{constant}$  planes of semi-major axis  $a_1 \equiv \sqrt{r_+^2 + a^2}$  and semi-minor axis  $a_2 \equiv r_+$ . This can be easily seen if we transform the Cartesian coordinates  $x, y, z$  to ellipsoidal

coordinates via

$$\begin{aligned}
 x &= \sqrt{r^2 + a^2} \sin \theta \cos \phi, \\
 y &= \sqrt{r^2 + a^2} \sin \theta \sin \phi, \\
 z &= r \cos \theta.
 \end{aligned}
 \tag{4.2}$$

Obviously, this still satisfies Eq.(4.1). When boosted, the black hole will not retain its ellipsoidal shape or axisymmetry except for boosts in the  $z$ -direction, which simply give more ‘compressed’ ellipsoids whose ‘height’ (length along the  $z$ -direction) get Lorentz contracted by a factor of  $\gamma = (1 - \beta^2)^{-1/2}$ . We present an example of this in Fig.4.1 where  $\gamma = 2$ . Visualizing the distortions of the Kerr horizon due to the boosts along the  $z$ -axis is almost trivial because of the axisymmetry of the black hole with respect to the  $z$ -axis. One simply Lorentz contracts the ‘height’ of the horizon as shown in Fig.4.1. Things become much less trivial once one boosts along directions that break the  $z$ -axis symmetry. The resulting distorted horizons will no longer be oblate spheroids but rather triaxial ellipsoids. There are several way of visualizing these distorted horizons. Here, we will present two of the three methods we have come up with. The reason for presenting two different methods is to strengthen the validity of our results; both methods give the same distorted surfaces as one will see below. As was done in Fig.4.1, instead of plotting 3-dimensional ellipsoids, we will suppress the  $y$ -direction for now and work with 2-dimensional  $x$ - $z$  cross-sections of the ellipsoids in sections 4.1, 4.2. In section 4.3, we will add the third dimension in and briefly look at 3-dimensional figures representing the

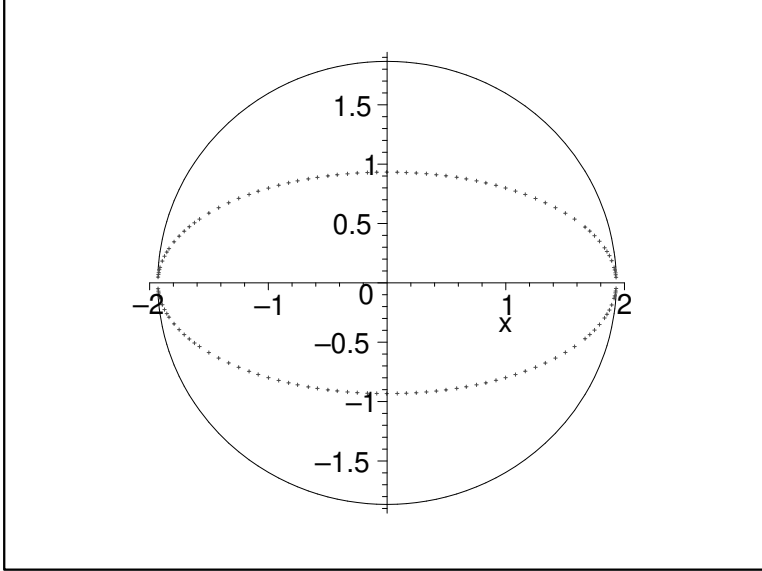


Figure 4.1:  $x$ - $z$  cross sections of an unboosted (solid) and a  $z$ -direction boosted (dotted) Kerr black hole with  $a = M/2$ , which gives  $r_+ = 1 + \sqrt{3}/2 = 1.866M$ . This gives  $a_1 = 1.932M$ ,  $a_2 = 1.866M$  for the  $x$ -, $z$ -axes, respectively. The Lorentz boost factor is  $\gamma = 2$ . In the figure and henceforth, we will set  $M = 1$ .

apparent horizons distorted by Lorentz boosts.

## 4.1 Discrete Tracer Line Method

The first method is what we call the *tracer line method* where we take 1-dimensional cross-sections of the undistorted  $x-z$  projection of the ellipsoid in the boost direction and replot the new distorted ellipse by Lorentz contracting the cross-sections along the boost direction by the factor  $\gamma \equiv (1 - \beta^2)^{-1/2}$ . The boost direction is specified by the latitudinal and azimuthal angles  $(\theta_\beta, \phi_\beta)$ . Since the initial undistorted horizon is azimuthally symmetric, we can rotate

our x-y axes so as to align the  $x = 0$  direction of the Kerr-Schild Cartesian coordinates with the  $\phi = \phi_\beta$  direction. Then the boost is specified by only the polar angle  $\theta = \theta_\beta$ . With the x-axis located at  $\phi = \phi_\beta$ , we can rewrite the boost direction in Cartesian coordinates as a line in  $x - z$  plane given by

$$z = \cot \theta_\beta x. \quad (4.3)$$

Therefore the cross-sections of the undistorted ellipse ( $x - z$  cut of the horizon) parallel to the boost direction are given by a line that runs parallel to the line given in Eq.(4.3). This line runs from one end of the ellipse to the other end. This is what we call the “tracer line”. It is given by the equation

$$z = \cot \theta_\beta x + z_0 \quad \text{where} \quad z_0 \in [z_{min}, z_{max}]. \quad (4.4)$$

Here,  $z_{min} = -z_{max}$  are the z-intercepts of the tracer line at either end of the ellipse where the tracer line is tangent to the ellipse (see Fig.4.2). For an ellipse with semi-major and minor axes  $a_1$ ,  $a_2$  and boost direction  $\theta_\beta$  the z-intercepts are

$$z_{max} = -z_{min} = \sqrt{a_2^2 + a_1^2 \cot^2 \theta_\beta}. \quad (4.5)$$

The intersection of the tracer line in Eq.(4.4) with the undistorted ellipse is given by a pair of points located on the *upper* and *lower* portions of the ellipse and are labelled with coordinates  $(x_1, z_1)$  and  $(x_2, z_2)$ , respectively (upper and lower with respect to a *reference line* that we define below). It is the distance between these two points that gets Lorentz contracted by a factor

of  $\gamma$ . We determine the location of the new points of the distorted ellipse by first finding a reference line from which we can measure the distance between  $(x_1, z_1)$  and  $(x_2, z_2)$ . Such a line needs to be orthogonal to the boost direction. The equation for this line is  $z = -\tan\theta_\beta x$  and it is shown as the dotted line in Fig.4.2. As can be seen clearly in the figure, the label 1 is for points of the ellipse above the line  $z = -\tan\theta_\beta x$ , and 2 is for points below. The intersection of the tracer line of Eq.(4.4) with this line is labelled  $(x_\times, z_\times)$ . Since we know the equations for both lines, we can easily solve for  $(x_\times, z_\times)$  by setting

$$-\tan\theta_\beta x_\times = \cot\theta_\beta x_\times + z_0 \quad (4.6)$$

which gives

$$x_\times = -\frac{z_0}{\cot\theta_\beta + \tan\theta_\beta}, \quad (4.7)$$

$$z_\times = -\tan\theta_\beta x_\times. \quad (4.8)$$

The point  $(x_\times, z_\times)$  is equidistant to both  $(x_1, z_1)$  and  $(x_2, z_2)$ . As the tracer line runs from  $z_{min}$  to  $z_{max}$ , we end up with a set of points labelled by ‘ $\times$ ’, ‘1’ and ‘2’. This now provides an easy way to locate the points  $(x'_1, z'_1)$ ,  $(x'_2, z'_2)$  of the distorted ellipse which we do by Lorentz contracting distances  $L_1, L_2$  between  $(x_\times, z_\times)$  and  $(x_1, z_1)$ , and between  $(x_\times, z_\times)$  and  $(x_2, z_2)$  given by

$$L_1 = \sqrt{(x_\times - x_1)^2 + (z_\times - z_1)^2}, \quad (4.9)$$

$$L_2 = \sqrt{(x_\times - x_2)^2 + (z_\times - z_2)^2}. \quad (4.10)$$

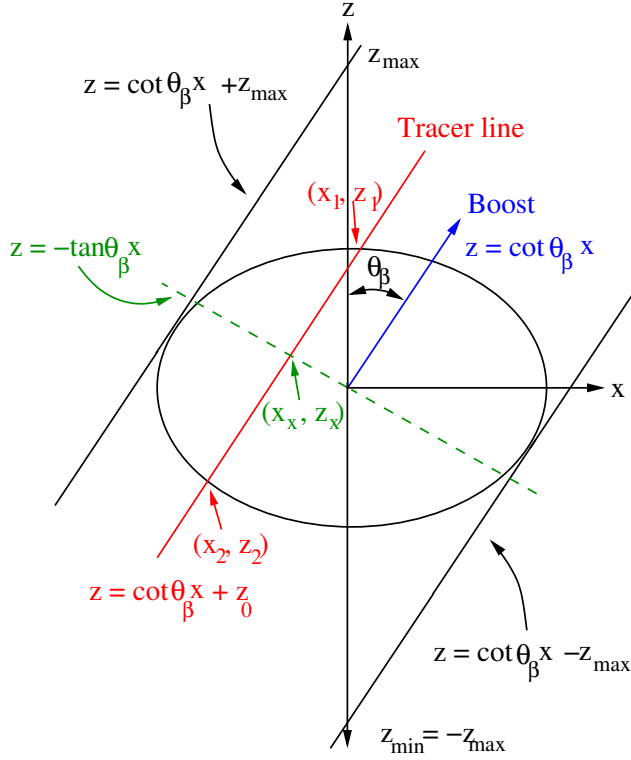


Figure 4.2: A schematic representation of the general lay-out for the tracer-line method. The red line is the tracer-line, which is parallel to the boost direction and sweeps the undistorted ellipse from left to right. The dashed line is perpendicular to the solid lines.  $\theta_\beta$  is the boost direction given by the polar angle  $\theta$  lying in the  $x$ - $z$  plane. The  $x$ -direction here does not necessarily coincide with the overall  $x$ -direction of the grid. We always rotate the coordinate grid so that the azimuthal boost direction  $\phi_\beta$  is reset to zero.



With everything in hand, we can finally write down the equations for the points  $(x'_1, z'_1)$ ,  $(x'_2, z'_2)$  of the boost distorted ellipse

$$x'_1 = x_\times + \text{sign}(z_1 - z_\times)L_1 \sin \theta_\beta/\gamma, \quad (4.11)$$

$$x'_2 = x_\times - \text{sign}(z_\times - z_2)L_2 \sin \theta_\beta/\gamma \quad (4.12)$$

$$z'_{1,2} = \cot \theta_\beta x'_{1,2} + z_0 \quad (4.13)$$

The ‘sign’ factor is needed for obtaining the correct shape at the very edges of the distorted ellipse (see Fig.4.2).

We now have an algorithm for drawing the distorted ellipse. Each value of  $z_0$  slides the tracer line from left to right, giving us the values for each  $(x_1, z_1)$ ,  $(x_2, z_2)$  and  $(x_\times, z_\times)$  which subsequently determines  $(x'_1, z'_1)$ ,  $(x'_2, z'_2)$  through Eqs.(4.11) and (4.12). As an example we present a numerical result where we pick 100 values for  $z_0$  between  $z_{min}$  and  $z_{max}$ . Specifying the value of  $z_0$  is sufficient for determining  $(x'_1, z'_1)$ ,  $(x'_2, z'_2)$  via the procedure described above. In Fig.4.3, we display the  $x - z$  cross-section of the horizon of a Kerr black hole of extremal spin  $a = 1$ , which gives  $r_+ = 1$  for the horizon location and  $a_1 = \sqrt{2}$ ,  $a_2 = 1$  for the axes. These values provide us with the shape of the undistorted horizon of the Kerr black hole (solid curve). For the boost direction, we pick  $\theta_\beta = \pi/6 = 30^\circ$  and a boost speed of  $\beta = \sqrt{3}/2$  which gives  $\gamma = 2$ . The dots in the figure give us the location of the distorted horizon under the Lorentz boost. We present a similar result in Fig.4.4 where we have repeated the same computation for a Kerr black hole with spin  $a = 0.75$  and Lorentz boost of  $\gamma = \sqrt{2}$  ( $\beta = \sqrt{2}/2$ ) in the direction  $\theta_\beta = 45^\circ$ . The axes of the

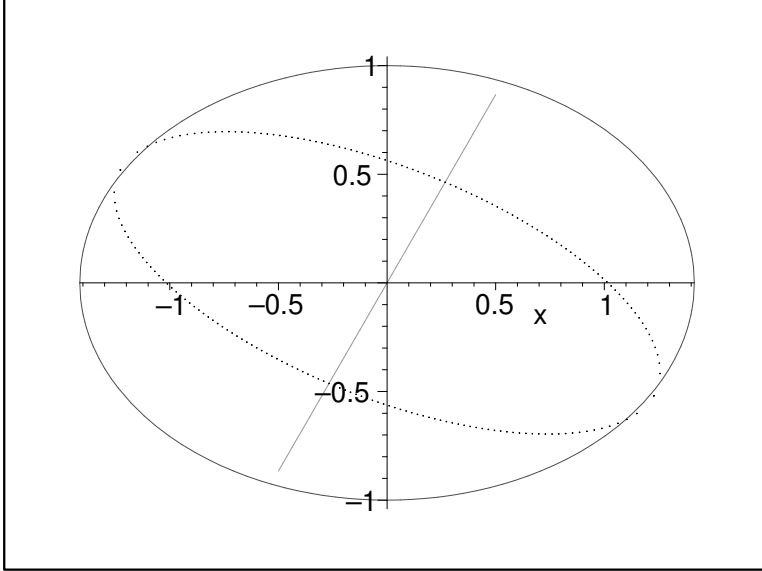


Figure 4.3: A  $\beta = \sqrt{3}/2$  ( $\gamma = 2$ ) boost of an extremal ( $a = 1$ ) Kerr black hole in the direction  $\theta_\beta = 30^\circ$ . The solid curve (the ellipse) is the undistorted horizon with semi-major axis  $a_1 = \sqrt{2}$  and semi-minor axis  $a_2 = 1$ . The distance units are normalized in terms of black hole mass  $M$ . The dotted warped/tilted ellipse is the new black hole horizon distorted under the Lorentz boost.

undistorted ellipse are  $a_1 = 1.822875656$ ,  $a_2 = 1.661437828$  (always in units of black hole mass  $M$ ). As in Fig.4.3, the solid curve represents the undistorted horizon and the dotted curve plots the horizon of the Lorentz boosted Kerr black hole. In appendix 1, we have included the details of the Maple code on how to execute this procedure specifically corresponding to the generation of Fig.4.4. The interested Maple aficionados are encouraged read that section. Final remark about this method concerns symmetry arguments. The Maple code provided in appendix 1 only gives the correct shape (distorted horizon) for the boost direction in the range  $0 \leq \theta_\beta \leq 90^\circ$  (first quadrant of the x-z

plane). For boost angles larger than  $90^\circ$ , the symmetry arguments used in appendix 1 need to be modified. Fortunately, one does not need to change the code to do that. One can simply use mirror reflections of the case with  $\theta_\beta$  lying in the first quadrant. For example, for boost angles in the second quadrant ( $90^\circ \leq \theta_\beta \leq 180^\circ$ ), one can simply compute the case for the boost in the first quadrant not using  $\theta_\beta$  for the boost direction but the complimentary angle  $\pi - \theta_\beta$  then mirror reflect each x-coordinate to obtain to correct shape. Similarly, one can mirror reflect the z-coordinate and obtain boosts whose direction vectors lie in the third or the fourth quadrants. In short, one only needs to compute for  $0 \leq \theta_\beta \leq 90^\circ$ . All other distorted surfaces (due to boosts in  $\theta > 90^\circ$  direction) can be obtained by subsequent parity transformations with respect to  $x = 0$  and/or  $z = 0$  lines. Although this method works very well and is very simple, it is a discrete method thus only as good as its resolution. The apparent horizon is a simply connected, smooth 2-dimensional surface so it might be better to try to reproduce the same distorted ellipses using transformations of continuous surfaces. Of course, one could always increase the resolution by using perhaps  $10^4$  data points as opposed to 100 or even more. After all, even a ‘continuous’ plot is not actually continuous when software plots it. With that said, let us move on to the next method.

## 4.2 Distorted Polar Coordinate Method

In this section, we present another method for drawing the distorted horizon. The advantage of this method over the previous one is that this one

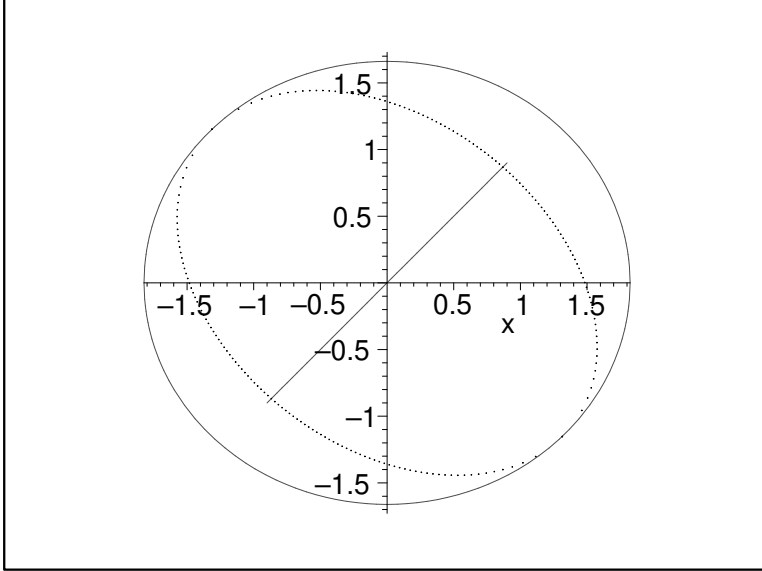


Figure 4.4: A  $\beta = \sqrt{2}/2$  ( $\gamma = \sqrt{2}$ ) boost of a Kerr black hole with spin  $a = 0.75$  in the direction  $\theta_\beta = 45^\circ$ . The solid curve (the ellipse) is the undistorted horizon with semi-major axis  $a_1 = 1.822875656$  and semi-minor axis  $a_2 = 1.661437828$ . As before, the dotted tilted ellipse is the Lorentz contracted black hole horizon.

gives a continuous surface as opposed to one that was plotted as a collection of discrete points. We begin with the equation of an ellipse (with semi-major and semi-minor axes  $a_1, a_2$ ) given in polar coordinates

$$\frac{x^2}{a_1^2} + \frac{z^2}{a_2^2} = 1 \quad \Longrightarrow \quad r(\theta) = \frac{a_1 a_2}{\sqrt{a_2^2 \cos^2 \theta + a_1^2 \sin^2 \theta}}. \quad (4.14)$$

As shown in Fig. 4.5, we decompose  $r(\theta)$  into its components that are parallel and perpendicular to the boost direction  $\theta_\beta$

$$r_{\parallel} = r(\theta) \cos \left[ \frac{\pi}{2} - (\theta + \theta_\beta) \right] = r(\theta) \sin(\theta + \theta_\beta), \quad (4.15)$$

$$r_{\perp} = r(\theta) \sin \left[ \frac{\pi}{2} - (\theta + \theta_\beta) \right] = r(\theta) \cos(\theta + \theta_\beta). \quad (4.16)$$

Here  $\theta_\beta$  is the boost angle measured with respect to the z-axis (as before) whereas  $\theta$  is measured from the x-axis. Under a Lorentz boost with  $\beta = v/c$

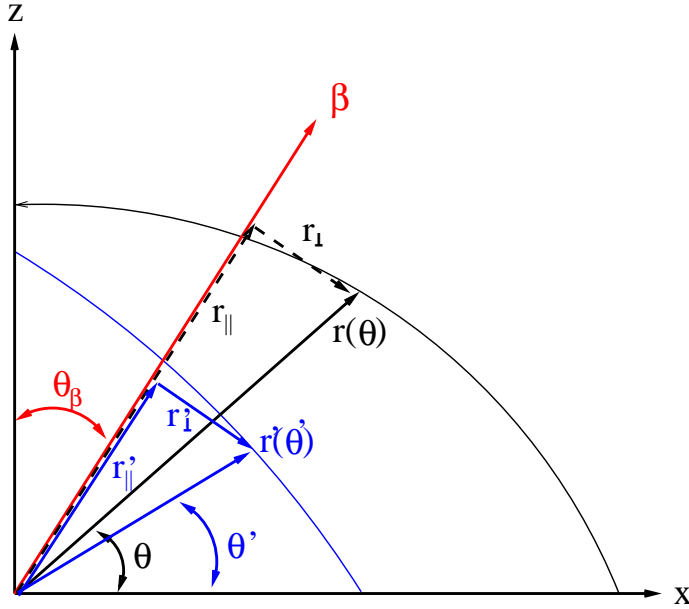


Figure 4.5: Schematic diagram showing the various angles and vectors used in determining the location of the distorted ellipse. The ellipses drawn here do not represent the actual distorted shapes.

giving a gamma factor of  $\gamma = (1 - \beta^2)^{-1/2}$ , the direction along the boost gets Lorentz contracted while the components orthogonal to the boost remain

unchanged , i.e.

$$r_{\parallel} \rightarrow r'_{\parallel} = \frac{r_{\parallel}}{\gamma} ; \quad r_{\perp} \rightarrow r'_{\perp} = r_{\perp}. \quad (4.17)$$

This gives us the components of the new polar vector  $r'(\theta)$ . Combining Eqs. (4.15) and (4.16) with the appropriate factor of  $\gamma$  we obtain the length of the new polar vector

$$\begin{aligned} r'(\theta) &= r(\theta) \sqrt{\gamma^{-2} \sin^2(\theta + \theta_{\beta}) + \cos^2(\theta + \theta_{\beta})} \\ &= \frac{a_1 a_2}{\sqrt{a_2^2 \cos^2 \theta + a_1^2 \sin^2 \theta}} \sqrt{1 - \beta^2 \sin^2(\theta + \theta_{\beta})}. \end{aligned} \quad (4.18)$$

As can be seen from Fig.4.5, the angle  $\theta$  of  $r(\theta)$  also gets rotated to the new angle  $\theta'$ , which is given by

$$\theta' = \frac{\pi}{2} - \theta_{\beta} - \tan^{-1} [\gamma \cot(\theta + \theta_{\beta})]. \quad (4.19)$$

Simply put, because of the Lorentz contraction, a point located at polar coordinates  $(r(\theta), \theta)$  shifts to a new location given by  $(r'(\theta'), \theta')$ .

In order to plot the distorted ellipse, we need to have an equation for it that is similar to Eq.(4.14). But because of the Lorentz contraction, the new ellipse should have different lengths for its semi-major and semi-minor axes. One now also expects to see  $xz$  crossterms in the Cartesian side of Eq.(4.14). To determine the lengths of the new axes, we need to find the “turning points” of the new ellipse. Meaning that just as the extrema of  $r(\theta)$  determine the angular location of the axes  $a_1, a_2$  so will the extrema of  $r'(\theta')$  determine the locations of the new turning points. In short, we need to extremize  $r'(\theta')$  by

looking at

$$\left. \frac{\partial r'(\theta')}{\partial \theta'} \right|_{\theta'=\theta'_{\substack{max \\ min}}} = 0$$

which is evaluated to be

$$\frac{\partial r'(\theta')}{\partial \theta'} = \frac{\partial r'}{\partial \theta} \frac{\partial \theta}{\partial \theta'} = \frac{\partial r'}{\partial \theta} \left( \frac{\partial \theta'}{\partial \theta} \right)^{-1}. \quad (4.20)$$

Although the derivatives of Eqs.(4.18) and (4.19) are trivial, displaying the analytical expression of Eq.(4.20) explicitly will crowd the page without serving much purpose. For this reason, we will pick specific values for  $\gamma$ ,  $\theta_\beta$ ,  $a_1$  and  $a_2$  and evaluate Eq.(4.20) numerically. We choose the following values

$$\gamma = 2, \theta_\beta = 30^\circ, a_1 = \sqrt{2}, a_2 = 1 \quad (4.21)$$

$(a_1, a_2) = (\sqrt{2}, 1)$  correspond to the extremal spin value of  $a = 1$  for the Kerr black hole. Evaluating Eq.(4.20), we get the following results

$r'_{\substack{max \\ min}}$	$\theta'_{\substack{max \\ min}}$	$\theta'_{\substack{max \\ min}} (^\circ)$
1.33487	-0.3773	-21.61
1.33487	2.7642	158.38
0.5297	1.1934	68.38
0.5297	-1.9481	-111.61

Table 4.1: Numerically determined values yielding the length of the distorted ellipse's long and short axes  $a'_1, a'_2$  as well as the angular locations  $\theta'_{\substack{max \\ min}}$  of those axes. In each column, the top two rows correspond to  $a'_1$  and bottom two to  $a'_2$ .

These values give us the lengths for the new axes of the ellipse as well as their angular locations. The new long and short axes have the following lengths

$$a'_1 = 1.33487, \quad a'_2 = 0.5297 \quad (4.22)$$

Keep in mind that these axes no longer point along the x, z-axes but are actually rotated by an angle given in table 4.1. The question is which one of  $\theta'_{max}$ 's give us the correct orientation for the distorted ellipse? In the x-z frame,  $r = a_1$  is located at  $\theta = 0^\circ$ . The same holds true for  $r' = a'_1$  in x'-z' frame, however that frame is rotated by an angle  $\theta'$  with respect to the x-z frame. From table 4.1, we see that  $r' = a'_1$  is given by  $\theta'_{max} = -21.61^\circ$  or  $158.38^\circ$ . By looking at the overall geometry, one can ascertain that the correct rotation angle is  $-21.61^\circ$  (otherwise the ellipse would tilt the wrong way). Let us call this rotation angle  $\Delta\theta$ . Now, it is simple to relate the x,z coordinates to the x',z' coordinates via a rotation matrix

$$\begin{pmatrix} x' \\ z' \end{pmatrix} = \begin{pmatrix} \cos \Delta\theta & \sin \Delta\theta \\ -\sin \Delta\theta & \cos \Delta\theta \end{pmatrix} \begin{pmatrix} x \\ z \end{pmatrix}. \quad (4.23)$$

Inverting this and solving for x and z we get

$$x = \cos \Delta\theta x' - \sin \Delta\theta z', \quad z = \sin \Delta\theta x' + \cos \Delta\theta z'. \quad (4.24)$$

The new version of Eq.(4.14) reads

$$\frac{(\cos \Delta\theta x' - \sin \Delta\theta z')^2}{a_1'^2} + \frac{(\sin \Delta\theta x' + \cos \Delta\theta z')^2}{a_2'^2} = 1 \quad (4.25)$$



Now, one easily sees the aforementioned  $xz$  cross terms. We solve for  $z'$  using the quadratic equation which has two solutions corresponding to the upper and lower halves of the distorted ellipse. We skip these trivial steps here and have Maple do it for us. The result that matters is the actual shape for the distorted ellipse, which is given in Fig.4.6 below. The details of how this figure

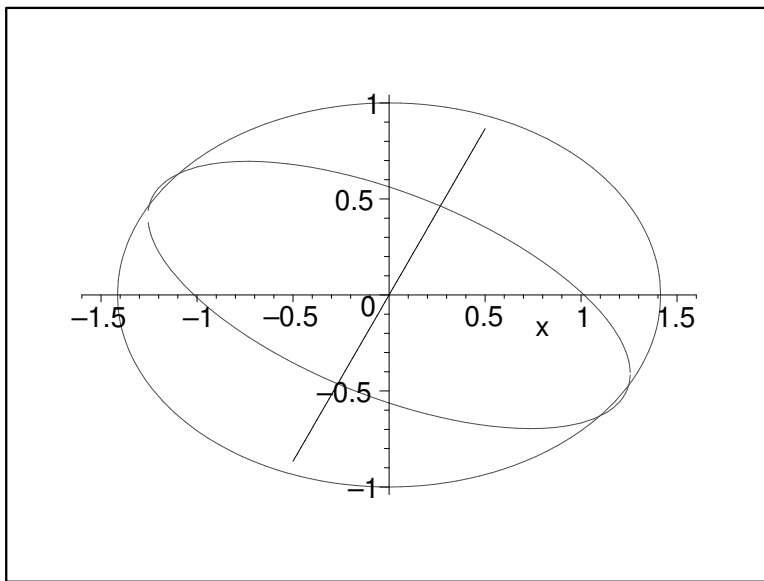


Figure 4.6: Horizon of a Kerr black hole with  $a = 1$  distorted by a Lorentz boost with  $\gamma = 2$  in the direction  $\theta_\beta = 30^\circ$ . This was plotted using the *polar plot* method.

is drawn using Maple are provided in appendix 2. The symmetry arguments made in section 4.1 hold here as well so we do not need to present cases with boost angle larger than  $90^\circ$  i.e.  $0^\circ \leq \theta_\beta \leq 90^\circ$  covers all possible angles using mirror reflections with respect to  $x$ - and  $z$ -axes.

### 4.2.1 Overlap Between The Two Methods

Here, we compare the results obtained by the two different methods mentioned above. The most straightforward way of doing this is to simply superimpose the distorted horizons obtained by these two methods. Once again, we stick with the  $a = 1$ ,  $\theta_\beta = 30^\circ$  case and simply plot the distorted ellipses on top of each other.

As can (or rather, can not) be seen from Fig.4.7, the overlap of the two ellipses is perfect. Without the colors, one would not be able to even tell that there are actually two superimposed ellipses. So, we have two distinct methods both yielding the same x-z cross-section for the Lorentz distorted ellipsoid. This clearly supports the validity of these results and the soundness of the methods used. There only remains the question of what the actual distorted ellipsoids look like embedded in 3-dimensional space.

## 4.3 Adding The Third Dimension

Although at first this may seem like an involved extra step, the inclusion of the third dimension (y-direction) is rather straightforward. Since we have constrained the distortions to the x-z plane, the distorted ellipsoid in three dimensions is given by adding the ‘y-term’ into Eq.(4.25). Let us demonstrate how to proceed by first doing this to a regular ellipse in the x-z plane given by

$$\frac{x^2}{a_1^2} + \frac{z^2}{a_2^2} = 1 \tag{4.26}$$

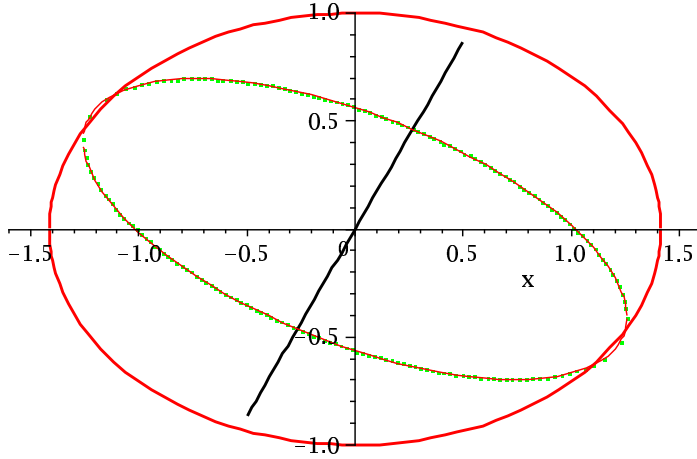


Figure 4.7: The overlap of the methods showing a perfect match. This figure shows an undistorted Kerr black hole with  $a = 1$  and the same black hole distorted by a  $\gamma = 2$  Lorentz boost with angle  $\theta_\beta = 30^\circ$  with respect to the  $z$ -axis.

which becomes an ellipsoid in 3-dimensions via

$$\frac{x^2 + y^2}{a_1^2} + \frac{z^2}{a_2^2} = 1. \quad (4.27)$$

Reapplying the same procedure to Eq.(4.25), we end up with

$$\frac{(\cos \Delta\theta x' - \sin \Delta\theta z')^2}{a_1'^2} + \frac{y'^2}{a_1^2} + \frac{(\sin \Delta\theta x' + \cos \Delta\theta z')^2}{a_2'^2} = 1 \quad (4.28)$$

Note that although the distorted ellipsoid acquires new axes  $a'_1, a'_2$  in the  $x, z$ -directions, the  $y$ -direction retains the original semi-major axis length  $a_1$ . This is because the boost lies in the  $x$ - $z$  plane thus does not have any effects along the  $y$ -direction. Using Maple's *plot3d* command, we can easily visualize this

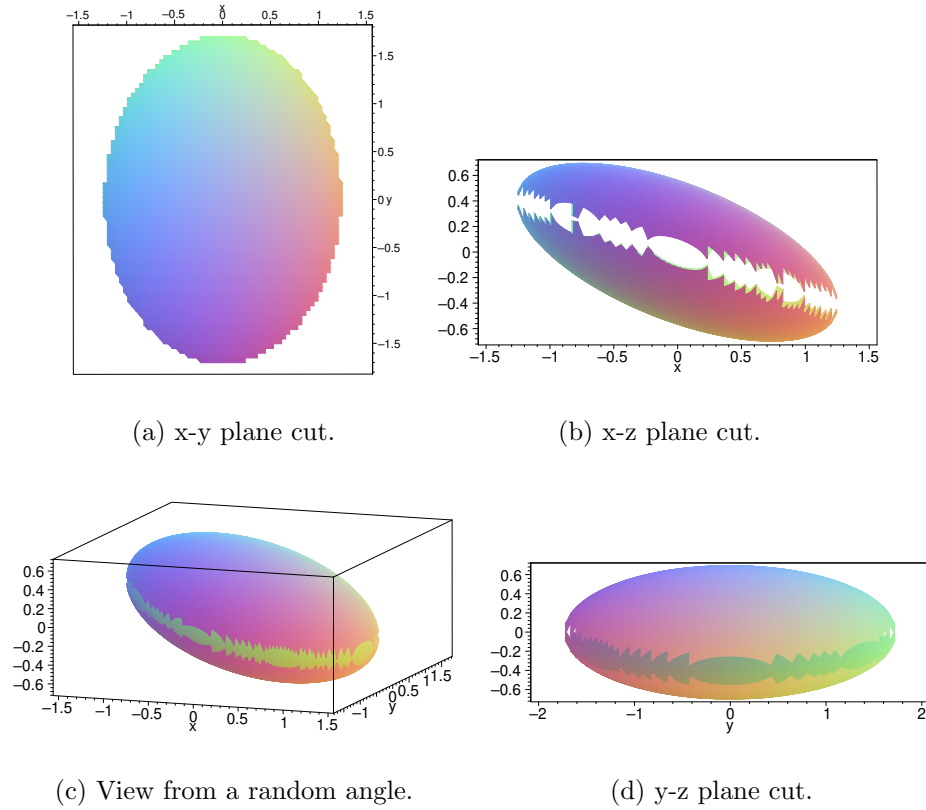


Figure 4.8: Different cross-sections of the triaxial ellipsoid which is an extremal Kerr black hole of spin  $a = 1$  distorted from its original shape by a  $\gamma = 2$  Lorentz boost toward  $\theta_\beta = 30^\circ$  direction which lies on the x-z plane. Starting from the upper left and going clockwise, the x-y, x-z, y-z cuts and the view from a random angle are displayed. The “jaws of doom” effect is an artifact of insufficient resolution, or rather, number of points used in generating the plots. Here, each plot contains 10,000 points. One can ‘close’ the jaws by increasing the number of particles at the expense of computing time.

triaxial ellipsoid in 3-dimensions. We apply this method to the case of a Kerr black hole with spin  $a = 1$  boosted toward  $\theta_\beta = 30^\circ$  with  $\gamma = 2$ . The resulting boost distorted ellipsoid is displayed from four different viewing angles in Fig.4.8. The “jaws of doom” effect in the figure is a resolution effect. These plots were made using 10000 particles (plot points) each. Increasing the number to something like  $10^7$  would greatly reduce the gap. However, this adds unnecessarily long computation times for compiling on a single machine.

#### 4.4 Elliptical Coordinates

Although the methods shown above suffice in providing us with the shape of the apparent horizon distorted by a boost. There is another way to obtain these surfaces using elliptical coordinates. Let us begin by once again looking at a simple ellipse in the x-z plane with long and short semi-axes given by  $a_1$  and  $a_2$  respectively. We begin with the equation of an ellipsoid written with a free parameter  $\xi \in [b, \infty)$  as given in [54]:

$$\frac{x^2 + y^2}{\xi^2 - a^2} + \frac{z^2}{\xi^2 - b^2} = 1 \quad (4.29)$$

For  $\xi > a$  we get a circle on the x-y plane with radius<sup>2</sup> =  $\xi^2 - a^2$ , and ellipses on the x-z and y-z planes.

We go from the rectangular coordinates  $x, y, z$  to the curvilinear (in this case ellipsoidal) coordinates  $\xi_1, \xi_2, \xi_3$  via the following relations given in

[54]

$$x = \xi_3 \sqrt{(\xi_1^2 + d^2)(1 - \xi_2^2)}, \quad (4.30)$$

$$y = \sqrt{(\xi_1^2 + d^2)(1 - \xi_2^2)(1 - \xi_3^2)}, \quad (4.31)$$

$$z = \xi_1 \xi_2. \quad (4.32)$$

$$(4.33)$$

Another coordinate transformation takes us from  $\xi_1, \xi_2, \xi_3$  to  $\mu, \theta, \phi$  with the following identifications

$$\xi_1 = d \sinh \mu; \quad \xi_2 = \cos \theta; \quad \xi_3 = \cos \phi \quad (4.34)$$

Combining Eqs.(4.33), (4.34), one can directly go from Cartesian  $x, y, z$  coordinates to ellipsoidal coordinates  $\mu, \theta, \phi$  with

$$x = d \cosh \mu \sin \theta \cos \phi, \quad (4.35)$$

$$y = d \cosh \mu \sin \theta \sin \phi, \quad (4.36)$$

$$z = d \sinh \mu \cos \theta. \quad (4.37)$$

The coordinate  $\mu$  acts as a radial distance and determines the ellipticity of the coordinate system.  $\mu \ll 1$  gives us a radial grid made up of very eccentric ellipses where as  $\mu = \infty$  gives us a perfectly circular radial grid. So as  $\mu$  increases, our grid goes from elongated ellipses near the origin to concentric circles very far away.

Finally, to truly accept the coordinates  $\mu, \theta, \phi$  as giving us ellipsoids we

must somehow obtain

$$\frac{x^2 + y^2}{a_1^2} + \frac{z^2}{a_2^2} = 1 \quad (4.38)$$

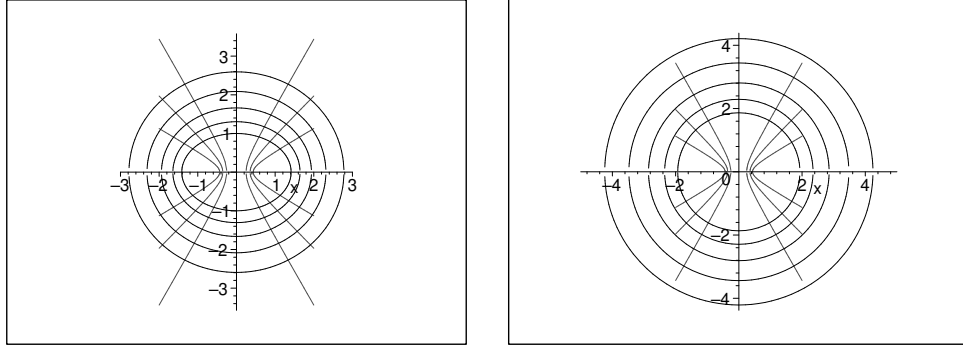
from the new identifications. This is accomplished by defining new constants

$$d^2 \equiv a_1^2 - a_2^2, \quad \mu_{min} = \tanh^{-1} \left( \frac{a_2}{a_1} \right). \quad (4.39)$$

A few simple steps of algebra using the well known identity  $\cosh^2 \mu - \sinh^2 \mu = 1$  gives us

$$d^2 \cosh^2 \mu_{min} = a_1^2, \quad d^2 \sinh^2 \mu_{min} = a_2^2.$$

We see that for  $\mu = \mu_{min}$ , the equation for an ellipsoid (Eq.(4.38)) is obtained with  $a_1, a_2$  as the axes. The value  $\mu_{min}$  is sometimes called the *mask radius* [55]. Using the ellipsoidal coordinates  $(\mu, \theta, \phi)$ , we can form a new coordinate grid around the black hole that starts at the horizon with  $\mu = \mu_{min}$  as the innermost ellipsoid and grows more and more spherical as  $\mu \rightarrow \infty$ . In Fig.4.9 below, we provide an example that uses different ellipsoidal grids around two different Kerr black holes. As before, we suppress the third dimension and only look at the x-z cuts ( $y = 0$  or  $\phi = \phi_\beta$ ) of the ellipsoids. So technically speaking, we are plotting the elliptical grid. The generalization to three dimensions is straightforward as shown in section 4.3. The hyperbolae in Fig.4.9 are curves of  $\theta = 60^\circ, 45^\circ, 30^\circ$ , respectively.  $\theta$  is similar to the usual polar angle of the spherical coordinates and asymptotically becomes identical to that.



(a) Kerr black hole with  $a = 1$ .

(b) Kerr black hole with  $a = 0.5$ .

Figure 4.9: Ellipsoidal coordinates for two Kerr black holes with spins  $a = 1, 0.5$  respectively. The innermost ellipses are the horizons. The hyperbolae are curves of  $\theta = 60^\circ, 45^\circ, 30^\circ$ , respectively.

#### 4.4.1 Elliptical Coordinates for Boosted Horizons

We now apply the polar coordinate rotation method of section 4.2 to the elliptical coordinates of the previous section. In fact, all we really need is the relevant information from that section. As one recalls, we need the new semi-major and semi-minor axis lengths  $a'_1, a'_2$  as well as the angle  $\Delta\theta$  by which the distorted ellipses rotate. For example, for a Kerr black hole with spins  $a = 1, 0.5$ , one gets, respectively

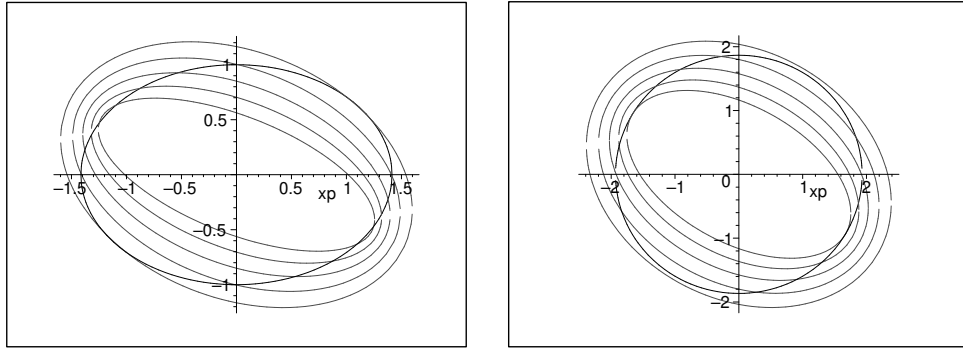
$$a'_1 = 1.33487, 1.91588 ;$$

$$a'_2 = 0.52972, 1.06663 ;$$

$$\Delta\theta = -0.3773, -0.50416 .$$



The distortion mostly comes from the crossterms in the equations for the ellipses such as the one in Eq.(4.25). Of course, here, our ellipses are written in terms of elliptical coordinates  $\mu, \theta$ , ( $\phi = \phi_\beta$ ) and new constants  $d$  and  $\mu_{\min}$ . We omit these details here and present them in appendix 4 which contains the relevant Maple code. We present the outcome in Fig.4.10 below where we have applied this method to Kerr black holes of spins  $a = 1$  and  $0.5$  for a boost of  $\gamma = 2$  along polar angle  $\theta_\beta = 30^\circ$  in the x-z plane as before.



(a) Kerr black hole with  $a = 1$ .

(b) Kerr black hole with  $a = 0.5$ .

Figure 4.10: Tilted ellipsoidal coordinates for two Kerr black holes with spins  $a = 1, 0.5$  respectively. The innermost ellipses are the horizons. The boost is in the x-z plane given by polar angle  $\theta_\beta = 30^\circ$  with  $\gamma = 2$  as before. The untilted ellipses represent the unboosted horizons. One can visually compare these figures with the figures obtained in sections 4.1, 4.2.

In summary, we have several methods that all yield the same shapes for the distorted horizons. Depending on what one wishes to do, one could either employ the discrete *tracer line* method or the continuous *polar plot* method. Or if one wishes, one could do everything in terms of ellipsoidal coordinates

from the start. Having different methods offers the user the option of picking the one that would suit his or her purposes best. Of course, the selling point of it all is that all of the methods agree on the shape and the size of the distorted apparent horizon.

## Chapter 5

# Area Invariance under Spin-Boost Transformations

Our calculation of the area invariance presented in chapter 3 is performed using a specific coordinate system and it is rather lengthy. It turns out that there is another way of showing the area invariance of a null surface using what is called a *spin-boost transformation* of a null tetrad. Such transformations are especially relevant in the so-called Newman-Penrose formalism of General Relativity [56]. The derivation of area invariance under spin-booster is presented in [38] by Poisson. There, Poisson shows that the 2-metric [of the 2-surface called the apparent horizon] is what remains invariant whereas we have shown that the 2-metric changes (in the specific coordinate system used), but the area of the horizon (the 2-dimensional integral of the determinant of the 2-metric) remains invariant. This crucial difference between these two methods is our first clue as to why one should not take the derivation in [38] as being compatible with the way we have shown the area invariance in Chapter 3, that is, under a Lorentz boost in the sense of a transformation to a moving coordinate system. More specifically, Poisson shows the area invariance under a specific class of transformations of a null tetrad in a spacetime

called a spin-boost transformation or a type III rotation. Although a spin-boost can be made to look very similar to a Lorentz transformation, below we will show that the spin-boost and the Lorentz boost as employed in this work yield different physical pictures. In Poisson’s own words [57]:

The phrase ‘Lorentz Boost’ is sometimes used to mean two different things. The usual meaning is ‘Lorentz transformation’, and this means a coordinate transformation to a moving frame; in this case the boost may change the form of the metric. The second meaning is mainly used in the context of Newman-Penrose formalism, and it means a change of the null tetrad...This does not change the form of the metric.

We will use the explicit example of a spin-boost transformation in Schwarzschild spacetime to illustrate the subtle but crucial differences between these seemingly identical transformations. First let us present Poisson’s derivation.

## 5.1 Poisson’s Derivation

The derivation below is identical to the one written in Poisson’s book [38] but provides a few more details.

Consider a null vector field  $\ell^\alpha$  tangent to the event horizon, and  $\lambda$ , the affine parameter for this vector field (i.e.  $\ell^\mu = \partial x^\mu / \partial \lambda$  thus  $\ell^\alpha \partial_\alpha \ell^\beta = \frac{\partial \ell^\beta}{\partial \lambda}$ ). The 2-dimensional cross-sections of the event horizon are what we call apparent

horizons and are orthogonal to  $\ell^\alpha$ . Under spin-boost transformations, the null vector changes its parametrization

$$\lambda \rightarrow \bar{\lambda}(\lambda, \theta^A) \quad (5.1)$$

where  $\theta^A$  ( $A = 1, 2$ ) are coordinates on the 2-dimensional cross sections transverse to the null vector  $\ell^\alpha$ . Here  $\bar{\lambda}$  is the new parameter given as a function of  $\lambda$  and  $\theta^A$ . Let us see how such a change of parametrization affects the geometry of the 2-surfaces. The differential form of Eq.(5.1) is

$$\begin{aligned} d\bar{\lambda} &= \left( \frac{\partial \bar{\lambda}}{\partial \lambda} \right)_{\theta^A} d\lambda + \left( \frac{\partial \bar{\lambda}}{\partial \theta^A} \right)_\lambda d\theta^A \\ &\equiv C d\lambda + c_A d\theta^A \end{aligned} \quad (5.2)$$

A displacement within the 3-dimensional null event horizon (parametrized by  $\lambda, \theta^A$  or  $\bar{\lambda}, \theta^A$ ) can be given in either coordinate system

$$\begin{aligned} dx^\alpha &= \ell^\alpha d\lambda + e_A^\alpha d\theta^A \\ &= \bar{\ell}^\alpha d\bar{\lambda} + \bar{e}_A^\alpha d\theta^A . \end{aligned} \quad (5.3)$$

where  $e_A^\alpha \equiv (\partial x^\alpha / \partial \theta^A)_\lambda$ .  $e_A^\alpha$  are the vector fields tangent to 2-dimensional cross sections (apparent horizons). Therefore, by construction  $\ell_\alpha e_A^\alpha = 0$ . The barred vector fields are given by

$$\bar{\ell}^\alpha \equiv (\partial x^\alpha / \partial \bar{\lambda})_{\theta^A} ; \quad \bar{e}_A^\alpha \equiv (\partial x^\alpha / \partial \theta^A)_{\bar{\lambda}} .$$

From Eq.(5.2), we see that the tangent vectors transform as

$$\bar{\ell}^\alpha = \frac{\partial x^\alpha}{\partial \bar{\lambda}} = \left( \frac{\partial \lambda}{\partial \bar{\lambda}} \right) \frac{\partial x^\alpha}{\partial \lambda} \equiv C^{-1} \ell^\alpha \quad (5.4)$$

and

$$\bar{e}_A^\alpha = e_A^\alpha + \ell^\alpha \left( \frac{d\lambda}{d\theta^A} \right)_{\bar{\lambda}} = e_A^\alpha - \ell^\alpha \frac{\partial \lambda}{\partial \bar{\lambda}} \frac{\partial \bar{\lambda}}{\partial \theta^A} = e_A^\alpha - c_A C^{-1} \ell^\alpha. \quad (5.5)$$

It can be easily verified that the barred vector fields are still orthogonal to each other. Since we are interested in the area of the apparent horizon, let us investigate what happens to the induced 2-metric of the cross sections. The 2-metric  $h_{AB}$  is defined as the projection (called a ‘pullback’ in differential geometry) of the 4-metric  $g_{\alpha\beta}$  onto the 2-surfaces via

$$h_{AB} \equiv g_{\alpha\beta} e_A^\alpha e_B^\beta \quad (5.6)$$

Under the reparametrization, the following changes take place

$$\begin{aligned} \bar{h}_{AB} &= g_{\alpha\beta} \bar{e}_A^\alpha \bar{e}_B^\beta \\ &= g_{\alpha\beta} (e_A^\alpha - c_A C^{-1} \ell^\alpha) (e_B^\beta - c_B C^{-1} \ell^\beta) \\ &= g_{\alpha\beta} e_A^\alpha e_B^\beta \\ &= h_{AB} \end{aligned} \quad (5.7)$$

From this, we see that the induced metric of the apparent horizon is invariant under a spin-boost transformation, therefore its area remains constant. This argument is made in a coordinate invariant manner. Basically, what is shown is that the tangent vectors to the horizon  $e_A^\alpha$  acquire a contribution in the

null direction under Lorentz the spin-boost transformation. Therefore, these contributions do not change the 2-metric given by Eq.(5.6).

There could be one reasonable objection to this derivation if one inspects Eq.(5.7) carefully. Then one would notice that in Eq.(5.7) we simply used the original spacetime metric  $g_{\alpha\beta}$  instead of using  $\bar{g}_{\alpha\beta}$  (the transformed spacetime metric). As we will show below this is not incorrect. This is because the transformation used in Eq.(5.1) is a spin-boost transformation and not a Lorentz coordinate transformation as it was used in Chapter 3. It turns out that the spacetime metric  $g_{\alpha\beta}$  remains invariant under these special transformations unlike in the case of a Lorentz boost. To see this, we must learn more about spin-boost (type III rotation) transformations and the null tetrad formalism of General Relativity.

## 5.2 Null Tetrad Formalism

Given any vacuum spacetime one can construct a basis made up of four linearly independent vectors whose coefficients depend on the spacetime variables. At each point  $\mathcal{P}$  in spacetime, one sets up a basis of four contravariant vectors. Let us denote this basis by  $e^\mu_{(a)}$  where  $\mu$  is the spacetime index and  $(a) = 1, \dots, 4$  is the tetrad index. We lower the spacetime index with the spacetime 4-metric as usual

$$e_{\mu(a)} = g_{\mu\nu} e^\nu_{(a)}.$$

The orthonormality conditions are given by the following

$$e^{\mu(a)}e_{\nu(a)} = \delta^{\mu}_{\nu}, \quad \text{and} \quad e^{\mu(a)}e_{\mu(b)} = \delta^{(a)}_{(b)}$$

where we raised the tetrad index using  $e^{\mu(a)} = \eta^{(a)(b)}e_{\mu(b)}$ .  $\eta^{(a)(b)}$  is the inverse of the “tetrad metric”  $\eta_{(a)(b)}$ , which is given to be

$$\eta_{(a)(b)} = e_{(a)}^{\mu}e_{\mu(b)}. \quad (5.8)$$

If one knows the tetrad a priori then one can construct the spacetime metric with

$$g_{\mu\nu} = e_{\mu}^{(a)}e_{\nu(a)}. \quad (5.9)$$

So far we have made no restrictions as to what kind of tetrad one can have. The Newman-Penrose formalism is a particular type of tetrad formalism where the four tetrad vectors are null vectors. In this formalism of General Relativity, one picks a null tetrad given by (we will be omitting the spacetime indices for the next few paragraphs)

$$e_{(a)} = (\ell, n, m, \bar{m}) \quad (5.10)$$

where each member of the tetrad is a null vector i.e.  $\ell^2 = n^2 = m^2 = \bar{m}^2 = 0$  and  $\bar{m}$  is the complex conjugate of  $m$ . In addition, one also must impose the following spacetime inner products on the tetrad

$$\ell \cdot n = -1 \quad \text{and} \quad m \cdot \bar{m} = 1 \quad (5.11)$$



with all other inner products equaling zero. It is not strictly necessary to impose the additional inner products in Eq.(5.11), but these extra conditions offer certain advantages which are mentioned in [40] that are beyond the scope of this thesis. With all the inner products known, we can now construct the tetrad metric

$$\eta_{(a)(b)} = \begin{pmatrix} 0 & -1 & 0 & 0 \\ -1 & 0 & 0 & 0 \\ 0 & 0 & 0 & 1 \\ 0 & 0 & 1 & 0 \end{pmatrix}. \quad (5.12)$$

Inverting this matrix and using it in  $e^{(a)} = \eta^{(a)(b)}e_{(b)}$ , we can determine the elements of the dual tetrad basis. They are

$$e^{(1)} = -n, \quad e^{(2)} = -\ell, \quad e^{(3)} = \bar{m}, \quad e^{(4)} = m. \quad (5.13)$$

Using these in Eq.(5.9) we obtain

$$g_{\mu\nu} = -\ell_\mu n_\nu - n_\mu \ell_\nu + m_\mu \bar{m}_\nu + \bar{m}_\mu m_\nu. \quad (5.14)$$

The null tetrad formalism is mainly used to extract gravitational waves from a given spacetime by looking at the so-called Weyl scalars ( $\Psi_0, \Psi_1, \Psi_2, \Psi_3, \Psi_4$ ), which are various contractions of the Weyl tensor  $C_{\alpha\beta\gamma\delta}$  with the members of the null tetrad. Our interest here does not lie with the Weyl scalars but rather with certain transformations of the null tetrad.

One transforms the null tetrad according to which Weyl scalar one wishes to remain constant. There are three such transformations. The one that is relevant here is called a *type III null rotation* of the tetrad. This is

also known as a ‘spin-boost transformation’. We will show below why this is a fitting term. In a type III transformation, one performs a rotation in the null  $m - \bar{m}$  plane and this results in the following changes for the null tetrad.

$$\ell \rightarrow A^{-1}\ell, \quad n \rightarrow A n, \quad m \rightarrow e^{i\theta}m, \quad \bar{m} \rightarrow e^{-i\theta}\bar{m} \quad (5.15)$$

where  $A$  and  $\theta$  are real valued parameters. There is one very special feature of this type of transformation and it is that it leaves the spacetime metric invariant. One could easily verify this by substituting the transformed vectors into Eq.(5.14) above. This is the reason why we used  $g_{\alpha\beta}$  in Eq.(5.7) and not  $\bar{g}_{\alpha\beta}$ . The two are the same under a type III rotation. What guarantee do we have that the transformation in Eq.(5.1) is a type III rotation? A quick look at Eqs.(5.4), (5.15) confirms that Eq.(5.1) is indeed a type III rotation which, as shown above, leaves  $g_{\alpha\beta}$  unchanged. The fact that  $g_{\alpha\beta}$  remains invariant is a clear indication that a type III rotation (spin-boost) is a transformation on the tetrad and not on the spacetime itself.

Having explained what spin-boost transformations are, let us now turn to the issue of why they might be relevant to the case of Lorentz boosts. To start, let us take a closer look at the spin-boost transformation. Given any two distinct null vectors  $\ell^\mu$  and  $n^\mu$  with  $\ell \cdot n = -1$ , one can construct a unit timelike vector  $t^\mu$  and a unit spacelike vector  $s^\mu$  out of these with

$$t = \frac{1}{\sqrt{2}}(\ell + n) \quad \text{and} \quad s = \frac{1}{\sqrt{2}}(\ell - n). \quad (5.16)$$

These equations are covariant so under the type III rotation (spin-boost) we get the following

$$\begin{aligned}
t \rightarrow \bar{t} &= \frac{1}{\sqrt{2}} (\bar{\ell} + \bar{n}) \\
&= \frac{1}{\sqrt{2}} (A^{-1}\ell + An) \\
&= \frac{A^2 + 1}{2A} t + \frac{1 - A^2}{2A} s.
\end{aligned} \tag{5.17}$$

For a suitable choice for the parameter A i.e.  $v/c \equiv \beta = (A^2 - 1)/(A^2 + 1)$  we obtain

$$\gamma = (1 - \beta^2)^{-1/2} = \left(1 - \frac{(A^2 - 1)^2}{(A^2 + 1)^2}\right)^{-1/2} = \frac{A^2 + 1}{2A}$$

and

$$\gamma\beta = \frac{(A^2 - 1)}{2A}$$

which change Eq.(5.17) to

$$\bar{t}^\mu = \gamma (t^\mu - \beta s^\mu) \tag{5.18}$$

where we have restored the spacetime index  $\mu$ . Similarly for  $s^\mu$  we get

$$\bar{s}^\mu = \gamma (s^\mu - \beta t^\mu). \tag{5.19}$$

Now, one clearly sees the connection between a type III rotation of the null tetrad and a Lorentz boost. Eqs.(5.18) and (5.19) look like Lorentz boost equations along vector  $s^\mu$ . It is for this reason that a type III rotation is also called a spin-boost transformation. That is, when this null rotation is applied

to a null tetrad, it gives a boost along  $s^\mu$  which looks just like a regular Lorentz boost.

It appears that we are now faced with a conundrum. We seemingly have a Lorentz transformation which, in one hand, changes the spacetime metric  $g_{\alpha\beta}$  as was done in chapter 3 and in the other hand, leaves  $g_{\alpha\beta}$  invariant as shown in this chapter. The inconsistency stems from the fact that a Lorentz boost can be taken to mean a coordinate transformation as in chapter 3 or a rotation of the tetrad as in this chapter. The point is that these two transformations result in fundamentally different physical pictures although often mistakenly grouped under the same name. We illustrate this explicitly by applying a spin-boost transformation to a well known black hole spacetime, namely the Schwarzschild solution. More precisely, what the spin-boost transformation does is a change of parametrization for the generators of the null tetrad, and not a transformation of the spacetime coordinates. So the basis vectors (null tetrad) change, but not the spacetime metric.

There is much more to Newman-Penrose formalism than what is mentioned here. In fact, this formalism plays a crucial role in gravitational wave extraction in spacetime which is especially relevant in Numerical Relativity and its applications toward gravitational wave detection. Interested readers can find more details in [58], [40] for example.

### 5.3 Spin-Boost Transformation for the Schwarzschild Spacetime

We are ultimately interested in connecting this formalism with boosted black holes. Therefore, in this section we will apply the spin-boost transformation to a Schwarzschild black hole. To begin, we must pick an appropriate null tetrad for our spacetime. The usual tetrad for the Schwarzschild spacetime will do just fine. This choice of tetrad picks a radially outgoing null vector for  $\ell^\mu$  and an ingoing one for  $n^\mu$ . The components in Schwarzschild coordinates  $(t, r, \theta, \phi)$  are

$$\begin{aligned}\ell^\mu &= \left( \left(1 - \frac{2M}{r}\right)^{-1}, 1, 0, 0 \right) \\ n^\mu &= \frac{1}{2} \left( 1, -\left(1 - \frac{2M}{r}\right), 0, 0 \right).\end{aligned}\tag{5.20}$$

Although we refer to the vectors  $\ell^\mu, n^\mu$  as the “null” tetrad, this is clearly misleading since a tetrad by definition requires four vectors. Here and for the rest of this chapter, we simply overlook the other two vectors of the tetrad  $(m^\mu, \bar{m}^\mu)$  as they are not relevant to our discussion. One can easily check that the conditions  $\ell^2 = n^2 = 0$  and  $\ell \cdot n = -1$  are satisfied. It can also be quickly verified that these vectors are null geodesics of Schwarzschild spacetime. However, because  $\ell$  and  $n$  are null, Eq.(5.20) is unique only up to a rescaling of the vectors. Any vector field of the form  $\ell^\mu = (f(r), g(r), 0, 0)$  satisfying the null condition  $\ell^2 = g_{tt}f(r)^2 + g_{rr}g(r)^2 = 0$  will be proportional to the explicit choice in Eq.(5.20). Another nice property of this tetrad is that the coordinate

$r$  is the affine parameter for  $\ell^\mu$  i.e.  $\ell^\alpha \partial_\alpha \ell^\beta = \frac{\partial \ell^\beta}{\partial r}$ . The tetrad in Eq.(5.20) is the most commonly used tetrad for Schwarzschild spacetime. However, we will show that this choice of tetrad is undesirable for a spin-boost transformation in the sense of a Lorentz transformation to a moving coordinate system. For the spacelike vector  $s^\mu$ , which is to be the boost direction, Eqs.(5.16) and (5.20) give a vector whose only non-zero spatial component is in the radial direction.

$$s^\mu = \frac{1}{\sqrt{2}} \left( \frac{r+2M}{2(r-2M)}, \frac{1}{2} \left( 3 - \frac{2M}{r} \right), 0, 0 \right) \quad (5.21)$$

If we now apply a spin-boost transformation on the tetrad of Eq.(5.20), the resulting Lorentz boost along  $s^\mu$  as given by Eqs.(5.18) and (5.19) translates to a boost in the *radial* direction as shown in Eq.(5.21). This is absurd as a Lorentz boost in the sense of a Lorentz transformation on the coordinates must always be *rectilinear* in direction and never radial. The concept of a ‘radial boost’ becomes especially vexing in the case of boosting a black hole. This would mean that all parts of the black hole would be boosted radially outward at once. This clearly makes no sense. So, although in a strict mathematical sense the spin-boost transformation equations (5.18) and (5.19) look just like a Lorentz transformation of coordinates, calling such a transformation a Lorentz boost of coordinates is misleading as the boost direction is radial in this case. Of course, the form of  $s^\mu$  completely depends on our initial choice of null tetrad vectors  $\ell^\mu$  and  $n^\mu$  and infinitely many choices exist. The exercise above simply shows us that the obvious tetrad choice in Schwarzschild spacetime is not the correct one. Let us see if we can actually find a proper tetrad so that

a spin-boost transformation would translate to a Lorentz boost in the sense of Lorentz transformation of coordinates in a *rectilinear* direction. Let us try a different coordinate system for our next attempt.

Kerr-Schild coordinates that we introduced in chapter 3 seem like a more suitable choice since by construction they are rectilinear. KS spatial coordinates  $(x, y, z)$  are related to Schwarzschild spatial coordinates in the same way as Cartesian coordinates relate to spherical. For example, the radial vector  $\mathbf{r}$  has components in KS coordinates given by  $\mathbf{r} = (x, y, z)$  with  $r^2 = x^2 + y^2 + z^2$  as was shown before in section 3.1. So, for ingoing KS coordinates, with the restriction  $\ell \cdot n = -1$ , we have

$$\ell^\mu = \frac{1}{2} \left( 1 - \frac{2M}{r} \right) \left( \frac{r+2M}{r-2M}, \frac{x}{r}, \frac{y}{r}, \frac{z}{r} \right) \quad \text{and} \quad n^\mu = \left( 1, -\frac{x}{r}, -\frac{y}{r}, -\frac{z}{r} \right) \quad (5.22)$$

which give

$$s^\mu = \frac{1}{\sqrt{2}} \left( \frac{r+2M}{r-2M} - \frac{1}{2} \left( 1 - \frac{2M}{r} \right), +\frac{1}{2} \left( 3 - \frac{2M}{r} \right) \left( \frac{x}{r}, \frac{y}{r}, \frac{z}{r} \right) \right) \quad (5.23)$$

and for outgoing KS, we have

$$\ell^\mu = \left( 1, \frac{x}{r}, \frac{y}{r}, \frac{z}{r} \right) \quad \text{and} \quad n^\mu = \frac{1}{2} \left( 1 - \frac{2M}{r} \right) \left( \frac{r+2M}{r-2M}, -\frac{x}{r}, -\frac{y}{r}, -\frac{z}{r} \right) \quad (5.24)$$

which give

$$s^\mu = \frac{1}{\sqrt{2}} \left( \frac{1}{2} \left( 1 + \frac{2M}{r} \right), \frac{1}{2} \left( 3 - \frac{2M}{r} \right) \left( \frac{x}{r}, \frac{y}{r}, \frac{z}{r} \right) \right). \quad (5.25)$$

In both Eqs.(5.23) and (5.25) the spatial component of the boost vector  $s^\mu$  points in the  $(\frac{x}{r}, \frac{y}{r}, \frac{z}{r})$  direction, which is nothing more than the radial vector  $r^{-1}\mathbf{r}$ . So once again, we ended up with a radial boost direction. This shows that standard choices for a null tetrad in any one of the three coordinate systems (Schwarzschild, ingoing KS, outgoing KS) yield radial directions for the boost, which are undesirable.

Let us approach this problem from another again. Let us first pick the rectilinear boost direction  $s^\mu$  instead of starting with the null tetrad. Then we will try to construct a null tetrad out of  $s^\mu$  and a suitable unit timelike vector. So, we will repeat the previous procedure in reverse order, that is, we will first determine the unit timelike and spacelike vectors then construct the null tetrad from these. To this end, it is more useful to look the Schwarzschild spacetime in Kerr-Schild (KS) coordinates. In order to determine a unit timelike vector  $T^\mu$  in a given spacetime with metric  $g_{\mu\nu}$  (we switch from  $t$  to  $T$  to avoid confusing the timelike vector  $T^\mu$  with the KS time coordinate  $t$ ) one must turn to the 3+1 ADM formalism of general relativity [60].

Given a spacetime  $(\mathcal{M}, g_{\mu\nu})$ , the ADM formalism foliates the 4-dimensional spacetime manifold  $\mathcal{M}$  with 3-dimensional spacelike hypersurfaces  $\Sigma_i$  (slices). This foliation is timelike meaning that for some scalar function  $\Phi$ , its gradient  $\nabla_\mu\Phi$  is normal to each spacelike slice of  $\Phi = \text{constant}$ , thus  $\nabla_\mu\Phi = \partial_\mu\Phi$  is timelike. The function  $\Phi$  is usually referred to as the global time function  $t$ . As the symbol  $t$  has already seen its fair share of use in this thesis, we will stick with  $\Phi$  here. The timelike separation between each slice is measured by



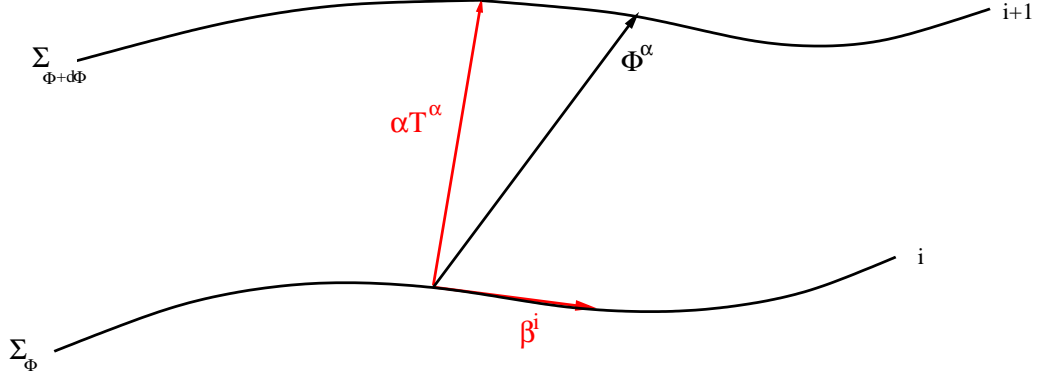


Figure 5.1: 3+1 ADM foliation of a spacetime into 3-dimensional spacelike hypersurfaces  $\Sigma$ .  $T^\mu$  is normal to each hypersurface and  $\Phi^\mu$  provides a direction of time flow.  $\beta^i$  accounts for the shift of each point on a given hypersurface. Two spatial dimensions have been suppressed.

a scalar called “the lapse”  $\alpha$ . Moreover, as each point on the  $i^{\text{th}}$  slice moves up in time to the  $(i + 1)^{\text{th}}$  slice, it might change its location in space due to changes in geometry or forces, that is, each point might *shift*. To account for this, one also introduces a 3-dimensional shift vector  $\beta^i$  (not to be confused with the boost parameter  $\beta$ ); here  $i$  denotes the spatial indices. Together the lapse  $\alpha$  and the shift  $\beta^i$  determine where in space and time each point on a hypersurface ends up. In short, they give us the time evolution i.e. the dynamics of a given spacetime. Fig. 5.1 illustrates the foliation of a spacetime.  $T^\mu$  is defined to be the unit timelike vector normal to each hypersurface. The timelike separation between each slice is given by  $\alpha T^\mu$ . If we let  $\Phi^\mu$  be the vector describing the infinitesimal spacetime displacement of a point from one hypersurface to the next, we can decompose this vector as follows:

$$\Phi^\mu = \alpha T^\mu + \beta^\mu \tag{5.26}$$

where  $\beta^\mu = (0, \beta^i)$  only has components in a given hypersurface.

Given a metric  $g_{\mu\nu}$  for a spacetime, the 3+1 ADM breakdown occurs as follows

$$g_{\mu\nu}dx^\mu dx^\nu = -(\alpha^2 - \beta^2)dt^2 + 2\beta_i dt dx^i + g_{ij} dx^i dx^j \quad (5.27)$$

where  $g_{ij}$  is called the *spatial metric* of the hypersurface and contains only the spatial components of  $g_{\mu\nu}$ . In order to determine the lapse and the shift of Schwarzschild spacetime in Kerr-Schild coordinates, we need to equate the metric of Eq.(5.27) with the Schwarzschild metric of Eq.(3.2). Let us display the metric of Eq.(3.2) explicitly in matrix format (symmetric entries have been left blank to avoid clutter)

$$g_{\mu\nu} = \begin{pmatrix} -\left(1 - \frac{2M}{r}\right) & \frac{2Mx}{r^2} & \frac{2My}{r^2} & \frac{2Mz}{r^2} \\ & 1 + \frac{2Mx^2}{r^3} & \frac{2Mxy}{r^3} & \frac{2Mxz}{r^3} \\ & & 1 + \frac{2My^2}{r^3} & \frac{2Myz}{r^3} \\ & & & 1 + \frac{2Mz^2}{r^3} \end{pmatrix}. \quad (5.28)$$

Here, as before,  $r^2 = x^2 + y^2 + z^2$ . The ADM formalism gives a unit timelike vector  $T^\mu$  normal to the 3-dimensional hypersurfaces in terms of the lapse function  $\alpha$  and the shift  $\beta^i$  by the following

$$T^\mu = (\alpha^{-1}, -\beta^i/\alpha). \quad (5.29)$$

From the metric in Eq. (5.28) we can immediately extract  $\beta_i = \frac{2M}{r^2}(x, y, z)$

and with a little work, we obtain  $\alpha, \beta^i$

$$\begin{aligned}\alpha &= \frac{1}{\sqrt{1 + \frac{2M}{r}}}, \\ \beta^i &= \frac{2M}{r^2} \left(1 + \frac{2M}{r}\right)^{-1} (x, y, z).\end{aligned}\tag{5.30}$$

With these, we can write the components  $T^\mu$  explicitly

$$T^\mu = \left( \sqrt{1 + \frac{2M}{r}}, -\frac{2M}{r^2} \left(1 + \frac{2M}{r}\right)^{-1/2} (x, y, z) \right).\tag{5.31}$$

A quick computation confirms that this is unit timelike i.e.  $T^2 = -1$ . We must now pick a spatial unit vector  $s^\mu$  such that the spin-boost transformation yields a rectilinear Lorentz boost direction. As we have seen above, the wrong choice might result in a meaningless direction for the boost. Let us pick the direction of the boost a priori then determine  $s^\mu$  accordingly. The x-direction will do as well as any. This means that once we construct  $\ell$  and  $n$  from  $T$  and  $s$  by inverting Eq.(5.16) and apply the spin-boost transformation on  $\ell$  and  $n$ , we should end up with a boost in the x-direction for the spacetime in Eqs.(5.18) and (5.19). However, simply picking  $s^\mu = X^\mu \equiv (0, 1, 0, 0)$  does not yield a unit spacelike vector. This needs to be properly normalized (i.e.  $s^2 = 1$ ) with respect to the KS metric of Eq.(5.28). The properly normalized unit spacelike vector spatially pointing in the x-direction now reads

$$s^\mu = \sqrt{\frac{r^3}{r^3 + 2Mx^2}} (0, 1, 0, 0).\tag{5.32}$$

A quick computation with the KS metric shows that this is indeed unit space-like ( $s^2 = 1$ ) and orthogonal to  $T^\mu$  ( $s \cdot T = 0$ ). Using Eqs.(5.16) to solve for  $\ell = (T + s)/\sqrt{2}$ , we obtain the null outgoing null vector

$$\ell^\mu = \begin{pmatrix} \frac{1}{\sqrt{2}} \sqrt{1 + \frac{2M}{r}} \\ \sqrt{\frac{r^3}{r^3 + 2Mx^2}} - \frac{2Mx}{r^2} \sqrt{\frac{r}{r+2M}} \\ -\frac{2My}{r^2} \sqrt{\frac{r}{r+2M}} \\ -\frac{2Mz}{r^2} \sqrt{\frac{r}{r+2M}} \end{pmatrix}. \quad (5.33)$$

Clearly  $\ell^\mu$  is null:  $\ell^2 = 0$  since  $T^2 = -1$ ,  $s^2 = 1$  and  $T \cdot s = 0$ . Similarly, we can easily obtain the ingoing null  $n^\mu$  via  $n = (T - s)/\sqrt{2}$ . Let us omit writing  $n^\mu$  explicitly.

To follow along with Poisson's formalism, we need to determine whether or not the vector field  $\ell^\mu$  is tangent to the event horizon and a geodesic of the Schwarzschild spacetime. The tangency condition is required because we want  $\ell^\mu$  to be a generator of the 3-dimensional event horizon. At a first glance, the answer to both questions seems to be negative. But let us do the computations properly anyway. We wish to determine whether Eq.(5.33) is a geodesic of the Schwarzschild spacetime or not. There are two ways to answer this question. One way would be to simply insert the vector field given in Eq.(5.33) into the geodesic equation in rectangular Kerr-Schild coordinates. Another way to go about this would be to transform  $\ell^\mu$  of Eq.(5.33) back to Schwarzschild spherical coordinates and use the geodesic equation in that coordinate system. As the metric in KS coordinates has no non-zero entries, it yields dozens of connection coefficients. Thus, it is more efficient to pick the

second method. So we will first transform the components of  $\ell^\mu$  in Eq.(5.33) to Schwarzschild spherical coordinates then insert that  $\ell^\mu$  into the geodesic equation. To that end, we first transform this vector field from KS Cartesian ( $\{x^\mu\}$ ) to Schwarzschild spherical coordinates ( $\{x^{\bar{\mu}}\}$ ). To do that, we must act on  $\ell^\mu$  with the Jacobian  $\Lambda_{\bar{\mu}}^\mu$  of the coordinate transformation. Let us interject here with a brief refresher on Jacobians (see [61] for a brief treatment).

Recall that any transformation from one coordinate system (say unbarred) to another (barred) is given by the Jacobian matrix  $\Lambda_{\bar{\mu}}^\mu$  with

$$\Lambda_{\bar{\mu}}^\mu = \frac{\partial x^\mu}{\partial x^{\bar{\mu}}} \quad \text{and} \quad \Lambda_{\mu}^{\bar{\mu}} = (\Lambda_{\bar{\mu}}^\mu)^{-1} = \frac{\partial x^{\bar{\mu}}}{\partial x^\mu} \quad (5.34)$$

where the second matrix is the inverse of the first and is used to go from barred to the unbarred coordinate system. Under these rules, a 1-form transforms according to

$$\ell_{\bar{\mu}} = \Lambda_{\bar{\mu}}^\mu \ell_\mu, \quad (5.35)$$

a vector according to

$$\ell^{\bar{\mu}} = \Lambda_{\mu}^{\bar{\mu}} l^\mu, \quad (5.36)$$

and finally the spacetime metric transforms as

$$\bar{g} = \Lambda^T g \Lambda \quad (5.37)$$

$$g = (\Lambda^T)^{-1} \bar{g} \Lambda^{-1}. \quad (5.38)$$

In the last two equations, we omitted writing the indices and left the transformation formulae in their schematic form to avoid unnecessary clutter.

Let us now put some specifics in. If one wishes to go from Schwarzschild spherical to Kerr-Schild Cartesian coordinates (to go the other way, one simply uses  $(\Lambda_{\bar{\mu}}^{\mu})^{-1} = \Lambda_{\mu}^{\bar{\mu}}$ ). The Jacobian matrix for this particular transformation is explicitly given to be

$$\Lambda_{\bar{\mu}}^{\mu} = \begin{pmatrix} 1 & -\frac{2M}{r-2M} \frac{x}{r} & -\frac{2M}{r-2M} \frac{y}{r} & -\frac{2M}{r-2M} \frac{z}{r} \\ 0 & x/r & y/r & z/r \\ 0 & \frac{\cos \theta \cos \phi}{r} & \frac{\cos \theta \sin \phi}{r} & -\frac{\sin \theta}{r} \\ 0 & -\frac{\sin \phi}{r \sin \theta} & \frac{\cos \phi}{r \sin \theta} & 0 \end{pmatrix}. \quad (5.39)$$

The inverse and the transpose of this Jacobian matrix can be obtained in a straightforward manner. There is one delicate detail that must be considered and that is determining which KS set of coordinates one is using. Given the Schwarzschild metric, one can write it in two equivalent but slightly different KS coordinates: ingoing and outgoing. The Jacobian matrix given above along with all the KS metrics displayed in this section are written with ingoing KS coordinates. If one wishes to use outgoing KS, one needs to make slight adjustments to the Jacobian, which consist of changing the signs of  $\Lambda_{11}$ ,  $\Lambda_{12}$ ,  $\Lambda_{13}$  components of the matrix in Eq.(5.39) (the time coordinate is labelled by 0th index.). Although the difference seems very subtle, it becomes pronounced when one compares Eqs.(5.22) with (5.24). The null vectors have different components in different KS coordinates.

Now that we have the explicit expression for the Jacobian at hand, using Eq.(5.36), we obtain  $\ell^{\bar{\mu}}$  in Schwarzschild coordinates. Omitting the algebraic

but hardly enlightening details, we get

$$\ell_{Sch}^{\bar{\mu}} = \frac{1}{\sqrt{2}} \begin{pmatrix} - \left(1 - \frac{2M}{r}\right)^{-1} \left( \frac{2Mx}{r^2} \sqrt{\frac{r^3}{r^3+2Mx^2}} - \sqrt{\frac{r}{r+2M}} \right) \\ \frac{x}{r} \sqrt{\frac{r^3}{r^3+2Mx^2}} - \frac{2M}{r} \sqrt{\frac{r}{r+2M}} \\ \sqrt{\frac{r^3}{r^3+2Mx^2}} \frac{1}{r} \cos \theta \cos \phi \\ - \sqrt{\frac{r^3}{r^3+2Mx^2}} \frac{\sin \phi}{r \sin \theta} \end{pmatrix} \quad (5.40)$$

where  $x = r \sin \theta \cos \phi$ . We left  $x$  as it is to save space in Eq.(5.40). Using Maple, we further confirmed these transformations and that the  $\ell_{Sch}^{\bar{\mu}}$  is null with respect to the Schwarzschild metric. Eq.(5.40) is the vector field that we want to investigate. A quick inspection of the components displayed in Eq.(5.40) is enough to hint that this vector field is probably not a geodesic of Schwarzschild spacetime. Indeed, inserting this vector field into the geodesic equation and letting Maple sort out the algebra, we confirm this: the vector field in Eq.(5.40) does not satisfy the geodesic equation in Schwarzschild spacetime. Furthermore, since it is not a geodesic, it is not affinely parametrized. In short, although this choice of the tetrad (assuming we also have  $n$ ,  $m$  and  $\bar{m}$ ) gives a boost in the x-direction  $(0, 1, 0, 0)$  under spin-boost transformation, the vector field  $\ell^\mu$  in Eq.(5.33) (which translates to  $\ell^{\bar{\mu}}$  given by Eq.(5.40) in Schwarzschild coordinates) can not be used in Poisson's derivation because it is not a generator of the event horizon. Once again, we came up short in our efforts to find a proper null tetrad that when transformed by spin-boosts yields a rectilinear Lorentz boost direction.

One reason why things did not work out when we picked  $s^\mu$  a priori

by making the choice  $s^\mu \propto X^\mu \equiv (0, 1, 0, 0)$  is because of the form of the timelike vector  $T^\mu$  in Eq. (5.31). It contains a shift in the spatial direction that naturally changes the spatial direction of  $s^\mu$  from  $X^\mu$  when one adds the two together to construct  $\ell^\mu$ . This means that whereas originally our vector was intended to point along the x-direction (spatially) because of the shift introduced by  $T^\mu$ , it will no longer point in that original direction. In fact, one could easily see this for oneself by simply taking the spatial components of  $\ell^\mu$  either in KS coordinates (Eq. (5.33)) or in Schwarzschild coordinates (Eq.(5.40)) and numerically evaluating them on a desired slice of  $r = 2M$  3-surface. For example, a  $\phi = 0$  slice would do. The result is that, the spatial component of  $\ell^\mu$  does not actually point outward toward the x-direction but instead it points inward with changing direction depending on one's latitude and longitude on the 2-sphere.

As a solution, one might propose to pick another unit timelike vector  $T^\mu$  that would not introduce such a shift. Unfortunately, a simple choice such as  $T^\mu = (1, 0, 0, 0)$  does not work because of the requirement that  $s \cdot T = 0$ . And because we have only two equations involving  $T^\mu$ :  $T^2 = -1$  and  $s \cdot T = 0$ , we do not have too many options when choosing the form of  $T^\mu$ . One could easily show that any choice of the form  $T^\mu = (A, Bx/r, By/r, Bz/r)$  will yield exactly the same vector as given in Eq. (5.31). In fact, we are limited to this choice by the structure of the ADM 3+1 breakdown as shown in Eq.(5.29). In KS coordinates, this  $T^\mu$  corresponds to a unit timelike vector that is orthogonal to  $t = \text{constant}$  (KS time) hypersurfaces. Not surprisingly, the explicit form



of the  $T^\mu$  is directly tied to the coordinates used.

The fact that  $\ell_{Sch}^{\bar{\mu}}$  in Eq.(5.40) is not a radially directed vector brings about other complications. Whereas in the radial case the vector fields  $e_A^\mu$  tangent to 2-dimensional spheres are orthogonal to  $\ell^\mu$  in Eq.(5.20) ( $l \cdot e_A = 0$ ), this certainly is not so with  $\ell_{Sch}^{\bar{\mu}}$  given in Eq.(5.40). Basically, this is yet another way of saying that this null vector field is not a generator of the event horizon as it is not orthogonal to  $r = \text{constant}$  surfaces. In other words, although it is null,  $\ell_{Sch}^{\bar{\mu}}$  is not tangent to the Schwarzschild event horizon. Recall that in order for Poisson's derivation of area invariance to work, one member of the null tetrad must be tangent to event horizon. Poisson emphasizes this point as well. Simply put,  $\ell_{Sch}^{\bar{\mu}}$  in Eq. (5.40) does not work.

Another objection can be directed toward the choice of the vector  $X^\mu = (0, 1, 0, 0)$  as pointing along the x-axis. That is,  $X^\mu$  may not be the true x-direction. One sees how this may be reasonable as the inner product of  $X^\mu$  with  $Y^\mu = (0, 0, 1, 0)$  and  $Z^\mu = (0, 0, 0, 1)$  does not equal zero, neither does  $Y \cdot Z$  by the way. In flat spacetime, these vectors would be orthogonal to each other but not so in a curved geometry like the Schwarzschild spacetime. In order for us to pick a more appropriate 'x-direction' (still referring to it as  $s^\mu$ ) than  $X^\mu$ , let us impose certain restrictions. Our choice should be orthogonal to  $Y^\mu = (0, 0, 1, 0)$  and  $Z^\mu = (0, 0, 0, 1)$  and should be unit spacelike. We can then write  $s^\mu$  as a linear combination of  $X^\mu, Y^\mu$  and  $Z^\mu$  as follows.

$$s^\mu = AX^\mu + BY^\mu + CZ^\mu$$

where the coefficients  $A$ ,  $B$  and  $C$  are our three unknowns determined by three equations

$$s \cdot Y = s \cdot Z = 0, \quad s^2 = 1 \quad (5.41)$$

This orthogonalization procedure is known as the Gram-Schmidt regularization. After a few pages of algebra we get

$$s^\mu = \frac{1}{r} \sqrt{\frac{r^3 + 2M(y^2 + z^2)}{r + 2M}} \left( 0, 1, -\frac{2Mxy}{r^3 + 2M(y^2 + z^2)}, -\frac{2Mxz}{r^3 + 2M(y^2 + z^2)} \right) \quad (5.42)$$

To make sure this is the correct vector, we further reconfirmed that  $s \cdot Y = s \cdot Z = 0$  and  $s^2 = 1$  using the solution we got in Eq.(5.42) and the metric of Eq.(5.28).

With the timelike vector given in Eq.(5.31) and the spacelike vector in Eq.(5.42) we can construct the null vector  $\ell^\mu$  as before. Once again, the vectors  $n$ ,  $m$  and  $\bar{m}$  are not relevant here but could be determined if needed. With  $\ell^\mu$  (and hypothetically  $n^\mu$ ) in hand, we can perform a spin-boost transformation on the vectors as was shown in Eq.(5.18). Following the same procedure from before we construct  $\ell^\mu$  whose components are even messier than our previous choice

$$\ell^\mu = \frac{1}{\sqrt{2}} \left( \begin{array}{c} \sqrt{\frac{r+2M}{r}} \\ \frac{1}{r\sqrt{r+2M}} \left( \sqrt{r^3 + 2M(y^2 + z^2)} - \frac{2Mx}{\sqrt{r}} \right) \\ -\frac{2My}{r\sqrt{r+2M}} \left( \frac{x}{\sqrt{r^3 + 2M(y^2 + z^2)}} + \frac{1}{\sqrt{r}} \right) \\ -\frac{2Mz}{r\sqrt{r+2M}} \left( \frac{x}{\sqrt{r^3 + 2M(y^2 + z^2)}} + \frac{1}{\sqrt{r}} \right) \end{array} \right). \quad (5.43)$$

From here on, we follow the same procedure of transforming Eq.(5.43) to

Schwarzschild coordinates then putting it into the geodesic equation in the Schwarzschild spacetime. We have chosen to omit all the tedious details here as they are not enlightening. Not surprisingly, we obtain the same result as before, that the vector field given in Eq.(5.43) is not a geodesic, nor tangent to the event horizon. As such, it is not suitable for use in Poisson's derivation.

To sum up the results of our failed attempts of the last few pages, we see that picking the direction  $s^\mu$  of the boost a priori and then constructing a null tetrad  $(\ell, n$  and the irrelevant  $m, \bar{m})$  from the vectors  $T^\mu$  and  $s^\mu$  fails at providing us with the necessary null vector  $\ell^\mu$  that would be a generator of the event horizon. In fact, we already know which vector fields are the generators of the event horizon in Schwarzschild spacetime. In Schwarzschild spherical coordinates, we have already seen that any vector field of the form

$$\ell^\mu = (f(r), g(r), 0, 0) \tag{5.44}$$

is a generator of the event horizon as long as the null vector condition

$$g_{00}f(r)^2 + g_{rr}g(r)^2 = 0 \tag{5.45}$$

is satisfied. However, as was shown above, any vector of this form projects a boost direction only radially. As we have discussed before, it does not make sense to talk about a boost in the radially outgoing or ingoing direction.

From what we have seen above, we can conclude that not all spin-boost transformations result in actual Lorentz boosts in the sense of Lorentz

transformations of the coordinates along a rectilinear direction. Sure enough, when one does a spin-boost transformation, one obtains equations (Eqs.(5.18) and (5.19)) that are identical to Lorentz transformation equations but one needs to keep in mind that one simply can not pick an arbitrary direction (the unit spacelike vector  $s^\mu$ ) for the boost. One might possibly end up with physically meaningless results such as a boost in the outgoing radial direction. The boost direction must be rectilinear. The main conclusion to draw from this is that spin-boost transformations should not be used to show the area invariance of apparent horizons under Lorentz boosts in the strict sense of what a Lorentz boost is usually understood to mean. This does not mean that Poisson's derivation is by any means wrong. All we are saying is that it is an incompatible way of showing the area invariance in the sense of chapter 3 of this thesis. Recall that, there we ended up with an altered 2-metric that still yielded an invariant area whereas Poisson's derivation in section 5.1 of this chapter results in an invariant 2-metric. As we have already mentioned in the beginning of this chapter, the reason for this disagreement is the fundamental but subtle difference between a spin-boost transformation and a Lorentz boost of coordinates. We have seen that, at least in the case of one explicit example using the Schwarzschild spacetime, the two boosts are not the same.

We had anticipated all of this at the beginning of this chapter and our tone is indicative of this with the punch line being the direct quote from Poisson. Let us close this chapter by once again reminding the reader of those words:

The phrase ‘Lorentz Boost’ is sometimes used to mean two different things. The usual meaning is ‘Lorentz transformation’, and this means a coordinate transformation to a moving frame; in this case the boost may change the form of the metric. The second meaning is mainly used in the context of Newman-Penrose formalism, and it means a change of the null tetrad, more specifically a rotation of it in the case of the spin-boost transformation. This does not change the form of the metric.

## Chapter 6

### Perturbations of a Boosted Black Hole

In this chapter, we will take another look at the spacetime metric describing a boosted black hole. By treating the boost velocity  $\beta \equiv v/c$  as a small perturbation parameter, we will rewrite the boosted metric up to  $\mathcal{O}(\beta^2)$  terms and expand the perturbed contributions [to the unperturbed background metric  $\mathring{g}_{\mu\nu}$ ] as tensor spherical harmonics [62]. We will then identify the modes of the perturbations and comment on the physical implications of each mode. Although we have mostly worked with Kerr black holes so far, here, we will focus on Schwarzschild black holes and include the Kerr case in the small spin limit ( $a \ll 1$ ) as a perturbation to the Schwarzschild background. A treatment of perturbations in the full Kerr background is beyond the scope of this thesis at this point. Black hole perturbation theory in Schwarzschild and Kerr backgrounds has been studied extensively and the literature in the subject is vast (see for example [40], [63], [65], [66]). Our notation and conventions will follow those of Regge & Wheeler [63] and Rezzolla [65].

We start by writing the metric of the spacetime as a background plus

a perturbation contribution

$$g_{\mu\nu} = \dot{g}_{\mu\nu} + h_{\mu\nu} \quad (6.1)$$

where  $|h_{\mu\nu}|/|\dot{g}_{\mu\nu}| \ll 1$ . Here  $\dot{g}_{\mu\nu}$  is the unperturbed background Schwarzschild metric given by  $\dot{g}_{\mu\nu} = \text{diag}(-1 + 2M/r, (1 - 2M/r)^{-1}, r^2, r^2 \sin^2 \theta)$ . Since the perturbation is due to a Lorentz boost, we should still have a vacuum spacetime, i.e.  $R_{\mu\nu} = \dot{R}_{\mu\nu} + \delta R_{\mu\nu} = 0$ .  $\delta R_{\mu\nu}$  is defined to be the contribution to the Ricci tensor coming from the perturbed sector of the metric, that is  $\delta R_{\mu\nu} = R_{\mu\nu}(h_{\mu\nu})$  (Keep in mind that  $R_{\mu\nu}$  is a second order differential operator acting on a metric).

In the usual perturbation scheme, one does not know the explicit form of  $h_{\mu\nu}$ . Instead, one solves  $R_{\mu\nu}(h_{\mu\nu}) = 0$  for the components of  $h_{\mu\nu}$ . The general technique for approaching this problem is to decompose  $h_{\mu\nu}$  into even and odd parity modes using tensor spherical harmonics. Given a tensor  $T_{\mu\nu}$ , one can break it down into components that behave differently under a parity transformation:

$$T_{\mu\nu}(t, r, \theta, \phi) = \sum_{\ell, m} a_{\ell m}(t, r) [A_{\ell m}^{\text{ax}}(\theta, \phi)]_{\mu\nu} + \sum_{\ell, m} b_{\ell m}(t, r) [B_{\ell m}^{\text{pol}}(\theta, \phi)]_{\mu\nu}. \quad (6.2)$$

Here,  $A_{\ell m}^{\text{ax}}$  and  $B_{\ell m}^{\text{pol}}$  represent the axial (odd) and the polar (even) tensorial

modes, which behave under the parity operator  $P$  in the following way

$$\begin{aligned}\text{axial : } P(A_{\mu\nu}) &= \tilde{A}_{\mu\nu} = (-1)^{\ell+1} A_{\mu\nu} , \\ \text{polar : } P(B_{\mu\nu}) &= \tilde{B}_{\mu\nu} = (-1)^\ell B_{\mu\nu} .\end{aligned}$$

The parity reversal operator  $P$  maps a point  $(\theta, \phi)$  on the 2-sphere to its mirror image via  $P : F(\theta, \phi) \rightarrow \tilde{F}(\pi - \theta, \phi + \pi)$ . Here,  $\ell$  carries the same integer values as in the case of ordinary spherical harmonics of quantum mechanics and electricity & magnetism (E&M), i.e.  $\ell = 0, 1, 2, \dots$  and  $-\ell \leq m \leq \ell$  as usual.

Following Regge & Wheeler [63], we can write down the most general perturbation contributions to the axial and polar modes

$$h_{\mu\nu}^{\text{ax}} = \begin{pmatrix} 0 & 0 & -h_0(t, r) \frac{1}{\sin\theta} \partial_\phi Y_{\ell m} & h_0(t, r) \sin\theta \partial_\theta Y_{\ell m} \\ 0 & 0 & -h_1(t, r) \frac{1}{\sin\theta} \partial_\phi Y_{\ell m} & h_1(t, r) \sin\theta \partial_\theta Y_{\ell m} \\ h_{t\theta} & h_{r\theta} & \frac{h_2(t, r)}{\sin\theta} (\partial_{\theta\phi}^2 - \cot\theta \partial_\phi) Y_{\ell m} & h_{\phi\theta} \\ h_{t\phi} & h_{r\phi} & \frac{h_2(t, r)}{2} \begin{pmatrix} \frac{1}{\sin\theta} \partial_\phi^2 + \cos\theta \partial_\theta \\ -\sin\theta \partial_\theta^2 \end{pmatrix} Y_{\ell m} & -h_2(t, r) \begin{pmatrix} \sin\theta \partial_{\theta\phi}^2 \\ -\cos\theta \partial_\phi \end{pmatrix} Y_{\ell m} \end{pmatrix} . \quad (6.3)$$

Above, we have omitted explicitly writing out all of the metric terms since the unspecified ones can easily be figured out using the symmetry of the metric ( $h_{\mu\nu} = h_{\nu\mu}$ ). Furthermore, we have used the notational convention  $\partial_{AB}^2 \equiv \partial^2 / \partial x^A \partial x^B$  with  $A, B = \theta, \phi$ . And, finally  $Y_{\ell m} = P_\ell(\cos\theta) e^{im\phi}$  are the standard spherical harmonics with  $P_\ell(\cos\theta)$  representing the usual Legendre polynomials.



In a similar fashion, one obtains the polar (even) perturbations:

$$h_{\mu\nu}^{\text{pol}} = \left( \begin{array}{cccc} (1 - 2M/r) H_0 & H_1 & h_0 \partial_\theta & h_0 \partial_\phi \\ H_1 & \frac{H_2}{1-2M/r} & h_1 \partial_\theta & h_1 \partial_\phi \\ h_{t\theta} & h_{r\theta} & r^2 (K + G \partial_\theta^2) & h_{\phi\theta} \\ h_{t\phi} & h_{r\phi} & r^2 G (\partial_\theta^2 - \cot \theta \partial_\phi) & r^2 \left[ \begin{array}{l} K \sin^2 \theta + \\ G (\partial_\phi^2 + \sin 2\theta \partial_\theta) \end{array} \right] \end{array} \right) \times Y_{\ell m} \quad (6.4)$$

It is implicitly assumed that all arbitrary functions  $H_0, H_1, h_0, h_1, K$  and  $G$  depend on  $t$  and  $r$ , i.e.  $H_0 = H_0(t, r)$  etc.

The above expressions (Eqs.(6.3) and (6.4)) for the axial (odd) and polar (even) modes of the perturbation metric  $h_{\mu\nu}$  can be further simplified by making a suitable *gauge transformation*. Consider the following infinitesimal coordinate transformation:

$$x'^{\mu} = x^{\mu} + \xi^{\mu} \quad (\xi^{\mu} \ll x^{\mu}) \quad (6.5)$$

then the perturbation changes according to

$$h_{\mu\nu}^{\text{new}} = h_{\mu\nu}^{\text{old}} + \xi_{\mu;\nu} + \xi_{\nu;\mu}. \quad (6.6)$$

This is quite similar to the gauge transformations one encounters in electromagnetism (cf. [67]). As in E&M, we are free to pick whatever form of  $\xi^{\mu}$  that would suit our purposes best. We can simply follow the gauge choice made in

the seminal work of Regge and Wheeler ([63]) now named after them. This allows one to ‘gauge away’ the unknown function  $h_2(t, r)$  in the odd case and the functions  $h_0(t, r), h_1(t, r), G(t, r)$  in the even case. Furthermore, Einstein equations in this gauge are independent of the axial harmonic number  $m$ . This means that the Schrödinger like radial wave equations (called Regge-Wheeler and Zerilli equations, cf. [63], [64]) do not change regardless of what the value for  $m$  may be. The reader is encouraged to consult [65], [66] for further explanations of this. Thus, without loss of generality, we can set  $m = 0$  and rewrite the results for the axial and polar perturbations to the spacetime metric of Schwarzschild black hole

$$h_{\mu\nu}^{\text{ax}} = \begin{pmatrix} 0 & 0 & 0 & h_0(t, r) \\ 0 & 0 & 0 & h_1(t, r) \\ 0 & 0 & 0 & 0 \\ h_0(t, r) & h_1(t, r) & 0 & 0 \end{pmatrix} \sin \theta \partial_\theta P_\ell(\cos \theta) \quad (6.7)$$

and

$$h_{\mu\nu}^{\text{pol}} = \begin{pmatrix} \frac{H_0(t, r)}{(1-2M/r)^{-1}} & H_1(t, r) & 0 & 0 \\ H_1(t, r) & \frac{H_2(t, r)}{1-2M/r} & 0 & 0 \\ 0 & 0 & r^2 K(t, r) & 0 \\ 0 & 0 & 0 & r^2 \sin^2 \theta K(t, r) \end{pmatrix} P_\ell(\cos \theta). \quad (6.8)$$

Using the expressions given in Eqs.(6.7) and (6.8) for the perturbation metric  $h_{\mu\nu}$  in Einstein’s equation  $\delta R_{\mu\nu} = 0$  leads one to the celebrated Regge-Wheeler and Zerilli equations of black hole perturbation theory. These equations look very much like the Schrödinger equation of quantum mechanics with non-zero

effective potentials  $V_{\text{eff}}(r)$  that are simply functions of the radial coordinate  $r$ . This is reached by assuming normal-mode like time behavior for the perturbations of the form

$$h_{\mu\nu} \sim \left( \begin{array}{c} 4 \times 4 \text{ matrix} \\ \text{that is a function} \\ \text{of } r \text{ only} \end{array} \right) e^{i\omega t} P_\ell(\cos \theta) \quad (6.9)$$

where  $\omega$  is the complex oscillation frequency. Solving the Schrödinger like differential equations yields the unknown functions that one needs to compute in order to determine the perturbations to the metric.

However, this will not be our approach here because we already know the cause of the perturbation (Lorentz boost) and the exact form of the perturbed metric (boosted Schwarzschild metric). For this reason, we will not choose this type of normal-mode behavior for the time dependence. Furthermore, one does not expect a boosted black hole to oscillate. In fact, a boosted black hole does not radiate since the Lorentz transformation is nothing more than replacing one inertial observer with another. We will show that this is indeed the case and that there is no radiation coming off the boosted Schwarzschild black hole expanded in terms of the boost parameter  $\beta$ . So, we will proceed in a manner that is the reverse of the usual procedure undertaken in perturbation theory. We will start with the boosted Schwarzschild metric expanded in powers of the perturbation parameter  $\beta$  up to  $\mathcal{O}(\beta^2)$ . Then, we will break the perturbation contributions down to their angular components which, in turn, will determine the  $\ell$  mode of each term.

## 6.1 Boosted Schwarzschild Black Hole

To perform the boost, we begin with the unperturbed Schwarzschild metric written in Cartesian-like Kerr-Schild coordinates just as we had done in chapter 3 (using the same barred notation)

$$\begin{aligned}
 ds^2 = & - d\bar{t}^2 + d\bar{x}^2 + d\bar{y}^2 + d\bar{z}^2 \\
 & + \frac{2M}{\bar{r}} \left[ \begin{aligned}
 & d\bar{t}^2 + \frac{\bar{x}^2}{\bar{r}^2} d\bar{x}^2 + \frac{\bar{y}^2}{\bar{r}^2} d\bar{y}^2 + \frac{\bar{z}^2}{\bar{r}^2} d\bar{z}^2 \\
 & - \frac{2\bar{x}}{\bar{r}} d\bar{t}d\bar{x} - \frac{2\bar{y}}{\bar{r}} d\bar{t}d\bar{y} - \frac{2\bar{z}}{\bar{r}} d\bar{t}d\bar{z} \\
 & + \frac{2\bar{x}\bar{y}}{\bar{r}^2} + \frac{2\bar{x}\bar{z}}{\bar{r}^2} d\bar{x}d\bar{z} + \frac{2\bar{y}\bar{z}}{\bar{r}^2} d\bar{y}d\bar{z}
 \end{aligned} \right] \quad (6.10)
 \end{aligned}$$

Since the Schwarzschild spacetime is spherically symmetric, one can boost in any direction one wishes. We shall pick the z-direction without loss of generality. As in section 3.1, we get the boost equations

$$\begin{aligned}
 \bar{t} = \gamma(t - \beta z) & \rightarrow d\bar{t} = \gamma(dt - \beta dz) \\
 & \rightarrow d\bar{t}^2 = \gamma^2(dt^2 - 2\beta dt dz + \beta^2 dz^2), \quad (6.11)
 \end{aligned}$$

$$\begin{aligned}
 \bar{z} = \gamma(z - \beta t) & \rightarrow d\bar{z} = \gamma(dz - \beta dt) \\
 & \rightarrow d\bar{z}^2 = \gamma^2(dz^2 - 2\beta dt dz + \beta^2 dt^2). \quad (6.12)
 \end{aligned}$$

Under these transformations the coordinate  $\bar{r}$  also will change as follows

$$\begin{aligned}
\bar{r} &= (\bar{x}^2 + \bar{y}^2 + \bar{z}^2)^{1/2} \\
&= (x^2 + y^2 + \gamma^2(z - \beta t)^2)^{1/2} \\
&\approx (x^2 + y^2 + z^2 - 2\beta t z)^{1/2} + \mathcal{O}(\beta^2) \\
&\approx r - \beta t \cos \theta + \mathcal{O}(\beta^2) \\
&\equiv r + \Delta r(\beta) + \Delta r(\beta^2)
\end{aligned} \tag{6.13}$$

where we already made use of  $z = r \cos \theta$ . Eq.(6.13) displays the shift in the radial coordinate as  $\mathcal{O}(\beta), \mathcal{O}(\beta^2)$  corrections  $\Delta r(\beta), \Delta r(\beta^2)$ , respectively. This polar tilt of  $r(\theta)$  was already seen in our visualizations of the boosted horizons (Section 4.2). To incorporate these changes in Eq.(6.10), we need to expand the following powers of  $\bar{r}$

$$\bar{r}^{-1} \approx r^{-1} \left( 1 + \frac{\beta t z}{r^2} \right), \tag{6.14}$$

$$\bar{r}^{-2} \approx r^{-2} \left( 1 + \frac{2\beta t z}{r^2} \right), \tag{6.15}$$

$$\bar{r}^{-3} \approx r^{-3} \left( 1 + \frac{3\beta t z}{r^2} \right). \tag{6.16}$$

The changes coming from  $\bar{r} - r \equiv \Delta r(\beta) \propto \mathcal{O}(\beta)$  will add extra terms to our perturbation expansion. We will compute these extra contributions separately and add them in at the end. For now, we will use  $\bar{r} = r$  and substitute the

Lorentz coordinate transformations into Eq.(6.10)

$$\begin{aligned}
ds_{\bar{r}=r}^2 &= -dt^2 + dx^2 + dy^2 + dz^2 & (6.17) \\
&+ \frac{2M}{r} \left[ \begin{aligned}
&\gamma^2(dt^2 - 2\beta dt dz + \beta^2 dz^2) + \frac{x^2}{r^2} dx^2 + \frac{y^2}{r^2} dy^2 \\
&+ \frac{\gamma^4}{r^2} (z^2 - 2\beta t z + \beta^2 t^2) (dz^2 - 2\beta dt dz + \beta^2 dt^2) \\
&- \frac{2\gamma}{r} (x dt dx - \beta x dx dz) - \frac{2\gamma}{r} (y dt dy - \beta y dy dz) \\
&- \frac{2\gamma^3}{r} \left( \begin{aligned}
&z dt dz - \beta z dt^2 - \beta t dt dz + \beta^2 t dt^2 \\
&- \beta z dz^2 + \beta^2 z dt dz + \beta^2 t dz^2 - \beta^3 t dt dz
\end{aligned} \right) \\
&+ \frac{2xy}{r^2} dx dy + \frac{2\gamma^2}{r^2} (x z dx dz - \beta x z dt dx - \beta t x dx dz + \beta^2 t x dt dx) \\
&+ \frac{2\gamma^2}{r^2} (y z dy dz - \beta y z dt dy - \beta t y dy dz + \beta^2 t y dt dy)
\end{aligned} \right].
\end{aligned}$$

where we have deliberately expanded all the terms in the metric with the anticipation of our next step, which will be grouping together all terms of  $\mathcal{O}(\beta)$  and  $\mathcal{O}(\beta^2)$  order. To this end, let us first explicitly evaluate the  $\gamma^n$ ,  $n = 1, 2, 3, 4$  terms.

$$\begin{aligned}
\gamma &= (1 - \beta^2)^{-1/2} \approx 1 + \beta^2/2 + \mathcal{O}(\beta^4) , \\
\gamma^2 &= (1 - \beta^2)^{-1} \approx 1 + \beta^2 + \mathcal{O}(\beta^4) , \\
\gamma^3 &= (1 - \beta^2)^{-3/2} \approx 1 + 3\beta^2/2 + \mathcal{O}(\beta^4) , \\
\gamma^4 &= (1 - \beta^2)^{-2} \approx 1 + 2\beta^2 + \mathcal{O}(\beta^4) ,
\end{aligned}$$

Substituting these expansions into the metric of Eq.(6.17), one obtains

$$\begin{aligned}
ds_{\bar{r}=r}^2 &= -dt^2 + dx^2 + dy^2 + dz^2 \\
&+ \frac{2M}{r} \left[ \begin{aligned}
&(1 + \beta^2)(dt^2 - 2\beta dt dz) + \frac{x^2}{r^2} dx^2 + \frac{y^2}{r^2} dy^2 \\
&(1 + 2\beta^2)(z^2 - 2\beta t z)(dz^2 - 2\beta dt dz)/r^2 \\
&-\frac{2}{r}(1 + \beta^2/2)(x dt dx - \beta x dx dz) - \frac{2}{r}(1 + \beta^2/2)(y dt dy - \beta y dy dz) \\
&-\frac{2}{r}(1 + 3\beta^2/2)(z dt dz - \beta z dt^2 - \beta t dt dz - \beta z dz^2) \\
&+\frac{2xy}{r^2} dx dy + \frac{2}{r^2}(1 + \beta^2)(xz dx dz - \beta x z dt dx - \beta t x dx dz) \\
&+\frac{2}{r^2}(1 + \beta^2)(yz dy dz - \beta y z dt dy - \beta t y dy dz)
\end{aligned} \right] \\
&+ \mathcal{O}(\beta^3) . \tag{6.18}
\end{aligned}$$

For starters, let us only look at the terms linear in  $\beta$  and see what kind of tensor spherical modes we get for  $h_{\mu\nu}$ . Now, we also insert the  $\mathcal{O}(\beta)$  adjustment coming from  $\bar{r} = r + \Delta r(\beta)$

$$\begin{aligned}
ds^2 &= - dt^2 + dx^2 + dy^2 + dz^2 \\
&+ \frac{2M}{r} [-dt + (x dx + y dy + z dz)/r]^2 \\
&+ \beta \times \frac{2M}{r} \left[ \begin{aligned}
&-2 dt dz - \frac{2}{r^2}(z^2 dt dz + t z dz^2) + \frac{2}{r} t dt dz \\
&+\frac{2}{r} x dx dz + \frac{2}{r} y dy dz + \frac{2}{r} z dt^2 + \frac{2}{r} z dz^2 \\
&-\frac{2}{r^2}(x z dt dx - t x dx dz - y z dt dy - t y dy dz)
\end{aligned} \right] \\
&+ \beta \times \frac{2M}{r} \frac{tz}{r^2} \left[ \begin{aligned}
&dt^2 + \frac{3}{r^2}(x^2 dx^2 + y^2 dy^2 + z^2 dz^2) \\
&-\frac{4}{r} dt (x dx + y dy + z dz) \\
&+\frac{6M}{r^2} (xy dx dy + xz dx dz + yz dy dz)
\end{aligned} \right] \\
&+ \mathcal{O}(\beta^2) . \tag{6.19}
\end{aligned}$$

The second  $\mathcal{O}(\beta)$  contribution comes from the corrections to the radial coordinate  $r$  as shown in Eqs.(6.13), (6.14) — (6.16). We call the line element due

to this perturbation  $h_{\mu\nu}^{\Delta r(\beta)} dx^\mu dx^\nu$ . We can put these  $\mathcal{O}(\beta)$  perturbations in matrix form

$$h_{\mu\nu} = \beta \frac{2M}{r} \begin{pmatrix} \frac{2z}{r} & -\frac{xz}{r^2} & -\frac{yz}{r^2} & \frac{t}{r} - \left(1 + \frac{z^2}{r^2}\right) \\ -\frac{xz}{r^2} & 0 & 0 & \frac{x}{r} \left(1 - \frac{t}{r}\right) \\ -\frac{yz}{r^2} & 0 & 0 & \frac{y}{r} \left(1 - \frac{t}{r}\right) \\ \frac{t}{r} - \left(1 + \frac{z^2}{r^2}\right) & \frac{x}{r} \left(1 - \frac{t}{r}\right) & \frac{y}{r} \left(1 - \frac{t}{r}\right) & \frac{2z}{r} \left(1 - \frac{t}{r}\right) \end{pmatrix} + h_{\mu\nu}^{\Delta r(\beta)} \quad (6.20)$$

where we have deliberately chosen to avoid displaying the matrix form of the  $\mathcal{O}(\beta)$  perturbation due to  $\bar{r} - r = \Delta r(\beta)$ . We must rewrite this entire perturbation metric in spherical coordinates in order to identify its proper spherical harmonic modes. The coordinate transformation from Kerr-Schild Cartesian coordinates to Schwarzschild spherical coordinates is straightforward. However, one needs to recall that Kerr-Schild time coordinate  $t_{KS}$  (labelled as  $t$  thus far in this chapter) is actually not the same as the Schwarzschild time coordinate  $t_{Sch}$ . The two are related via

$$dt_{KS} = dt_{Sch} - \frac{dr}{1 - \frac{2M}{r}}, \quad (6.21)$$

$$t_{KS} = t_{Sch} - r - 2M \ln(r - 2M). \quad (6.22)$$

We must make this coordinate substitution for the Kerr-Schild time coordinate used in Eq.(6.19). Despite the potential for confusion, we will now use  $t$  to denote the Schwarzschild time coordinate instead of the Kerr-Schild time coordinate. Furthermore, we need the following Cartesian to spherical coordinate



transformation equations:

$$x = r \sin \theta \cos \phi , \quad (6.23)$$

$$y = r \sin \theta \sin \phi , \quad (6.24)$$

$$z = r \cos \theta \quad (6.25)$$

and

$$dx = dr \sin \theta \cos \phi + d\theta r \cos \theta \cos \phi - d\phi r \sin \theta \sin \phi , \quad (6.26)$$

$$dy = dr \sin \theta \sin \phi + d\theta r \cos \theta \sin \phi + d\phi r \sin \theta \cos \phi , \quad (6.27)$$

$$dz = dr \cos \theta - d\theta r \sin \theta . \quad (6.28)$$

With all our coordinate substitutions at hand, we are now ready to transform the metric of Eq.(6.19). The algebra is straightforward but tedious which is why we choose to omit many steps here. However, we will include a few sample calculations then jump to the final result instead of dwelling over laborious details. Let us begin with the  $\Delta r$  contribution. Recall that, the perturbation to the line element due to this polar shift in  $r$  is given in Eq.(6.19)

$$\begin{aligned} h_{\mu\nu}^{\Delta r(\beta)} dx^\mu dx^\nu &= \beta \times \frac{2M}{r} \frac{t}{r} \frac{z}{r} \left[ dt^2 - \frac{4}{r} dt (x dx + y dy + z dz) \right. \\ &\quad \left. + \frac{3}{r^2} \left( x^2 dx^2 + y^2 dy^2 + z^2 dz^2 \right. \right. \\ &\quad \left. \left. + 2xy dx dy + 2xz dx dz + 2yz dy dz \right) \right] \\ &= \beta \frac{2M}{r} \frac{t}{r} \cos \theta \left[ dt^2 + \frac{3}{r^2} (r dr)^2 - \frac{4}{r} dt dr \right] \\ &= \beta \frac{2M}{r} \frac{t}{r} [dt^2 + 3dr^2 - 4dt dr] . \end{aligned} \quad (6.29)$$

Last step for this term is replacing the Kerr-Schild time coordinate with the Schwarzschild time coordinate. Rewriting Eqs.(6.21) and (6.22) schematically as

$$dt = dt_{Sch} + f dr \rightarrow t = t_{Sch} + F \quad (6.30)$$

where  $f = f(r)$  and  $F = \int f dr$ , we get (now using  $t$  to label  $t_{Sch}$ )

$$h_{\mu\nu}^{\Delta r(\beta)} dx^\mu dx^\nu = \beta \frac{2M}{r} \frac{t + F}{r} \cos \theta [dt^2 - 2dt dr + (f^2 - 4f + 3)dr^2] \quad (6.31)$$

where  $f = -(1 - 2M/r)^{-1}$  and  $F = -r - 2M \ln(r - 2M)$ . Next, let us return to the other  $\mathcal{O}(\beta)$  perturbation in Eq.(6.19) and transform it into spherical coordinates. We will not include the entire calculation here for reasons that have already been mentioned above. So, let us pick the  $tt$ - and  $xz$ -component of Eq.(6.19) to work with as examples.

$$\begin{aligned} \frac{2}{r} z dt_{KS}^2 &= 2 \cos \theta \left( dt^2 - \frac{2dt dr}{1 - \frac{2M}{r}} + \frac{dr^2}{\left(1 - \frac{2M}{r}\right)^2} \right) \\ \frac{2x}{r} \left(1 - \frac{t_{KS}}{r}\right) dx dz &= 2 \sin \theta \cos \phi \left( 2 - \frac{t}{r} + \frac{2M}{r} \ln(r - 2M) \right) \\ &\quad \times \left[ \begin{aligned} &dr^2 \sin \theta \cos \theta \cos \phi + dr d\theta r \cos 2\theta \\ &-d\theta^2 r^2 \sin \theta \cos \theta \cos \phi - dr d\phi r \sin \theta \cos \theta \sin \phi \\ &+d\theta d\phi r^2 \sin^2 \theta \sin \phi \end{aligned} \right]. \end{aligned}$$

We have a total of seven such terms, all of which must be rewritten in spherical coordinates then recombined as components of a rank-2 tensor in spherical coordinates. Once again, we will omit explicitly constructing each component and only display a few illustrative cases. For starters, it is not hard to see that

all  $h_{\mu\phi} = h_{\phi\mu}$  components should be equal to zero because the axial coordinate  $\phi$  is orthogonal to the boost direction  $z$  and thus does not change. Therefore, the metric should have only polar perturbations and no axial perturbations whatsoever. Let us demonstrate this explicitly. For example

$$h_{t\phi} \propto 2r \sin^2 \theta \cos \theta \sin \phi \cos \phi - 2r \sin^2 \theta \cos \theta \sin \phi \cos \phi = 0. \quad (6.32)$$

Similarly, we get

$$h_{r\phi} = h_{\theta\phi} = h_{\phi\phi} = 0. \quad (6.33)$$

Next, we present a less trivial computation for a non-zero component. Factoring out the  $\beta \times 2M/r$  for the time being, we have

$$\begin{aligned} \frac{r}{2M\beta} h_{t\theta} &= 2r \sin \theta \left( -\cos^2 \theta \cos^2 \phi - \cos^2 \theta \sin^2 \phi + 1 + \cos^2 \theta \right) \\ &\quad + \left( 1 - \frac{t}{r} + \frac{2M}{r} \ln(r - 2M) \right) \\ &= 2r \sin \theta \left( 2 - \frac{t}{r} + \frac{2M}{r} \ln(r - 2M) \right). \end{aligned}$$

The computation for other non-zero components of  $h_{\mu\nu}$  is similar and hence will be omitted. Combining all the results and writing the perturbation out in matrix form once again, we obtain the spherical coordinate version of the first line of Eq.(6.20)

$$\begin{aligned} h_{\mu\nu}^{\mathcal{O}(\beta), \bar{r}=r} &= \beta \times \frac{2M}{r} \cos \theta \quad (6.34) \\ &\times \begin{pmatrix} 2 & [2f - 2 + \frac{t+F}{r}] & r \tan \theta \left( 1 - \frac{t+F}{r} \right) & 0 \\ h_{tr} & 2 \left[ (1-f) \left( 1 - f - \frac{t+F}{r} \right) \right] & -2r \tan \theta \left( 1 - \frac{t+F}{r} \right) \left( \frac{r-M}{r-2M} \right) & 0 \\ h_{t\theta} & h_{r\theta} & 0 & 0 \\ 0 & 0 & 0 & 0 \end{pmatrix} \end{aligned}$$

where  $f = -(1 - 2M/r)^{-1}$  and  $F = -r - 2M \ln(r - 2M)$  as was shown in Eqs.(6.21) and (6.22). To this, we must also add the contribution from Eq.(6.31), which was due to  $\bar{r} - r \sim \mathcal{O}(\beta)$  as one might recall. Written out in matrix form, this perturbation looks like

$$h_{\mu\nu}^{\Delta r(\beta)} = \beta \times \frac{2M}{r} \cos \theta \begin{pmatrix} \frac{t+F}{r} & -\frac{t+F}{r} & 0 & 0 \\ -\frac{t+F}{r} & f^2 - 4f + 3 & 0 & 0 \\ 0 & 0 & 0 & 0 \\ 0 & 0 & 0 & 0 \end{pmatrix}. \quad (6.35)$$

The total perturbation at linear order in  $\beta$  is the sum of the metrics in Eqs.(6.34) and (6.35), which is given by

$$h_{\mu\nu}^{\mathcal{O}(\beta)} = \beta \times \frac{2M}{r} \cos \theta \quad (6.36)$$

$$\times \begin{pmatrix} 2 + \frac{t+F}{r} & 2(f-1) & r \tan \theta \left(1 - \frac{t+F}{r}\right) & 0 \\ h_{tr} & \begin{pmatrix} 3f^2 - 8f + 5 \\ -2(1-f)\frac{t+F}{r} \end{pmatrix} & -2r \tan \theta \left(1 - \frac{t+F}{r}\right) \left(\frac{r-M}{r-2M}\right) & 0 \\ h_{t\theta} & h_{r\theta} & 0 & 0 \\ 0 & 0 & 0 & 0 \end{pmatrix}.$$

It was already clear that, there are no axial modes of perturbation in this spacetime. This is once again confirmed when one compares the metric of Eq.(6.36) with Eqs.(6.7) and (6.8); and matches it with the polar perturbations given by Eq.(6.8). At this point, all that remains is to identify the mode of the perturbation. We do this by equating Eq.(6.36) with Eq.(6.8) and solving for the unknown spherical harmonic(s)  $Y_{\ell m}$ . On the way, we also determine

the perturbation metric functions  $H_0, H_1, H_2, h_0, h_1$ . Recalling that

$$Y_{10} = \sqrt{\frac{3}{4\pi}} \cos \theta.$$

We match the metrics term by term. For example, setting the  $tt$ -component of Eq.(6.36) equal to that of Eq.(6.8), we get

$$h_{tt} = \left(2 + \frac{t+F}{r}\right) \cos \theta = \left(1 - \frac{2M}{r}\right) H_0(t, r) Y_{\ell m} \quad (6.37)$$

which gives  $\ell, m = 1, 0$  and  $H_0(t, r) = \left(2 + \frac{t+F}{r}\right) \sqrt{\frac{4\pi}{3}} \left(1 - \frac{2M}{r}\right)^{-1}$ . Similarly,

$$h_{tr} = 2 \cos \theta (f - 1) = H_1(t, r) Y_{\ell m} \quad (6.38)$$

which results in  $\ell, m = 1, 0$  and

$$H_1(t, r) = 2 \sqrt{\frac{4\pi}{3}} (f - 1). \quad (6.39)$$

It should be expected that each matched term should yield the same spherical harmonic mode  $\ell, m = 1, 0$  otherwise something would have been wrong with our expansion. Instead of continuing to match all of the remaining metric terms, we simply present the result. That is

$$\text{Eq.(6.36)} = \begin{pmatrix} H_0 \left(1 - \frac{2M}{r}\right) & H_1 & h_0 \partial_\theta & 0 \\ H_1 & H_2 \left(1 - \frac{2M}{r}\right)^{-1} & h_1 \partial_\theta & 0 \\ h_0 \partial_\theta & h_1 \partial_\theta & 0 & 0 \\ 0 & 0 & 0 & 0 \end{pmatrix} Y_{10}. \quad (6.40)$$

The unknown perturbation metric functions are now completely determined

$$H_0(t, r) = -\sqrt{\frac{4\pi}{3}} f \left( 2 + \frac{t+F}{r} \right), \quad (6.41)$$

$$H_1(t, r) = 2\sqrt{\frac{4\pi}{3}} (f - 1), \quad (6.42)$$

$$H_2(t, r) = \sqrt{\frac{4\pi}{3}} \left( -3f + 8 + 2 \left( \frac{1}{f} - 1 \right) \frac{t+F}{r} - \frac{5}{r} \right), \quad (6.43)$$

$$h_0(t, r) = -\sqrt{\frac{4\pi}{3}} r \left( 1 - \frac{t+F}{r} \right), \quad (6.44)$$

$$h_1(t, r) = 2\sqrt{\frac{4\pi}{3}} r \left( \frac{r-M}{r-2M} \right) \left( 1 - \frac{t+F}{r} \right) \quad (6.45)$$

where, once again

$$f(r) = -\frac{1}{1 - \frac{2M}{r}} \quad \text{and} \quad F(r) = -r - 2M \ln(r - 2M)$$

The important result to focus on is the harmonic mode of the perturbation, which is  $\ell = 1$  at the linear order in  $\beta$ . This is indeed what one should expect to obtain for several reasons: (1) Because of the formulation of the perturbation theory, at the linear order, one should expect to see only linear corrections, which come from the  $\ell = 1$  mode. (2) The act of boosting imparts momentum to the black hole. Momentum =  $mv$ , is the first time derivative of the gravitational dipole ( $\ell = 1$ ) moment, which is mass $\times$ distance. As can be seen from Eqs.(6.41) — (6.45), the  $\ell = 1$  mode has a non-zero time derivative coming from the terms that contain  $\partial[(t+F)/r]/\partial t = 1/r \neq 0$ , thus this mode imparts some momentum to the black hole. This picture agrees with what one physically expects from boosting a black hole. With that said, it is

obvious from the work thus far that there are no modes higher than  $\ell = 1$  at  $\mathcal{O}(\beta)$  so let us look at higher order perturbations next.

## 6.2 Slow Spin Kerr as a Perturbation of Schwarzschild

Let us now incorporate the Kerr spacetime into this scheme. There are detailed studies of perturbation theory in full Kerr background (cf. [40], [68], [69]) but the machinery and the background needed to do perturbation calculations in fully Kerr background is very involved and would add at least another 100 pages to this thesis (possibly 600 pages according to Chandrasekhar). As such, we will consider the Kerr spacetime only in the *slow spin* limit ( $a \ll 1$  in dimensionless mass units) and treat it as a perturbation of the Schwarzschild background. The Kerr metric for the  $a \ll 1$  case is given by

$$ds^2 = - \left( 1 - \frac{2M}{r} \right) dt^2 + \frac{dr^2}{1 - \frac{2M}{r}} + r^2 d\Omega^2 - \frac{4Ma}{r} \sin^2 \theta dt d\phi \quad (6.46)$$

where  $d\Omega^2$  is the metric on the 2-sphere. It is clear from the  $dt d\phi$  term that the spin dependent perturbation will contribute to the axial modes. Recalling from Eq.(6.7) that axial modes scale as  $h_{(0 \text{ or } 1)}(t, r) \sin \theta \partial_\theta Y_{\ell m}$ , the  $\sin^2 \theta$  term in  $h_{t\phi}$  is seen to come from  $\sin \theta \partial_\theta \cos \theta \propto \sin \theta \partial_\theta Y_{10}$ , indicating the harmonic to be the  $\ell = 1, m = 0$  mode. This  $\ell = 1$  mode is now associated with the *angular* momentum of the black hole. Just as the  $\mathcal{O}(\beta)$  boost perturbation resulted in a non-radiating  $\ell = 1$  mode, this off-diagonal perturbation to the Schwarzschild metric also only yields a non-radiating  $\ell = 1$  mode. This, of

course, is necessary on general principles since it is well known that only modes with  $\ell \geq 2$  radiate (cf. [61], [30]) and more importantly that the Kerr solution does not radiate whatsoever. After all, what we considered in Eq.(6.46) simply is the slow spin limit of the Kerr solution. With the perturbation due to the spin in the unboosted case classified, we can now boost this spacetime along the z-axis and investigate the outcome.

### 6.2.1 Slow Spin Kerr Boosted

In order to boost, the  $\mathcal{O}(a)$  perturbation needs to be rewritten in unboosted (barred) Kerr-Schild coordinates

$$\begin{aligned}
h_{\mu\nu}^{\mathcal{O}(a)} dx^\mu dx^\nu &= -\frac{4Ma}{\bar{r}} \sin^2 \bar{\theta} d\bar{t}_{Sch} d\bar{\phi} \\
&= -\frac{4Ma}{\bar{r}} \sin^2 \bar{\theta} \left( d\bar{t}_{KS} + \frac{d\bar{r}}{1 - \frac{2M}{\bar{r}}} \right) d\bar{\phi} \\
&= -\frac{4Ma}{\bar{r}^3} (\bar{x}^2 + \bar{y}^2) \left( d\bar{t}_{KS} + \frac{\bar{x}d\bar{x} + \bar{y}d\bar{y} + \bar{z}d\bar{z}}{\bar{r} - 2M} \right) d\bar{\phi}. \tag{6.47}
\end{aligned}$$

In the above equation,  $\bar{x}, \bar{y}$  and  $\bar{\phi}$  coordinates will remain unchanged under the boost since they are orthogonal to the boost direction. We have also once again distinguished between the Schwarzschild and the Kerr-Schild time coordinates by use of proper labelling. But now, we will go back to simply using  $t$  to label  $t_{KS}$  as was done before. Next, we boost along the z-axis and the  $t, z$  coordinates change according to Eqs.(6.11) and (6.12). We also need to take the  $\Delta r(\beta)$  shift into account because of  $\bar{r}^{-3}$ . With the new adjustments,



Eq.(6.47) becomes

$$\begin{aligned}
h_{\mu\nu}dx^\mu dx^\nu &= -\frac{4Ma}{r}\sin^2\theta\left[dt - \beta dz + \frac{xdx + ydy + (z - \beta t)(dz - \beta dt)}{r - 2M}\right]d\phi \\
&\quad -\frac{4Ma}{r}\sin^2\theta\left(1 + \frac{3t\beta}{r}\cos\theta\right)\left[dt + \frac{xdx + ydy + zdz}{r - 2M}\right]d\phi + \mathcal{O}(a\beta^2) \\
&= \text{Eq.}(6.47) + h_{\mu\nu}^{\mathcal{O}(a\beta)}dx^\mu dx^\nu + \mathcal{O}(a\beta^2)
\end{aligned} \tag{6.48}$$

where

$$\begin{aligned}
h_{\mu\nu}^{\mathcal{O}(a\beta)}dx^\mu dx^\nu &= \frac{4a\beta M}{r}\sin^2\theta\left[dz + \frac{zdt + tdz}{r - 2M}\right]d\phi \\
&\quad -\frac{4a\beta M}{r}\frac{3t}{r}\sin^2\theta\cos\theta\left[dt + \frac{rdr}{r - 2M}\right]d\phi
\end{aligned} \tag{6.49}$$

$$\tag{6.50}$$

Transforming the remaining terms to spherical coordinates, at  $\mathcal{O}(a\beta)$ , we obtain

$$h_{t\phi}^{\mathcal{O}(a\beta)} = a\beta \times \frac{2M}{r^2} \left(1 - \frac{6t}{r}\right) \sin^2\theta \cos\theta, \tag{6.51}$$

$$h_{r\phi}^{\mathcal{O}(a\beta)} = a\beta \times \frac{2M}{r^3} \left[1 + \frac{t}{r - 2M}\right] \sin^2\theta \cos\theta, \tag{6.52}$$

$$h_{\theta\phi}^{\mathcal{O}(a\beta)} = -a\beta \times \frac{2M}{r^2} \left[1 + \frac{t}{r - 2M}\right] \sin^3\theta. \tag{6.53}$$

If one wishes, one can further transform the Kerr-Schild time coordinate  $t$  back to Schwarzschild time coordinate as was done before. As this does not add new insight to the calculation, we choose to omit this step in this section. Matching these metric elements with the appropriate components of Eq.(6.7)

we get

$$\begin{aligned}
h_{t\phi}^{\mathcal{O}(a\beta)} &= h_0(t, r) \sin \theta \partial_\theta Y_{\ell m}, \\
h_{r\phi}^{\mathcal{O}(a\beta)} &= h_1(t, r) \sin \theta \partial_\theta Y_{\ell m}, \\
h_{\theta\phi}^{\mathcal{O}(a\beta)} &= \frac{1}{2} h_2(t, r) (\cos \theta \partial_\theta - \sin \theta \partial_\theta^2) Y_{\ell m}.
\end{aligned}$$

Term by term matching each time yields the same harmonic for this  $\mathcal{O}(a\beta)$  perturbation:  $Y_{\ell m} = Y_{20}$ . That is, under the boost, the  $\mathcal{O}(a)$ ,  $\ell = 1$  mode has yielded an  $\mathcal{O}(a\beta)$ ,  $\ell = 2$  mode. This should not be surprising because of the particular formulation of the perturbation scheme. The linear perturbations gave a contribution in the  $\ell = 1$  mode and the quadratic order perturbations are expected to contribute in the  $\ell = 2$  mode. Here, since both  $a$  and  $\beta$  are used as linear perturbation parameters,  $\mathcal{O}(a\beta)$  terms are taken to be quadratic order perturbations to  $\mathring{g}_{\mu\nu}$ .

The real question is whether these  $\ell = 2$  modes radiate or not. It is well known that gravitational radiation is due to the third time derivative of the quadrupole moment in the leading order (cf. [70], [30]). A closer look at Eqs.(6.51), (6.52) and (6.53) gives us our functions  $h_0(t, r)$ ,  $h_1(t, r)$  and  $h_2(t, r)$ . Note that  $h_0, h_1$  and  $h_2$  are all linear in  $t$ . Thus, we see that the quadrupole contribution to the background metric has no third order time derivative ( $\partial^3/\partial t^3$ ) and therefore does not emit gravitational radiation. Once again, using perturbation theory, we have confirmed that at least in the small spin limit, boosted Kerr black holes do not radiate. Let us close this chapter with a similar computation of the perturbations to second order but this time

for the  $\mathcal{O}(\beta^2)$  contribution to the Schwarzschild background.

### 6.3 Boosted Schwarzschild to Second Order

We go back to the Schwarzschild black hole boosted along the z-direction as given in Eq.(6.18) and extract the  $\mathcal{O}(\beta^2)$  terms. This gives

$$h_{\mu\nu}^{\mathcal{O}(\beta^2)} dx^\mu dx^\nu = \frac{2M\beta^2}{r} \left[ \begin{array}{l} dz^2 + dt^2 + \frac{2}{r^2} z^2 dz^2 + \frac{4}{r^2} tz dt dz \\ -\frac{1}{r}(x dt dx + y dt dy) - \frac{5}{r} z dt dz - \frac{2}{r}(tdz^2 + tdt^2) \\ + \frac{2}{r^2} xz dx dz + \frac{2}{r^2} yz dy dz + \frac{t^2}{r^2} dz^2 + \frac{z^2}{r^2} dt^2 \\ + \frac{2}{r^2} tx dt dx + \frac{2}{r^2} ty dt dy \end{array} \right] + h_{\mu\nu}^{\mathcal{O}(\beta)\Delta r(\beta)} + h_{\mu\nu}^{\Delta r(\beta^2)} \quad (6.54)$$

where  $t$  is the Kerr-Schild time coordinate  $t_{KS}$ . The first term, now labelled  $^{(I)}h_{\mu\nu}^{\mathcal{O}(\beta^2)}$ , comes from the  $r = \bar{r}$  approximation and the  $h_{\mu\nu}^{\mathcal{O}(\beta)\Delta r(\beta)}$  term is due the coupling of  $\mathcal{O}(\beta)$  elements of the ‘bare’ perturbed metric of Eq.(6.20) with the  $\mathcal{O}(\beta)$  correction to  $\bar{r}$ . Of course, now we also need to add the perturbations due to  $\bar{r} - r$  at the second order in  $\beta$ . Re-Taylor expanding powers of  $\bar{r}$  to  $\mathcal{O}(\beta^2)$  we obtain the following corrections

$$\bar{r}^{-1} = r^{-1} \left( 1 + \beta \frac{t}{r} \cos \theta + \frac{3}{2} \beta^2 \frac{t^2}{r^2} \cos^2 \theta \right) \quad (6.55)$$

$$\bar{r}^{-2} = r^{-2} \left( 1 + 2\beta \frac{t}{r} \cos \theta + 4\beta^2 \frac{t^2}{r^2} \cos^2 \theta \right) \quad (6.56)$$

$$\bar{r}^{-3} = r^{-3} \left( 1 + 3\beta \frac{t}{r} \cos \theta + \frac{15}{2} \beta^2 \frac{t^2}{r^2} \cos^2 \theta \right) \quad (6.57)$$

The  $\mathcal{O}(\beta^2)$  perturbed line element due to Eqs.(6.55) – (6.57) equals

$$h_{\mu\nu}^{\Delta r(\beta^2)} = \frac{2M\beta^2}{r} \frac{t^2}{r^2} \frac{z^2}{r^2} \left[ \frac{3}{2} dt^2 + 8 dt dr + \frac{15}{2} dr^2 \right] \quad (6.58)$$

The  $\Delta r(\beta)$  coupling with  $\mathcal{O}(\beta)$  terms yields the following perturbation

$$h_{\mu\nu}^{\mathcal{O}(\beta)\Delta r(\beta)} dx^\mu dx^\nu = \frac{4M\beta^2}{r} \frac{t}{r} \frac{z}{r} \quad (6.59)$$

$$\times \left[ \begin{aligned} & -\frac{3}{r^2} ((x dx + y dy)(z dt + t dz) + t z dz^2 + z^2 dt dz) \\ & -2 dt dz + \frac{2}{r} ((x dx + y dy) dz + z dt^2 + z dz^2 + t dz dt) \end{aligned} \right].$$

Once again, Eq.(6.54) must be rewritten in spherical Schwarzschild coordinates. Let us start with the  $\Delta r(\beta^2)$  perturbation of Eq.(6.58). This term is very straightforward to evaluate. As always, we must include the change in the time coordinate given by Eqs.(6.21), (6.22) and Eq.(6.30), which results in

$$h_{\mu\nu}^{\Delta r(\beta^2)} = \frac{2M\beta^2}{r} \frac{(t+F)^2}{r^2} \cos^2 \theta \quad (6.60)$$

$$\times \left[ \frac{3}{2} dt^2 + (3f+8) dt dr + \left( \frac{3}{2} f^2 + 8f + \frac{15}{2} \right) dr^2 \right].$$

For Eq.(6.59), we use transformation equations (6.23) through (6.28) and also employ the identity

$$d(x^2 + y^2) = d(r^2 \sin^2 \theta) = dr r \sin^2 \theta + d\theta r^2 \sin \theta \cos \theta. \quad (6.61)$$

Eq.(6.59) now becomes

$$\begin{aligned}
h_{\mu\nu}^{\mathcal{O}(\beta)\Delta r(\beta)} dx^\mu dx^\nu &= \frac{4M\beta^2 t}{r} \frac{t}{r} \cos \theta \\
&\times \left[ \begin{aligned} &2r \cos \theta dt^2 + [2(t-r) - 3r \cos^2 \theta] dt dz \\ &(dr r \sin^2 \theta + d\theta r^2 \sin \theta \cos \theta) \left( \left(2 - \frac{3t}{r}\right) dz - 3 \cos \theta dt \right) \\ &+(2r \cos \theta - 3t \cos \theta) dz^2 \end{aligned} \right].
\end{aligned} \tag{6.62}$$

In this equation, we have deliberately avoided expanding all the Cartesian coordinates in terms of their corresponding spherical variables to avoid further clutter. We will continue our notational ‘sloppiness’ and use  $t$  to denote  $t_{Sch}$  from now on. Using all the proper transformation equations, we simply rewrite Eq.(6.62) in Schwarzschild coordinates. For the sake of saving space, we omit many pages of intensive algebra and present the final expression as components of  $h_{\mu\nu}^{\mathcal{O}(\beta)\Delta r(\beta)}$

$$h_{tt}^{\mathcal{O}(\beta)\Delta r(\beta)} = \frac{4M\beta^2 t}{r} \frac{t}{r} \cos^2 \theta \tag{6.63}$$

$$h_{tr}^{\mathcal{O}(\beta)\Delta r(\beta)} = \frac{4M\beta^2 t}{r} \frac{t}{r} \left[ 2 \left( \frac{t}{r} - \frac{5}{2} \right) + 4f \right] \cos^2 \theta \tag{6.64}$$

$$h_{t\theta}^{\mathcal{O}(\beta)\Delta r(\beta)} = -\frac{4M\beta^2 t}{r} \frac{t}{r} 2 \left( \frac{t}{r} - 1 \right) \sin \theta \cos \theta \tag{6.65}$$

$$h_{rr}^{\mathcal{O}(\beta)\Delta r(\beta)} = \frac{4M\beta^2 t}{r} \frac{t}{r} \left[ 2 \left( \frac{t}{r} - \frac{5}{2} + f \right) f + \left( 2 - \frac{3t}{r} \right) \right] \cos^2 \theta \tag{6.66}$$

$$h_{r\theta}^{\mathcal{O}(\beta)\Delta r(\beta)} = \frac{4M\beta^2 t}{r} \frac{t}{r} [(3t - 2r) - 2(t - r)f] \sin \theta \cos \theta \tag{6.67}$$

$$h_{\theta\theta}^{\mathcal{O}(\beta)\Delta r(\beta)} = 0$$

We follow the same procedure for the  ${}^{(I)}h_{\mu\nu}^{\mathcal{O}(\beta^2)}$  metric term explicitly given in Eq.(6.54). The line element from this perturbation metric equals

$$\begin{aligned}
{}^{(I)}h_{\mu\nu}^{\mathcal{O}(\beta^2)} dx^\mu dx^\nu = & \frac{2M\beta^2}{r} & (6.68) \\
\times & \left[ \begin{aligned} & \left( 1 - \frac{2(t+F)}{r} + \cos^2 \theta \right) dt^2 \\ & + \left[ \begin{aligned} & \left( 2f + \frac{2F}{r} + \frac{2t}{r} - 1 - \frac{4f(t+F)}{r} \right) \\ & + \left( 2f + \frac{2F}{r} + \frac{2t}{r} - 4 \right) \cos^2 \theta \end{aligned} \right] dt dr \\ & + 2(2r - F - t) \sin \theta \cos \theta dt d\theta \\ & + \left[ \begin{aligned} & f(f-1) \left( 1 - \frac{2(t+F)}{r} \right) \\ & + \left( 3 - 4f + \frac{2(f-1)(t+F)}{r} + f^2 + \left( \frac{t+F}{r} \right)^2 \right) \cos^2 \theta \end{aligned} \right] dr^2 \\ & + 2 \left[ (t+F)(2-f) + 2(f-1)r - \frac{1}{r}(t+F)^2 \right] \sin \theta \cos \theta dr d\theta \\ & + [r^2 - 2r(t+F) + (t+F)^2] \sin^2 \theta d\theta^2 \end{aligned} \right]
\end{aligned}$$

where  $t$  is already taken to be the Schwarzschild time coordinate and  $f, F$  have the usual meanings. In Eq.(6.68), we have tried to visually separate terms that have angular dependence from those that do not. To this perturbation, we must add the  $\Delta r(\beta^2)$  contribution given by Eq.(6.60) and the  $\mathcal{O}(\beta)\Delta r(\beta)$  terms coming from Eqs.(6.63) — (6.67). The total perturbation is given by

$$h_{\mu\nu}^{\mathcal{O}(\beta^2)} = {}^{(I)}h_{\mu\nu}^{\mathcal{O}(\beta^2)} + h_{\mu\nu}^{\mathcal{O}(\beta)\Delta r(\beta)} + h_{\mu\nu}^{\Delta r(\beta^2)}. \quad (6.69)$$

There is no point in carrying out the algebra explicitly. Here, we are only interested in the harmonic modes of the perturbations. Therefore, we will proceed by inspection. A through survey of each metric term by comparing with Eq.(6.4) yields the following  $\mathcal{O}(\beta^2)$  corrections to the Schwarzschild

metric written out in schematic fashion

$$\begin{aligned}
h_{tt} &\sim H_0^{\ell=0} + H_0^{\ell=2} \cos^2 \theta \propto H_0^{\ell=0}(t, r) Y_{00} + H_0^{\ell=2}(t, r) Y_{20} \\
h_{tr} &\sim H_1^{\ell=0} + H_1^{\ell=2} \cos^2 \theta \propto H_1^{\ell=0}(t, r) Y_{00} + H_1^{\ell=2}(t, r) Y_{20} \\
h_{rr} &\sim H_2^{\ell=0} + H_2^{\ell=2} \cos^2 \theta \propto H_2^{\ell=0}(t, r) Y_{00} + H_2^{\ell=2}(t, r) Y_{20} \\
h_{t\theta} &\sim h_0(t, r)^{\ell=2} \sin \theta \cos \theta \propto h_0^{\ell=2} \partial_\theta Y_{20} \\
h_{r\theta} &\sim h_1(t, r)^{\ell=2} \sin \theta \cos \theta \propto h_1^{\ell=2} \partial_\theta Y_{20} \\
h_{\theta\theta} &\sim \sin^2 \theta \propto Y_{00} \text{ terms} + Y_{20} \text{ terms}
\end{aligned}$$

All  $\mathcal{O}(\beta^2)$  perturbations are in  $\ell = 2$  and  $\ell = 0$  modes.  $\ell = 0$  is a correction to the mass (monopole) and is expected to be there since under boosts mass increases by a factor of  $\gamma \approx 1 + \mathcal{O}(\beta^2)$ . As for the  $\ell = 2$  contribution, a closer look at Eq.(6.68) reveals that perturbation metric functions are at most quadratic in  $t$  of the form  $(t + F(r))^2$ . Therefore, their third time derivative is zero. As we expected, these  $\mathcal{O}(\beta^2)$  modes do not radiate either.

Let us summarize our results in the following table

Spacetime	Order	Mode	Gravitational Radiation
Boosted Sch.	$\mathcal{O}(\beta)$	$\ell = 1$ polar	No
Boosted Sch.	$\mathcal{O}(\beta^2)$	$\ell = 2$ polar	No
		$\ell = 0$ polar	No
Kerr ( $a \ll 1$ )	$\mathcal{O}(a)$	$\ell = 1$ axial	No
Boosted Kerr ( $a \ll 1$ )	$\mathcal{O}(a\beta)$	$\ell = 2$ axial	No

Table 6.1: Summary of all perturbations that contribute to the background Schwarzschild metric. Here, we have included the Kerr metric in the slow spin ( $a \ll 1$ ) limit as a perturbation to the Schwarzschild background. Quadratic terms give modes up to  $\ell = 2$ . However, as expected, there is no radiation coming from these modes.



## Chapter 7

### Conclusions

In this thesis, we took a long look at apparent horizons in General Relativity. We began in chapter 1 by defining various black hole boundaries used in the literature and presented the generally agreed definition for the apparent horizon (AH) of a black hole. Because apparent horizons are 2-dimensional cross-sections (in non-dynamical spacetimes) of the event horizon, which is a null 3-dimensional hypersurface, the area of the AH does not change under Lorentz boosts. We presented a lengthy calculation in chapter 3 that explicitly showed the area invariance for apparent horizons in Schwarzschild and Kerr spacetimes under arbitrary Lorentz boosts. We also provided numerical results where we computed the horizon masses ( $M_H$ ) (Area =  $4\pi M_H^2$ ) of two Schwarzschild black holes boosted toward each other. Our numerically solved initial data for this configuration confirmed the area invariance of AH as expected. In chapter 4, we presented several compatible methods for visualizing the shapes of boost distorted horizons. Our results agreed with former results derived by Huq in [71] but we have generalized the method to include any boost direction as well as providing 3-dimensional figures for these triaxial ellipsoids. Chapter 5 opened with an elegant calculation showing the area invariance un-

der what is known as a spin-boost transformation. Although the resulting coordinate transformation equations under the spin-boost looked like Lorentz boost equations; by explicitly applying this method to the Schwarzschild metric, we showed the subtle but fundamental difference between a Lorentz boost on spacetime coordinates and a spin-boost transformation (a rotation of the null tetrad). Finally in chapter 6, we investigated the perturbations induced on the Schwarzschild spacetime by a Lorentz boost and investigated the resulting modes of perturbation up to quadratic order in perturbation parameters  $\beta$  (boost parameter) and  $a$  (black hole spin parameter). Despite obtaining quadrupole mode ( $\ell = 2$ ) contributions to the background metric, we showed that none of these quadrupole modes emit gravitational radiation, hence confirming the well known fact that boosted black holes do not radiate.

We can further extend some of the work we have done here. The numerical work presented in section 3.2 can be generalized to include the head-on collision of spinning Kerr black holes. The collision can also be modified to be off-center and thus become a “grazing” collision with some impact parameter  $b$  representing the closest point of approach for the black holes. With these adjustments, the binding energy and horizon mass curves of figures 3.2 and 3.3 will certainly look different. On the analytical front, we can accompany the numerical work by determining explicitly the terms that add to the divergence of the binding energy  $E_b$  from the  $1/r$  Newtonian behavior. To this end, we plan to use post-Newtonian theory to figure out the higher order contributions, which will scale in powers of  $GM_{total}/r$ . We have already stated in section 3.2

that the leading order correction to the binding energy is a term that scales as  $1/r^2$ . The inclusion of spin for the black holes will further introduce  $\mathbf{S}_1 \cdot \mathbf{S}_2$  type spin-spin coupling terms. Moreover, the off-axis collision will add orbital angular momentum to the system that previously would have had none. This will add  $\mathbf{L} \cdot \mathbf{S}$  type spin-orbit coupling terms to the total energy of the system and thus modify the binding energy even more. All of these contributions can be written down analytically up to fifth or seventh post-Newtonian order meaning that the scaling goes as  $(v/c)^5$  or  $(v/c)^7$ . The analytical results from post-Newtonian expansion can be compared with the numerical results to see how closely the expressions match.

On another front, one can use the area invariance of the horizon (or invariance of the horizon mass  $M_H$ ) as a tool to gauge the accuracy of initial data used in a General Relativistic simulation. Of course, one needs to keep in mind that the apparent horizon area is an adiabatic invariant, which means that it grows adiabatically (as separation distance  $r$  decreases) in the presence of strong gravity due to another black hole. However, for black holes that are sufficiently far apart ( $r > 20M$  will do, see Fig.3.3), the invariance of  $M_H$  is pretty robust and becomes exact at the limit  $r \rightarrow \infty$ . Since the ultimate goal of numerical relativity is to start runs with very large orbital separations and observe the binary execute hundreds, maybe even thousands of orbits (this is especially relevant for extreme mass ratio inspirals [72] in the context of the upcoming Laser Interferometer Space Antenna (LISA)) prior to the merger; the potential use of apparent horizon area invariance to measure the accuracy

of initial data will certainly become a more relevant test in the future.

## Appendix

## Appendix 1

### Maple Code for The Tracer Line Method

Here, we display the Maple code used to compute the shape and location of horizons distorted by Lorentz boosts. The code presented here pertains to the ‘tracer line method’ of section 4.1.

```
> with(plots):
```

```
Warning, the name changecoords has been redefined
```

Kerr black hole has spin  $a = 0.75M$ , Lorentz gamma factor of root of 2 and boosted

at a 45 degree angle.

```
> M:=1: J:=1: beta:=sqrt(3)/2: g:=1/sqrt(1-beta^2):
```

```
> theta:=Pi/6:
```

The Kerr horizon is located at  $r_{\text{plus}}$ , which is given by

```
> rp:=M+sqrt(M^2-J^2):
```

$a_1$  and  $a_2$  label the long and short axes of the ellipse on the x-z plane

```

> a1:=sqrt(rp^2+ J^2); a2:=rp;
      a1 :=  $\sqrt{2}$ 
      a2 := 1

```

Next, we plot the undistorted horizon. This will be an ellipse with a1 and a2 labeling the axes.

Instead of immediately displaying the plot, we store it as 2 curves e1 and e2 for the upper

and lower halves of the ellipse, respectively. We also plot a line l1 indicating the boost direction.

```

> e1:=plot(a2*sqrt(1-x^2/a1^2),x=-a1..a1, thickness=2):
> e2:=plot(-a2*sqrt(1-x^2/a1^2),x=-a1..a1, thickness=2):
> l1:=plot(cot(theta)*x,x=-0.9..0.9,thickness=2):

```

we add 1/10000 to z\_max, otherwise Maple's numerical roundoff gives imaginary values

for x1 for j=0 and j =100.

```

> zmax:=sqrt(a2^2+a1^2*(cot(theta))^2)+1/10000;
      zmax :=  $\sqrt{7} + \frac{1}{10000}$ 
> unassign('j');

```

Since our tracer line runs from  $z_0 = z_{\max}$  to  $z_{\min}$ , we trace by assigning 100 discrete values to  $z_0$  in this interval.

```
> z0:=zmax-2*zmax*j/100:
```

Now, we define the points  $(x_1, z_1)$ ,  $(x_2, z_2)$  on the undistorted ellipse.

$$x_1 := \frac{-a_1^2 z_0 \cot(\theta) + a_1 a_2 \sqrt{z_{\max}^2 - z_0^2}}{a_2^2 + a_1^2 \cot(\theta)^2}$$

$$x_2 := \frac{-a_1^2 z_0 \cot(\theta) - a_1 a_2 \sqrt{z_{\max}^2 - z_0^2}}{a_2^2 + a_1^2 \cot(\theta)^2}$$

```
> z1:=(cot(theta))*x1+z0:
```

```
> z2:=(cot(theta))*x2+z0:
```

$x_{\text{int}}$  and  $z_{\text{int}}$  label what we have labeled as  $x_{\times}$ ,  $z_{\times}$  in chapter 4.

```
> xint:=-z0/(cot(theta)+tan(theta)): zint:=-tan(theta)*xint:
```

```
> L1:=sqrt((x1-xint)^2+(z1-zint)^2):
```

```
> L2:=sqrt((x2-xint)^2+(z2-zint)^2):
```

$x_{p1}, x_{p2}$  and  $z_{p1}, z_{p2}$  label the points bounding the boost distorted ellipse.

```
> xp1:=xint+signum(z1-zint)*L1*sin(theta)/g:
```

```
> xp2:=xint-L2*sin(theta)/g:
```

```
> zp1:=(cot(theta))*xp1+z0:
```

```
> zp2:=(cot(theta))*xp2+z0:
```



Since we will need to plot a list of 100 points, we save each coordinate as a Maple

array with 100 entries.

```
> A:=array(0..100):B:=array(0..100):  
> C:=array(0..100): E:=array(0..100):
```

Now, we execute the 'j-loop' which gives us the x,z coordinates of each of the 100 points

on the distorted ellipse. Because of the obvious symmetry of the distorted ellipsoid with

respect to the line parallel to the boost direction going through the origin.

We only evolve

half the points (j=0 to 50) and let the symmetry provide the values for the other half (j = 51 to 100).

```
> for j from 0 by 1 to 50 do A[j]:=evalf(xp1); B[j]:=evalf(zp1);  
C[j]:=evalf(xp2); E[j]:=evalf(zp2) end do:
```

```
> for j from 51 by 1 to 100 do A[j]:=-C[100-j]; B[j]:=-E[100-j];  
C[j]:=-A[100-j]; E[j]:=-B[100-j]; end do:
```

The next we commands are used to convert the entries of each array into 100 (x,z) coordinate pairs.

A gives the x-component of the points on the upper half of the distorted ellipsoid.

```
> listX1:=convert(A,'list');
```

B is for the z-component.

```
> listZ1:=convert(B,'list');
```

Now, we convert the x,z-lists into an ordered pair.

```
> pair1:=(listX1,listZ1) -> [listX1, listZ1]:
```

Call the ordered pair "mainlist1".

```
> mainlist1:=array(zip(pair1, listX1, listZ1)):
```

Similarly, C and E give the x,z-components of the points on the lower half of the

distorted ellipsoid.

```
> listX2:=convert(C,'list');
```

```
> listZ2:=convert(E,'list');
```

Once again, convert each individual list to an ordered pair and call it "mainlist2".

```

> pair2:=(listX2,listZ2) -> [listX2, listZ2]:
> mainlist2:=array(zip(pair2, listX2, listZ2)):

```

The reason for creating (x,z) ordered pairs is so that we can use Maple's "pointplot"

command to scatter plot the total of 200 points whose x,z-coordinates are given by

mainlist1 and mainlist2. Maple treats these as data files and pointplot extracts the

coordinates of each j=integer point from this list and plots it on the x-z plane.

p1 plots the 100 points of the upper half and p2 plots the 100 points of the lower

half of the distorted ellipsoid.

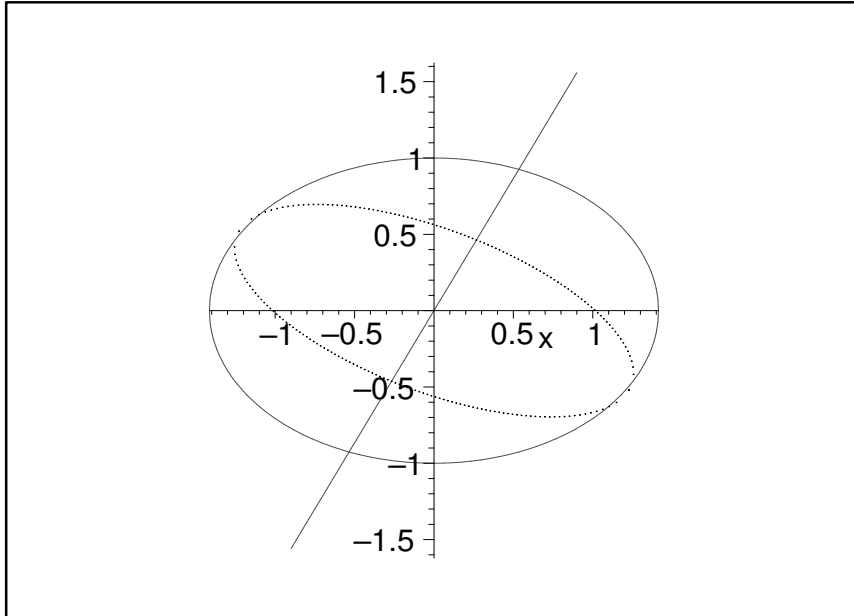
```

> p2:=pointplot(mainlist2, symbol=point, symbolsize=10000):
> p1 := pointplot(mainlist1,symbol = point,symbolsize = 10,scaling =
CONSTRAINED)

```

We finally display all the plotted curves.

```
> display(p1,p2,e1,e2,l1);
```



## Appendix 2

### Maple Code for the Polar Plot Method

In this section, we display the Maple code used to draw the distorted horizon using the 'polar plot method'. The code exhibited here is used to draw Fig. 4.6 in section 4.2.

```
> with(plots):
```

```
Warning, the name changecoords has been redefined
```

input parameters for a Kerr black hole with spin  $a=1$ ,  $\gamma = 2$

```
> M:=1: J:=0.5: beta:=sqrt(3)/2: g:=1/sqrt(1-beta^2):
```

```
> alpha[Beta]:=Pi/6: unassign('theta'):
```

$r_{\text{plus}}$  is the horizon location. It is given by

```
> rplus:=M+sqrt(M^2-J^2);
```

```
rplus := 1.866025404
```

$a_1$  and  $a_2$  label the long and short axes of the ellipse on the  $x$ - $z$  plane

```
> a1:=sqrt(rplus^2+ J^2); a2:=rplus;
```

```
a1 := 1.931851653
```

```
a2 := 1.866025404
```

We write the equation of the undistorted ellipse in polar coordinates,  $r$  stands for  $r(\theta)$ .

```
> r:=((cos(theta))^2/a1^2+(sin(theta))^2/a2^2)^(-1/2);
```

$$r := \frac{1}{\sqrt{.2679491923 \cos(\theta)^2 + .2871870788 \sin(\theta)^2}}$$

Similarly,  $rp$ , which stands for  $r'$ , traces out the distorted ellipse.

```
> rp:=r*sqrt((1-beta^2*(sin(theta+alpha[Beta]))^2));
```

$$rp := \frac{1}{2} \frac{\sqrt{4 - 3 \sin(\theta + \frac{1}{6} \pi)^2}}{\sqrt{.2679491923 \cos(\theta)^2 + .2871870788 \sin(\theta)^2}}$$

$\theta'$  is  $\theta'$ , given by

```
> theta:=theta+arctan(cot(alpha[Beta]+theta))-arctan(g*cot(theta+alpha[Beta]));
```

$$\theta' := \theta + \frac{1}{2} \pi - \operatorname{arccot}(\cot(\theta + \frac{1}{6} \pi)) - \arctan(2 \cot(\theta + \frac{1}{6} \pi))$$

Solution to the equation below should tell us where  $r$  prime of  $\theta$  reaches maximum and minimum lengths.

```
> evalf(solve(diff(rp,theta)/diff(theta,theta)));
```

```
2.656851854, -2.084676022, 1.056916632, -.4847407994
```

```
> evalf(solve(diff(rp,theta)));
```

```
1.120736347, -2.020856307, 2.904568886, -.2370237680
```

Construct an array with these 4 values for  $\theta'$  called  $\theta'$ ext.

```
> thetaext:=array(1..4,[2.656851854,-2.084676022,1.056916632,-.484740799
4]);
```

```
thetaext := [2.656851854, -2.084676022, 1.056916632, -.4847407994]
```

For each value of  $i$ , we obtain  $r'$  and  $\theta'$ . These values are displayed in Table 4.1.

```
> for i from 1 by 1 to 4 do theta:=thetaext[i]; evalf(rp);
> evalf(thetap); end do;
```

```
 $\theta := 2.656851854$ 
```

```
1.915881771
```

```
2.637430202
```

```
 $\theta := -2.084676022$ 
```

```
.9407898530
```

```
-2.074958777
```

```
 $\theta := 1.056916632$ 
```

```
.9407898530
```

```
1.066633878
```

```
 $\theta := -.4847407994$ 
```

```
1.915881771
```

```
-.504162451
```

$d\theta$  is what we call  $\Delta_{\theta}$ .

```
> dtheta:=abs(-.504162451);
```

```
dtheta := .504162451
```

```
> s:=sin(dtheta); co:=cos(dtheta);
```

```
s := .4830742692
```

```
co := .8755793799
```

a1new and a2new denote a'\_1 and a'\_2.

```
> a1new:=1.915881771; a2new:=1.066633878;
```

```
a1new := 1.915881771
```

```
a2new := 1.066633878
```

A, B, and C are the generic a, b, and c terms one gets from solving the quadratic equation for z'.

```
> C:=(co^2/a1new^2+s^2/a2new^2)*x^2-1:
```

```
> B:=-2*co*s*(1/a1new^2-1/a2new^2)*x:
```

```
> A:=(s^2/a1new^2+co^2/a2new^2):
```

z1 and z2 give the upper and lower halves of the distorted ellipse.

```
> z1:=(-B+sqrt(B^2-4*A*C))/2/A;
```

```
> z2:=(-B-sqrt(B^2-4*A*C))/(2*A);
```

```
z1 := -.3478908085 x + .6780386905  $\sqrt{-.9578374954 x^2 + 2.949684181}$ 
```

```
z2 := -.3478908085 x - .6780386905  $\sqrt{-.9578374954 x^2 + 2.949684181}$ 
```

```
> plot1:=plot(z1,x=-2..2,thickness=2):
```

```
> plot2:=plot(z2,x=-2..2,scaling=CONSTRAINED,thickness=2):
```



```

> e1:=plot(a2*sqrt(1-x^2/a1^2),x=-a1..a1,thickness=2):
> e2:=plot(-a2*sqrt(1-x^2/a1^2),x=-a1..a1,thickness=2):
> l1:=plot(cot(alpha[Beta])*x,x=-0.5..0.5,color=black):

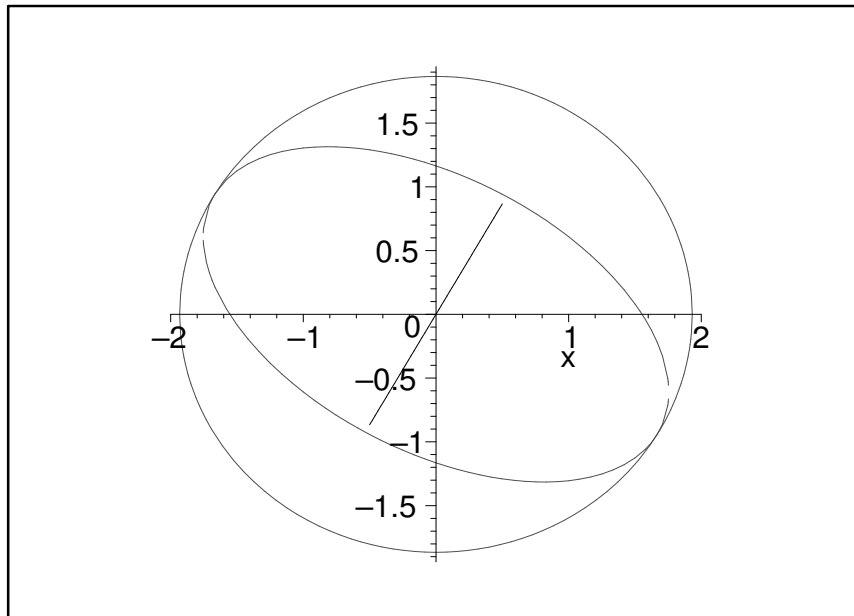
```

We also plot the undistorted horizon and the boost direction along with the distorted horizon.

```

> display(plot1,plot2,e1,e2,l1);

```





## Appendix 3

### Maple Code for Plotting using Ellipsoidal Coordinates

We suppress one dimension and actually only provide the code for using elliptical coordinates here. The generalization to three dimensions is straightforward but not very enlightening here. All the ellipses are plotted on the x-z plane.

```
> with(plots):
```

h1...h6 denote the hyperbolae  $\theta = 60, 45, 30$  degrees, obtained from  $x = a \cosh r \sin(\theta)$ ,

$z = a \sinh r \cos(\theta)$  in  $x^2/a_1^2 + z^2/a_2^2 = 1$ .

```
> h1:=sqrt(x^2-d^2/2):h2:=-sqrt(x^2-d^2/2):
```

```
> h3:=sqrt(3*(x^2-d^2/4)):
```

```
> h4:=-sqrt(3*(x^2-d^2/4)): h5:=sqrt(x^2/3-d^2/4):
```

```
> h6:=-sqrt(x^2/3-d^2/4):
```

Usual parameters for  $a=1$  Kerr black hole give us the semimajor and semiminor

axes of the horizon.

```
> a1:=sqrt(2);a2:=1;
```

$$a1 := \sqrt{2}$$

$$a2 := 1$$

Next, we determine our constant  $d$  and  $r_{\min}$ . Here we are using  $r_{\min}$  instead of  $\mu_{\min}$ .

```
> d:=sqrt(a1^2-a2^2); rmin:=evalf(arctanh(a2/a1));
```

$$d := 1$$

$$rmin := .8813735866$$

```
> unassign('j');
```

```
> r:=rmin+j/5;
```

$$r := .8813735866 + \frac{1}{5}j$$

We set up arrays with 6 entries for the concentric ellipses.  $Z$  plots the upper and lower

portions of each ellipse.

```
> e1:=array(0..5); e2:=array(0..5);
```

```
> z:=a*sinh(r)*sqrt(1-(x^2)/(a^2*(cosh(r))^2));
```

$$e1 := \text{array}(0..5, [])$$

$$e2 := \text{array}(0..5, [])$$

$$z := \sinh(.8813735866 + \frac{1}{5}j) \sqrt{1 - \frac{x^2}{\cosh(.8813735866 + \frac{1}{5}j)^2}}$$

> for j from 0 by 1 to 5 do

e1[j]:=plot(z, x=-3..3,scaling=CONSTRAINED,color=black, thickness=2):

e2[j]:=plot(-z, x=-3..3,scaling=CONSTRAINED,color=black, thickness=2):

end do:

Next, we plot surfaces of constant theta

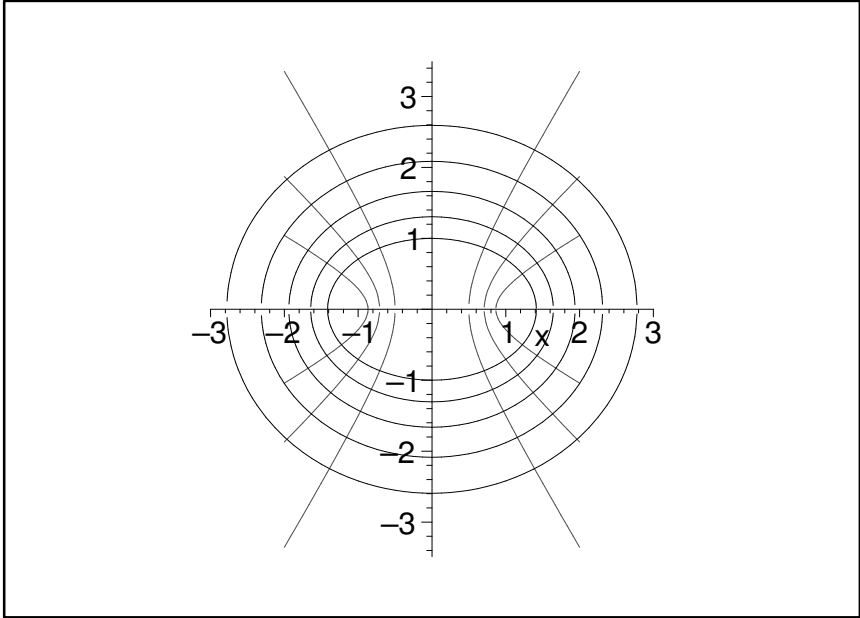
> p1:=plot(h1,x=-2..2): p2:=plot(h2,x=-2..2): p3:=plot(h3,x=-2..2):

> p4:=plot(h4,x=-2..2):

p5:=plot(h5,x=-2..2):p6:=plot(h6,x=-2..2,scaling=constrained):

> display(e1[0], e1[1], e1[2], e1[3], e1[4], e2[0], e2[1], e2[2], e2[3],

e2[4], p1, p2, p3, p4, p5, p6);



## Appendix 4

### Maple Code for using Tilted Ellipsoidal Coordinates

Following appendix 3, we now plot the actual distorted ellipses using the same elliptical coordinate method but now for ellipses distorted by a Lorentz boost of  $\gamma = 2$  and x-z plane polar angle direction  $\theta_\beta = 30^\circ$ .

```
> M:=1: theta:=.504162451:
> with(plots):
> unassign('j');
> a2:=1.066633878:
> a1:=1.915881771:
> a:=sqrt(a1^2-a2^2):
```

We use r and r\_min instead of mu and mu\_min.

```
> rmin:=arctanh(a2/a1):
> r:=rmin+j/10:
```

Create an array for various concentric ellipse plots.

```
> p1:=array(0..10): p2:=array(0..10):
```

x\_min,max and y\_min,max below determine our plot range.

```
> xmin:=-a*cosh(r): xmax:=a*cosh(r):
```

A, B and C are the individual terms that go into the equation of an ellipse.

xp stands for x\_prime.

$$A := \frac{\sin(\theta)^2}{\cosh(r)^2} + \frac{\cos(\theta)^2}{\sinh(r)^2}$$

$$B := \frac{\sin(2\theta) xp}{(\sinh(r) \cosh(r))^2}$$

$$C := \left( \frac{\cos(\theta)^2}{\cosh(r)^2} + \frac{\sin(\theta)^2}{\sinh(r)^2} \right) xp^2 - a^2$$

z1p and z2p form the upper and lower portions of the tilted ellipses.

```
> z1p:=(-B+sqrt(B^2-4*A*C))/(2*A):
> z2p:=(-B-sqrt(B^2-4*A*C))/(2*A):
> for j from 0 by 1 to 10 do

> p1[j]:=plot(z1p, xp=-xmin..xmin,thickness=2):

> p2[j]:=plot(z2p, xp=-xmin..xmin,scaling=CONSTRAINED):
```



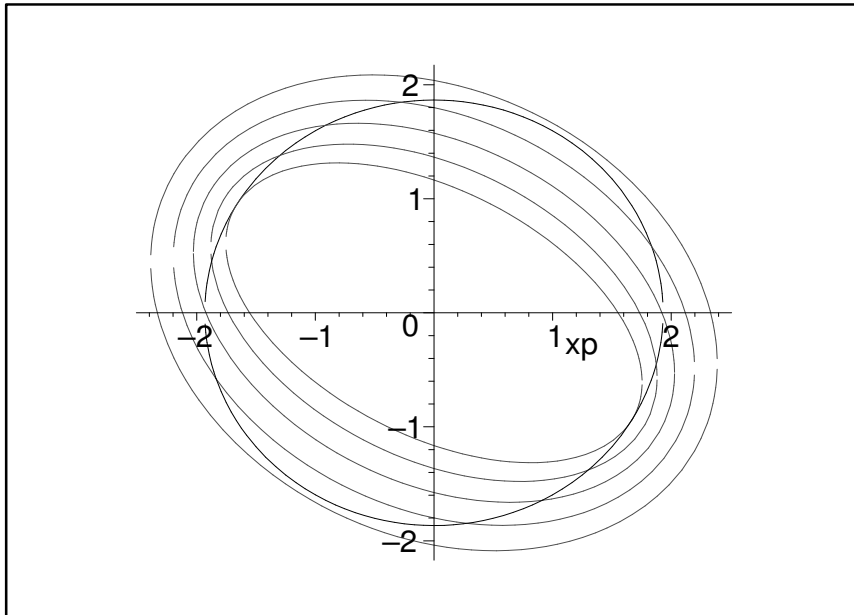
> end do:

$e1$  and  $e2$  are the halves of the original undistorted ellipsoid, the undistorted black hole horizon.

```
 $e1 := \text{plot}(1.866025404 \sqrt{1 - \frac{x^2}{1.931851653^2}}, x = -2..2, \text{?}, \text{thickness} = 2)$ 
```

```
 $e2 := \text{plot}(-1.866025404 \sqrt{1 - \frac{x^2}{1.931851653^2}}, x = -2..2, \text{thickness} = 2)$ 
```

```
display( $p1_0, p1_1, p1_2, p1_3, p1_4, e1, e2, p2_0, p2_1, p2_2, p2_3, p2_4$ )
```





## Bibliography

- [1] C. DeWitt, B.S. DeWitt, “Black Holes: Proceedings of the 23rd Les Houches Summer School”, Gordon and Breach, New York (1973).
- [2] S.W. Hawking, G.F.R. Ellis, *Large Scale Structure of Space-Time* (Cambridge University Press, Cambridge, 1973).
- [3] A. Raychaudhuri, *Pyhs. Rev.* **98**, 1123, (1955).
- [4] Robert E. Wald, V.Iyer, *Phys. Rev.* **D44**, R3719, (1991).
- [5] Binary Black Hole Grand Alliance, *Phys. Rev. Lett.* **80**, 2512-2516, (1998).
- [6] R.E. Wald, *General Relativity* (The University of Chicago Press, Chicago, 1984).
- [7] R. Penrose, *Physical Review Letters* **14**, 57, (1964).
- [8] A. Ashtekar, B. Krishnan, *Isolated and Dynamical Horizons and Their Applications*, gr-qc/0407042 (2005).
- [9] A. Ashtekar, B. Krishnan, *Dynamical Horizons and Their Properties*, gr-qc/0308033, (2003).
- [10] A. Ashtekar, B. Krishnan, *Isolated and Dynamical Horizons and Their Applications*, <http://relativity.livingreviews.org/Articles/lrr-2004-10/>, (2004).

- [11] A. Ashtekar, J. Baez, K. Krasnov, *Adv.Theor.Math.Phys.*, 1, (2000).
- [12] T. Thiemann, *Modern Canonical Quantum General Relativity*, (Cambridge University Press, Cambridge, 2008).
- [13] J. M. M. Senovilla, *Journal of High Energy Physics* **11**, 46, (2003).
- [14] B. Carter in *Les Astres Occlus* ed. by B. DeWitt, C. M. DeWitt, (Gordon and Breach, New York, 1973).
- [15] Sean A. Hayward, *Phys. Rev.* **D49**, 6467, (1994).
- [16] I. Booth, “Black Hole Boundaries”, [arxiv.org/gr-qc/0508107](https://arxiv.org/abs/gr-qc/0508107), (2005).
- [17] E. Shettner, F. Hermann, D. Pollney, *Phys. Rev* **D71**, 044033, (2005).
- [18] M. Campanelli, C. Lousto, Y. Zlochower, *Phys. Rev.* **D73**, 061501, (2006).
- [19] I. Booth, L. Brits, J. Gonzalez, Chris Van Den Broeck, “Marginally Trapped Tubes and Dynamical Horizons”, [arxiv.org/gr-qc/0506119](https://arxiv.org/abs/gr-qc/0506119), (2005).
- [20] D. Bernstein, D. Hobill, E. Seidel, L. Smarr, *Phys. Rev.* **D50**, 3760 (1994).
- [21] P. Anninos, D. Bernstein, S. R. Brandt, D. Hobill, E. Seidel, L. Smarr, *Phys. Rev.* **D50**, 3801 (1994).
- [22] P.C. Vaidya, “Newtonian Time in General Relativity”, *Nature* **171**, 260, (1953).

- [23] A. S. Eddington, *Nature* **113**, 192, (1924).
- [24] D. Finkelstein, *Phys. Rev* **110**, 965, (1958).
- [25] Reissner, H., *Annals of Physics (Germany)*, **50**, 106, (1916).
- [26] Nordström, G., *Proc. Kon. Ned. Akad. Wet.* **20**, 1238, (1918).
- [27] R. P. Kerr, *Phys. Rev. Lett.* **11**, 237 (1963).
- [28] T.A. Apostolatos, C. Cutler, G.J. Sussman, K.S. Thorne, *Phys. Rev.* **D49**, 6274, (1994).
- [29] Birkhoff, G. D. *Relativity and Modern Physics*, (Harvard University Press, Cambridge, 1923).
- [30] C. W. Misner, K. S. Thorne, and J. A. Wheeler, *Gravitation* (W.H. Freeman, New York, 1970).
- [31] R. Genzel, R. Schödel, T. Ott, A. Eckart, T. Alexander, F. Lacombe, D. Rouan and B. Aschenbach, *Nature* **425**, 934, (2003).
- [32] R. Shafee, J. E. McClintock, R. Narayan, S. W. Davis, L. Li, R. A. Remillard, *The Astrophysical Journal* **636**, L113, (2006).
- [33] A. Broderick, V. L. Fish, S. S. Doeleman, A. Loeb, arXiv.org: 0809.4490, (2008).
- [34] R.P. Kerr, A. Schild, “A New Class of Vacuum Solutions of the Einstein Field Equations”, in *Proceedings of the Galileo Galilei Centenary Meeting*

- on General Relativity, Problems of Energy and Gravitational Waves*, ed. G. Barbera (1965).
- [35] Mijan Firdous Huq, “Apparent Horizon Location in Numerical Spacetimes” Ph.D. Thesis, The University of Texas at Austin, (2004).
- [36] R. Matzner, M. F. Huq and D. Shoemaker, *Phys. Rev.* **D59**, 024015, (1999), [arXiv:gr-qc/9805023].
- [37] M. F. Huq, M. Choptuik and R. A. Matzner, *Phys. Rev.* **D66**, 084024, (2002), [arXiv:gr-qc/0002076].
- [38] E. Poisson, *A Relativist’s Toolkit* (Cambridge University Press, Cambridge, 2004).
- [39] M.P. Hobson, G. Efstathiou, and A.N. Lasenby, *General Relativity* (Cambridge University Press, Cambridge, 2006).
- [40] S. Chandrasekhar, *The Mathematical Theory of Black Holes* (Oxford University Press, Oxford, 1983).
- [41] F. Pretorius, *Phys. Rev. Lett.* **95**, 121101, (2005), [arXiv:gr-qc/0507014].
- [42] J.G. Baker, J. Centrella, D. I. Choi, M. Koppitz and J. van Meter, *Phys. Rev. Lett.* **96**, 111102, (2006), [arXiv:gr-qc/0511103].
- [43] M. Campanelli, C. O. Lousto, P. Marronetti and Y. Zlochower, *Phys. Rev. Lett.* **96**, 111101, (2006), [arXiv:gr-qc/0511048].

- [44] J. A. Gonzalez, M. D. Hannam, U. Sperhake, B. Brügmann and S. Husa, arXiv:gr-qc/0702052, (2007).
- [45] M. Campanelli, C. O. Lousto, Y. Zlochower and D. Merritt, *Phys. Rev. Lett.* **98**, 231102, (2007) [arXiv:gr-qc/0702133].
- [46] B. Brügmann, J. A. Gonzalez, M. Hannam, S. Husa and U. Sperhake, arXiv:0707.0135, (2007).
- [47] S. Brandt, B. Brügmann, *Phys. Rev. Lett.* **78**, 3606, (1997).
- [48] R. A. Matzner, M. J. Huq, D. Shoemaker, *Phys. Rev.* **D59**, 024015, (1998).
- [49] R. A. Matzner, A. Nerozzi, P. Walter, “openGR”, 2009, in preparation.
- [50] U. Sperhake, V. Cardoso, F. Pretorius, E. Berti, J. A. Gonzalez, *Phys. Rev. Lett.* **101**, 161101, (2008).
- [51] M. Shibata, H. Okawa, T. Yamamoto, *Phys. Rev.* **D78**, 101501, (2008).
- [52] E. Bonning, P. Marronetti, D. Neilsen, R. A. Matzner, *Phys. Rev.* **D68**, 044019, (2003).
- [53] S. Hawley, M. Vitalo, R. A. Matzner, arXiv:gr-qc/0604100, (2006).
- [54] Philip M. Morse & Herman Feshbach. *Methods of Theoretical Physics*, (Mc-Graw Hill, 1953).

- [55] Matt Anderson, “Constrained Evolution in Numerical Relativity”, Ph.D. Thesis, The University of Texas at Austin, (2004).
- [56] E. Newman, R. Penrose, *J. Math. Phys.* **3**, 566, (1962).
- [57] Eric Poisson, private communication, 2007.
- [58] Andrea Nerozzi, “Towards BH-NS Merger Simulations: Initial Data, Evolution and Wave Extraction” Ph.D. Thesis, Univeristy of Portsmouth, Portsmouth, UK, (2004).
- [59] R. Penrose, W. Rindler, *Spinors in Space-time*, (Cambridge University Press, Cambridge, 1984).
- [60] R. Arnowitt, S. Deser, C. W. Misner, *Gravitation: An Introduction to Current Research*, (Wiley, New York, 1962).
- [61] B. F. Schutz, *Geometrical Methods of Mathematical Physics*, (Cambridge University Press, Cambridge, 1980).
- [62] K. S. Thorne, *Rev. Mod. Phys.* **52**, 299, 1980.
- [63] J. A. Wheeler, T. Regge, *Phys. Rev* **108**, 1063, (1957).
- [64] F. J. Zerilli, *Phys. Rev.* **D2**, 2141, (1970).
- [65] L. Rezzolla, “Gravitational Waves from Perturbed Black Holes and Relativistic Star”, arXiv:gr-qc/0302025, (2003).



- [66] K. D. Kokkotas, B. G. Schmidt, *Quasi-normal Modes of Stars and Black Holes*, <http://relativity.livingreviews.org/Articles/lrr-1999-02/>, (1999).
- [67] J. D. Jackson, *Classical Electrodynamics*, (Wiley, New York, 1999).
- [68] S. A. Teukolsky, *Phys. Rev. Lett***29**, 1114, 1972.
- [69] S. Chandrasekar, *Proc. Roy. Soc. (London)* **A358**, 421, 1978.
- [70] B. F. Schutz, “An Introduction to General Relativity”, Cambridge Univ. Press, Cambridge, UK (1984).
- [71] M. J. Huq, “Apparent Horizons in Numerical Relativity”, Ph.D. Thesis, The University of Texas at Austin, (2002).
- [72] K. Glampedakis, *Class.Quant.Grav.* **22**, S605-S659, (2005).

## Vita

Sarp Akcay graduated top of his class from Lafayette High School in Williamsburg, Virginia, in 1998. That same year he entered the College of William & Mary in Williamsburg, Virginia and began majoring in physics. During the summer of 2000 he conducted research in solid state physics with the Physics Department at The Ohio State University in Columbus, Ohio. He graduated Magna Cum Laude with a Bachelor of Science in Physics in 2002. Sarp entered the Graduate School at the University of Texas Department of Physics in 2002. He will be taking up a postdoctoral research position with The University of Southampton in Southampton, UK starting Fall 2009.

Permanent Address: 18 Windbluff Ct  
Owings Mills, MD, 21117

This dissertation was typeset with  $\text{\LaTeX}$ <sup>1</sup> by the author.

---

<sup>1</sup> $\text{\LaTeX}$  is an extension of  $\text{\TeX}$ .  $\text{\TeX}$  is a collection of macros for  $\text{\TeX}$ .  $\text{\TeX}$  is a trademark of the American Mathematical Society. The macros used in formatting this dissertation were written by Dinesh Das, Department of Computer Sciences, The University of Texas at Austin, and extended by Bert Kay, James A. Bednar, and Ayman El-Khashab.